MASTER OF SCIENCE DEGREE IN
MECHANICAL ENGINEERING

Contribution to the Structural Analysis of a Modified Railway Wagon for Wooden Transportation

Author

Nuno António Simão da Cruz

Supervisors

Luis Manuel Ferreira Roseiro

Raquel Almeida de Azevedo Faria

Coimbra, February 2022

DEFINITIVO

INSTITUTO POLITÉCNICO
DE COIMBRA

INSTITUTO SUPERIOR
DE ENGENHARIA
DE COIMBRA

isec Engenharia

DEPARTAMENTO DE ENGENHARIA MECÂNICA

Contribuição para a Análise Estrutural de um Vagão Ferroviário Modificado para Transporte de Madeira

Relatório de Trabalho de Projeto para a obtenção do grau de Mestre em Engenharia Mecânica

Especialização em Construção e Manutenção de Equipamentos Mecânicos

Autor

Nuno António Simão da Cruz

Orientadores

Luis Manuel Ferreira Roseiro

Raquel Almeida de Azevedo Faria

Coimbra, Fevereiro 2022

INSTITUTO POLITÉCNICO
DE COIMBRA

INSTITUTO SUPERIOR
DE ENGENHARIA
DE COIMBRA

RESUMO

Adquirir ou desenhar e criar novos vagões ferroviários para transportes de bens específicos implica investimentos elevados que nem sempre justificam o tráfego esperado. A tendência é melhorar e atualizar o material rolante existente para colmatar da forma mais eficiente as necessidades verificadas.

Nesta tese é apresentado o trabalho desenvolvido no âmbito de um projeto iniciado pela Medway Maintenance & Repair, onde se pretende converter uma frota de vagões plataforma universais para o transporte de madeira em rolaria. Descreve a análise estrutural realizada ao chassis do vagão plataforma para avaliar a viabilidade de implementação de um sistema de fueiros para transporte de madeira em rolaria, tendo por base as normas e diretrizes aplicáveis a este tipo de modificação.

Envolve um processo de engenharia inversa para obtenção da geometria do chassis e para a caracterização das propriedades mecânicas do material de base. É demonstrada a obtenção dos Modelos de Elementos Finitos utilizados para avaliação da integridade estrutural do vagão, pré e pós modificação, e são propostos reforços estruturais estratégicos para o caso em estudo com base nos resultados obtidos.

Palavras-chave: Ferrovia, Vagão plataforma, Análise estrutural, MEF

ABSTRACT

Acquiring or designing and creating new freight wagons for transporting specific goods implies high investments that do not always justify the expected traffic. The trend is to improve and update the existing rolling stock to meet the verified needs as efficiently as possible.

This thesis presents the work developed within the scope of a project initiated by Medway Maintenance & Repair, which intends to convert a fleet of universal flat wagons to transport wooden logs. It describes the structural analysis carried out on the wagon's underframe to assess the feasibility of implementing a stanchion system for transporting wooden logs following the standards and guidelines applicable to this type of modification.

It entailed a reverse engineering process for obtaining the wagon's underframe geometry and characterizing the base material's mechanical properties. It also demonstrates the development of the Finite Element Models (FEM) used to assess the structural integrity of the wagon before and after modification. Finally, strategic structural reinforcements are proposed for the case in study based on the results obtained.

Keywords: Railways, Flat wagon, Structural analysis, FEM

COLABORAÇÃO INSTITUCIONAL

Este trabalho de projeto foi desenvolvido em colaboração Institucional entre o Instituto Superior de Engenharia de Coimbra e a empresa Medway Maintenance & Repair.

AGRADECIMENTOS

Ao Senhor Professor Luis Roseiro, meu orientador, por todo o apoio e incentivo prestado ao longo do desenvolvimento deste projeto e pelo papel fundamental que teve no meu percurso académico. Agradeço os conselhos sábios e o seu tempo valioso.

À Senhora Professora Raquel Faria, minha orientadora, pelo apoio prestado no processo de pesquisa e pela disponibilidade sempre demonstrada no desenvolvimento do projeto.

Ao Senhor Professor Vítor Maranha pela motivação e encorajamento constante.

À empresa Medway M&R., pelo privilégio concedido para trabalhar neste projeto e por me introduzir ao mundo complexo da Ferrovia. Um agradecimento especial ao Senhor Engenheiro João Martins, ao Senhor Engenheiro Paulo Alves e ao Senhor Engenheiro Paulo Oliveira pela disponibilidade prestada.

Aos colegas do Laboratório de Mecânica Aplicada, por partilharem comigo os dias de trabalho e a recompensa ao esforço no decurso desta etapa académica.

Uma palavra de agradecimento a todos os Professores deste Mestrado por transmitirem o seu conhecimento e experiência e fomentaram o meu gosto pela Engenharia Mecânica.

À minha família e amigos acima de tudo, pelo apoio e compreensão sempre presentes nesta etapa.

INDEX

FIGURE INDEX

TABLE INDEX

GRAPHIC INDEX

SYMBOLS

δ	Displacement [mm]
L	Distance between bogies [mm]
F_L	Longitudinal force [N]
ν	Poisson coefficient [adm.]
ε	Strain [adm.]
F_t	Transversal force [N]
σ_u	Ultimate strength [MPa]
σ_y	Yield-strength [MPa]
E	Young modulus [GPa]

ABBREVIATIONS

CAD	Computer Aided Design
DOF	Degree Of Freedom
FE	Finite Element
FEM	Finite Element Method
INE	Instituto Nacional de Estatística
IP	Infraestruturas de Portugal
MEF	Método dos Elementos Finitos
TSI	Technical Specification of Interoperability
3D	Three-dimensional
2D	Two-dimensional
UIC	Union internationale des chemins de fer

1 INTRODUCTION

Railway freight transportation is amongst the most environmentally friendly and sustainable freight modes of transportation, providing high transport volume with speed and security. According to INE (National Institute of Statistics), 8.7 million tons of goods were transported in Portugal in 2020, despite current global crisis caused by the COVID pandemic.

In Portugal, 70,8% of the railways are electrified and, as the concerns regarding climate change increase, the shifting towards "green freight" modes becomes prominent as investments in these sustainable technologies gain traction. This puts pressure on the railway industry to renovate the rolling stock and infrastructures with modern technology to enhance energy efficiency, reduce carbon dioxide emissions, and lower freight costs. IP (Portugal Infrastructures) has been renovating the national railway's rails over the years, having most of the leading freight routes falling in classification UIC D4, allowing 22.5 ton/axle or 8 ton/m.

According to INE, and regarding the rolling stock, there are 2719 wagons in the railway park in Portugal, 66% of them flat wagons. No accurate data regarding the mean age of these vehicles were found. Still, the wagons have been in circulation for at least three decades and don't support loads that take full advantage of the infrastructure's capacity. Because acquiring or designing, and building new wagons requires high investments, to keep up with the referred necessity of modernization, the tendency is to improve the existing wagons with recent technologies.

Medway Maintenance & Repair (M&R) is a company of the Medway group, a subsidiary of the Mediterranean Shipping Company (MSC). Medway M&R started operations of repair and maintenance of rolling stock material in 2019, performing interventions in locomotives and freight wagons, with 11575 interventions in wagons in its first year.

The present project is a contribution to the Medway M&R wagon renewal strategy, which was launched in 2019 in response to the current demand and the growth perspective in the National and Iberian traffic of wooden logs. Following the logic of upgrading the existing vehicles, the goal is to adapt an existing fleet of flat wagons to the transportation of wooden logs, optimizing its load capacity in the process. This thesis was integrated into this project as a contribution to the structural calculations required for future homologation of the modification and respective optimization.

The work focuses on the analysis of the chassis of the existing wagon. Given the lack of information, firstly, a reverse engineering process of the chassis was made to obtain its 3D model. Then, the mechanical characteristics of the material were determined from experimental tests on specimens collected from the wagon.

Based on existing standardization and available works in the open literature, finite element models were implemented to analyze the structural behaviour of the chassis in its original configuration and the modified version with additional structures to transport wooden logs. The results obtained revealed areas with insufficient mechanical strength.

Thus, an optimization of the chassis is proposed, applying reinforcements in particular areas, in an iteration process based on the finite element model for the most unfavorable conditions.

1.1 Outline of the thesis

After this brief introduction, chapter 2 will present the main technical characteristics of freight wagon vehicles and identify the particularities of wooden logs transportation.

In chapter 3, similar works and projects are identified and their methodologies noted. Technical specifications for interoperability (TSIs) are reviewed, and the state-of-the-art application of numerical methods for certification of sub-systems in the railway industry is assessed.

Chapter 4 describes the reverse engineering methods applied to develop a virtual geometric model of the wagon's chassis and the experimental tests performed to determine the wagon's material properties. Then, the load cases studied for the wagon "as-is", and the finite element models employed for the analysis are described. Stress and displacements are assessed for the wagon "as-is" to benchmark the already certified vehicle body for further comparisons.

In Chapter 5, the load cases considered for the case study of wooden logs transport are described. Then, the used FE model for the analysis is detailed. An assessment of the impact that the addition of a sub-system for wooden logs transportation is made based on the results of the simulations performed. The viability of implementation of the timber bunk system was evaluated.

In chapter 6, the conclusions of the work regarding the attained results are presented, as well as some future works suggestions.

2 FREIGHT WAGONS

Freight wagons, goods wagons or simply wagons are the terminologies used when referring to unpowered railway vehicles used to carry cargo. This chapter presents some types of freight wagons common in Europe, as well as technical characteristics relevant to the present work.

Due to the wide range of goods being transported via railways, namely with different sizes and shapes, several types of vehicles are required to accommodate these goods optimally. Since the beginning of the mass usage of the railway lanes, several kinds of wagons have been developed. Except for some highly specialized ones, the difference between wagon is mainly the so-called "superstructure" where the goods are placed. The remaining components are quite similar and many of them standardized. Figure 1 depicts some common types of freight wagons from Medway fleet, as well as the products they typically convey.

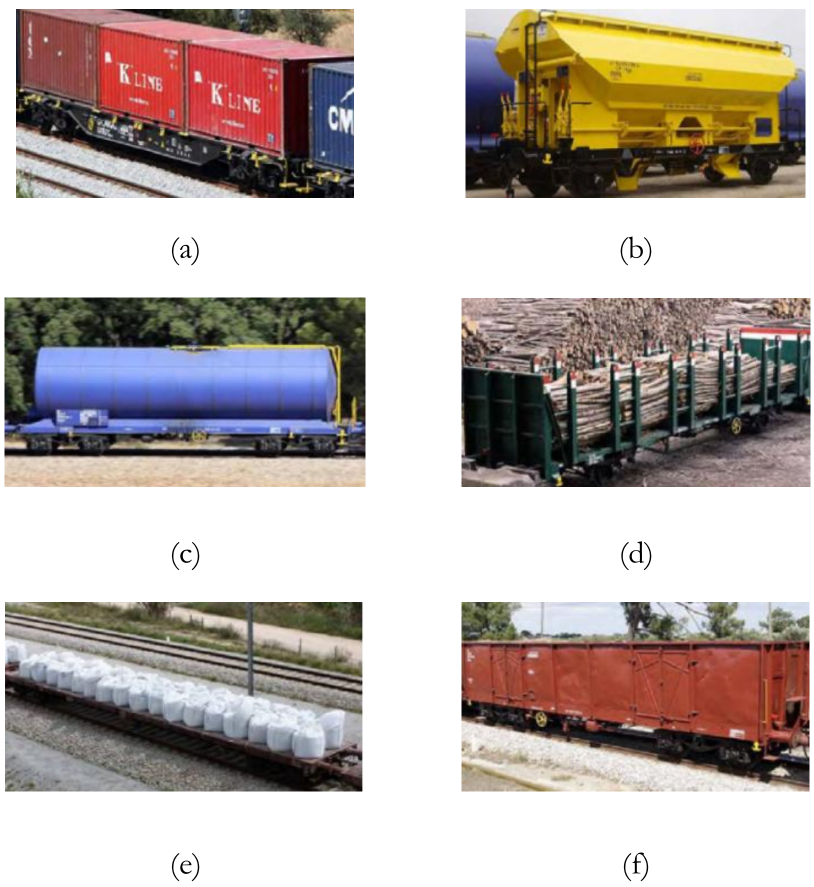

Figure 1 - Types of wagons (source: medway-iberia.com). (a) Flat wagon for transporting containers; (b) Hopper wagon for grain transportation; (c) Tank wagon for biodiesel transportation; (d) Flat wagon for wooden logs transportation; (e) Flat wagon transporting cement bags; (f) Open wagon for scrap-metal transportation;

One element that isn't necessarily standardized but exists in all freight wagons is the wagon's underframe or chassis, which is the structure in analysis in the present work. The chassis is the framework that supports the "superstructures" if they exist, and all the components necessary for operation. It supports all the loads that occur during transportation and handling processes

The majority of wagon underframes in use today are built of construction steel. Nonetheless, some newly manufactured wagons are made of high-performance alloys and composites to improve transportation efficiency, and numerous of studies have been undertaken on them (Ulianov, Shaltout, & Balan, 2015), (Ulianov, Önder, & Peng, 2018).

The underframe of a wagon is typically made up of a series of longitudinal and transversal beams that can be arranged in various ways, depending on the manufacturer and type of items being transported. The key locations and designations of a flat wagon chassis are shown in figure 2.

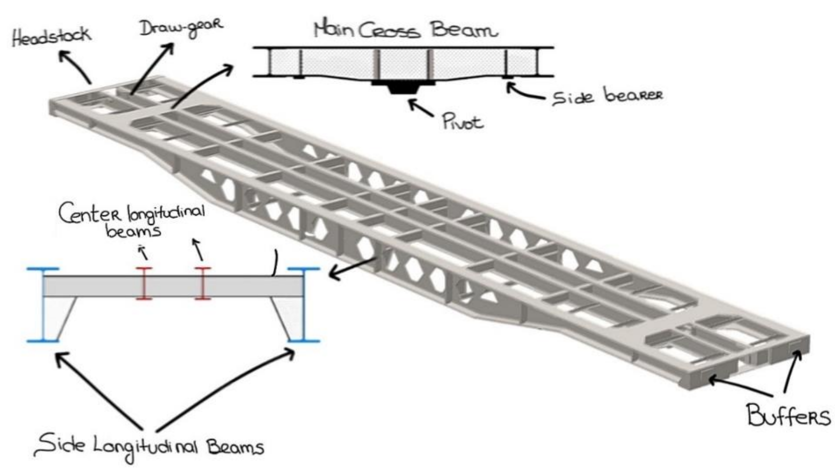

Figure 2 - Main features of flat wagon's underframes.

The coupling components required to mate the wagons to each other are fixed to the underframe. In Europe, the coupling systems are still predominantly buffer and screw type. These systems are manual and consist in three main components: buffers, hooks, and screws.

As illustrated in figure 3, to couple the rolling stock, the link in series with the screw is placed in the towing hook of the following vehicle and the screw is manually tensioned until the buffers are in slight compression.

Buffers are the components fixed in the chassis headstock that use springs and/or rubber rings to absorb compression shocks between vehicles during operation.

The draw-gear is the wagon-mounted arrangement that sustains the tension forces transmitted from the coupling system.

Figure 3 – UIC standard coupling system (source: IET 51 IMTT).

All the components that run passively on the rails, e.g., wheels, axles, vehicle frame, are denominated as running gear (figure 4). Their main functions are:

- Even transmission and distribution of the vertical load on the rail through the wheels;
- Vehicle guidance along the rails;
- Application of the braking efforts;
- Containment of dynamic efforts resulting from irregularities in the line, curves, and movements between vehicles.

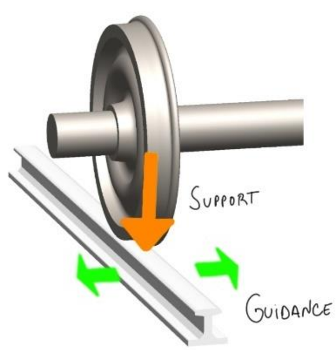

Figure 4 - Running gear – rail interaction.

Wagon's guidance can be of rigid or free (figure 5). Rigid guidance vehicles have been used since the beginning of railways because they are light and of simple construction. In this wagon type, equipments like suspension and brakes are attached directly to the structure.

Rigid guidance vehicles have lower payload capacity because they only have two wheelsets per vehicle, whilst most free-guidance vehicles have two bogies, each with two wheelsets. Also, they have lower payload capacity because slipping has to occur for them to perform curves, which involves high magnitude forces, especially in relatively small radius curves. On the other hand, in vehicles equipped with bogies (free guidance), the slipping forces are much smaller because the bogies are able to rotate relative to the underframe, allowing better performances in smaller radius curves.

Nowadays, the disadvantages of rigid guidance have led to its less use relative to free guidance.

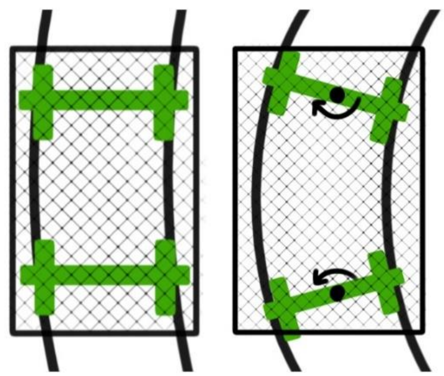

Figure 5 - Rigid guidance (left), Free guidance (right).

Standard wagons equipped with bogies typically have two bogies, each with 2 axles or wheelsets. The bogies support the vehicle's mass and use the wheels to guide the vehicle on the tracks. Among other things, this subsystem houses the brake and suspension system.

Bogies come in different configurations depending on the type of service and manufacturer. Three-piece bogies design, which is the type of bogie used on the wagon in analysis, are the most common type for freight wagons. The wagon's underframe sits on the side bearers that are attached to the transverse member called bolster. As shown in figure 6, the bolster is rigidly connected to the bogie's frame, which is in series with the suspension system, providing some damping for the vehicle resting on the side bearers.

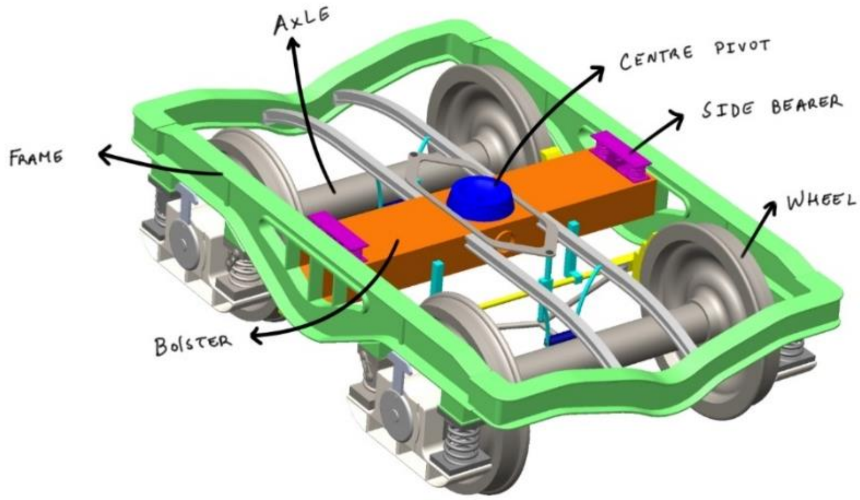

Figure 6 - Bogie main components.

Understanding the interaction between the bogie and the wagon's underframe is crucial to an accurate definition of the simulation model.

The underframe only interacts with the bogie's bolster. This interaction occurs in three points: the two side bearers and the pivot. The side bearers only constrain vertical displacements to allow the wagon's underframe to rotate freely around the pivot.

According to the reference system in figure 7, in the pivot there are transversal, and vertical reactions and on the side bearers only vertical reaction. Figure 8 depicts the free-body diagram of the wagon's underframe.

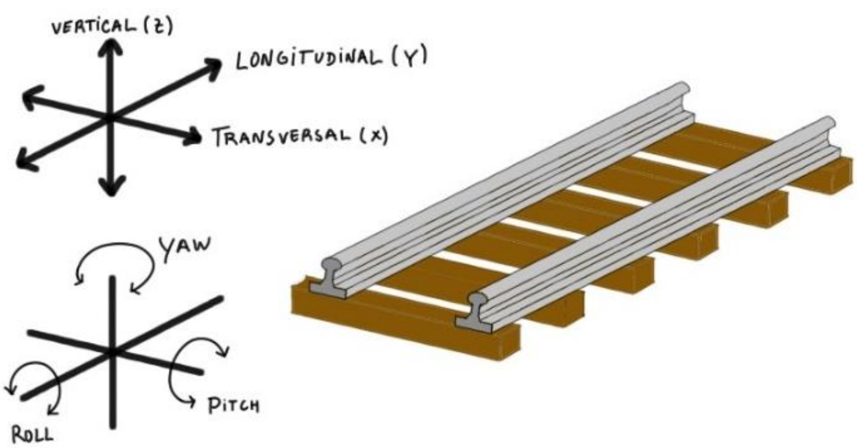

Figure 7 - Reference system for vehicle movements.

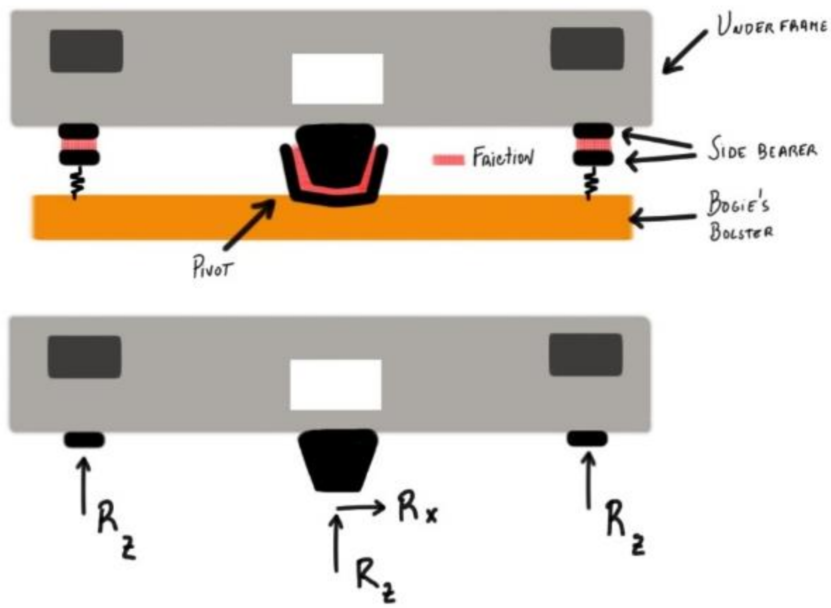

Figure 8 – Free body diagram the wagon's underframe.

2.1 Wagon in study

The wagon in analysis is a Rlps 81 94 383 2 001/065. According to UIC classification the letters Rlps stand for:

R – Ordinary flat wagon with bogies;

l – No stakes;

p – No end wall;

s – Permitted in trains up to 100 km/h.

Medway owns a fleet of dozens of wagons of this type. These have recently been mainly used to transport cement bags, but they are appropriate to carry any typical item suitable for flatbed transport. There's no record of issues reported regards the structural integrity of this wagon's chassis.

Aside from some non-structural features, the wagon's chassis is symmetrical along both longitudinal and transverse axis. of the vehicle.

The main characteristics of the wagon are listed in table 1. The wagon is shown in figure 1(e) and some structural details are presented in figure 9.

Table 1 – Wagon main technical data.

Manufacturer	Belgian Franc* and Cometna**
Year of manufacturing	1969* and 1971**
Vehicle tare	22.900 kg
Maximum payload	57.100 kg
Useful area	51.2 m^2
Vehicle length (with buffers)	19900 mm
Guidance system	Bogie
Bogie weight	4500 kg
Bogie combined load capacity	90.000 kg

Figure 9 – Structural details of the wagon in analysis.

2.2 Wooden logs transportation in railways

Wood as a raw material is a highly valued asset. After being cut, it goes from the forest to factories to be processed. This is not always a direct trajectory, and the raw material goes through a series of transportation methods, called multimodal or intermodal transportation. Typically, it is firstly transported in trucks and, when logistically advantageous, is also transported by train or ship (Timber Transport Forum, 2020).

Vehicles equipped with side stanchions are typically used to transport goods with cylindrical shapes like wood logs or steel tubes. These components are usually found in freight wagons and truck trailers and are responsible for containing the logs transversally. They can either be permanently fixed to the vehicle's structure or removable/interchangeable. Some vehicles are equipped with swivelling stanchions with fast decoupling mechanisms, allowing ease switch of vehicle's configuration for flatbed transportation. These tend to be used to transport long steel beams like rails, cement "big bags", concrete railway sleepers, and others, rather than wood, where transversal loads are low or non-existent. For transporting wooden logs specifically, high-strength posts fixed to the structure are the most utilized type of structure.

The vehicles can also be transporting the wooden logs in "timber cassettes" (figure 10c). These consist of structures with some sets of stanchions that fit in the mounting points of regular shipping containers and can be intermodally transported as such (Castagnetti, Toubol, & Rizzi, 2016).

Additionally, the vehicles can either be designed initially with stanchions and respective mounting systems or fitted with "after-market" systems for this effect. Figure 10 shows wagons with stanchions applied in different ways.

(a) (source:medway-iberia.com)

(b) (source:exte.se)

(c) (source: WASCOSA)

(d) (source:exte.se)

Figure 10 - Types of timber bunks systems. (a) Wagon with fixed stanchions; (b) Wagon with UIC sockets; (c) Timber cassette wagon; (d) Flat wagon equipped with ExTe timber bunks.

Several brands offer solutions for modifying existing wagons to transport wooden logs. These systems are known as "Timber Bunk's", and all feature the same main elements, shown in figure 11. These are almost always made of high-strength steel and are approved by notified bodies for railway applications.

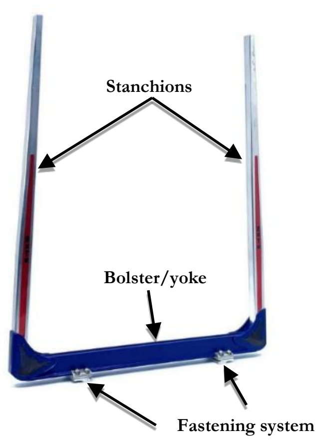

(a)

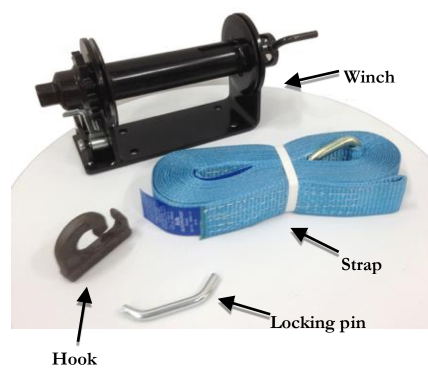

(b)

Figure 11 - (a) Timber bunk components; (b) Winch system. (Source: exte.se)

Fixed systems can either be welded directly to the vehicle's chassis, bolted, or clamped (figure 12). Depending on the application, each one presents pros and cons.

(a) (b) (c)

Figure 12 - Types of fixtures for the timber-bunks. (a) Over-yoke bolted; (b) Welded; (c) Clamped.

In the Timber bunks the wooden logs are vertically supported by the yoke and transversally by the stanchions. A tensioned strap (figure 12) is then placed as a safety measure, "hugging" the logs, preventing them from sliding in the event of a severe deceleration (Timber Transport Forum, 2020).

End-walls are also often installed on wagons transporting wooden rolls to prevent longitudinal sliding of the rolls beside the vehicle boundaries. These can have different geometries and play an essential role in the vehicle's aerodynamic efficiency.

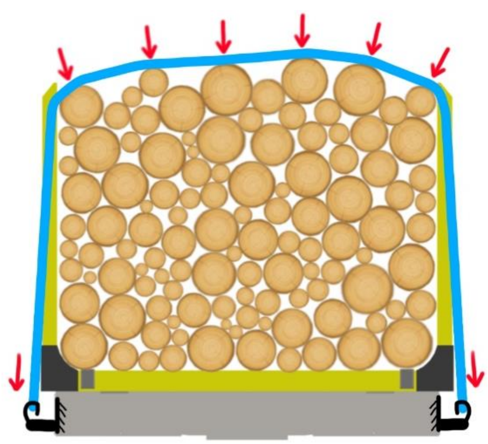

Figure 13 - Forces exerted by tensioned strap.

2.3 Equipment considered in this work

It was already established that the timber-bunks and end-walls to be used were from a Swedish company named ExTe. Medway intends to install seven sets of ExTe SR8+ Timber Bunk G1 and Winch-system 602 to each wagon. Figure 14 presents the main dimensions and technical data of this equipment. Regarding the material, the manufacturer only mentions that it is high-strength steel.

An over-yoke fastening system was adopted. It would have been possible to use a clamped type of system, but it would require some frame areas to be cut off to fit it.

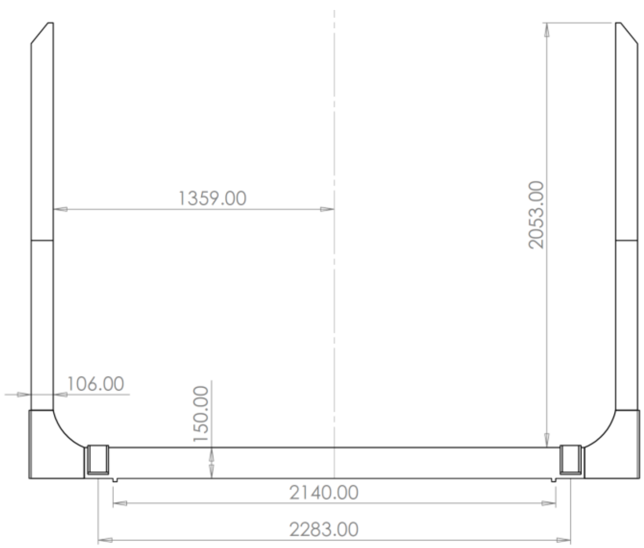

Timber bunk's own weight	160 kg
Loading area	5.55 m^2
Maximum payload per set	8 ton

Figure 14 - ExTe SR8+ Timber bunk system main technical data.

When this work began, a prototype wagon was already being converted in Medway M & R facilities, where ExTe SR8+ Timber bunks and end-walls with a less restricted gauge had been assembled. In figure 15 are presented some pictures of the prototype wagon.

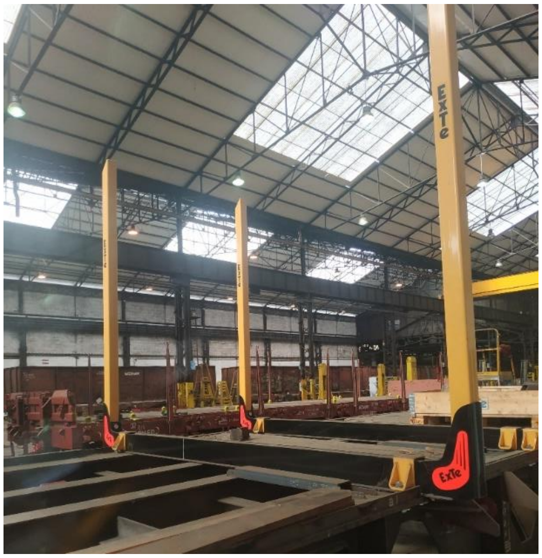

(a)

(b)

(c)

(d)

Figure 15 – Prototype wagon. (a) ExTe timber bunk system fitted; (b) Over-yoke fastening system; (c) Steel end-wall; (d) End-wall attachment to the wagon's underframe.

3 PROCESS OF VALIDATION OF A WAGON'S UNDERFRAME

Before any vehicle is allowed to circulate in the European rail system is mandatory that compatibility with the network is assured so that no safety issues arise in its life cycle and the capability of this system is optimized.

Technical specifications for interoperability (TSIs) comprises the essential technical requirements that each subsystem of the railway system must meet. These tend to become stricter and more complex as technologies progress.

The specifications expressed in Freight Wagons-TSI (2013) applies to all the new, renewed or upgraded freight wagons and conformity assessment procedures are presented in this document. As stated in ANNEX IV of the TSI, these procedures must be carried out by notified bodies so that the subsystem can be homologated and commissioned into service with 'EC' Declaration of Conformity. In practice, the tests are often overviewed and may not be carried in total accordance with the applicable standards due to client desire and still approved by notified bodies (Stoilov V. , Slavchev, Maznichki, & Purgic, 2019).

The wagon in analysis in the present study has been in circulation since 1970, and little data besides the one presented in chapter 2.1 was available.

According to the manufacturer, the timber bunk system intended to be installed is certified by notified bodies, as mentioned before in chapter 2.3. Since the two are certified, only the interaction between them and their interaction with other railway subsystems, such as the surrounding infrastructure, must be assessed.

To assess if the requirements are fulfilled, usually, the systems must go through a series of functional tests that require the usage of specialized and expensive pieces of equipment on dedicated facilities. The process for validating the structural subsystem of an already certified vehicle might not be as extensive and, in some cases, not even imply a new 'EC' declaration of verification. Nowadays, the tendency in the processes of testing and certification is to utilize virtual tools such as numerical simulation as much as possible to reduce testing costs and time. Reviews of the state of the art of application of these methods can be found in works conducted by Juris, et al. (2019), Batista, et al. (2017) and issued by Ahmad, Cole, Spiryagin, Spiryagin, & Sun (2015).

The validation program given at EN12663-2, 2010 must be followed to assess conformity on the strength requirements. This standard indicates that the structural strength of an evolved wagon can be demonstrated based on a comparison between a previously approved design if similar service conditions are applied. Different requirements scenarios for various case studies are described. The present work fits the description of an identical design for a new application, which, according to this table, requires no field tests or a reduced test program. However, it is unclear when experimental tests must be performed, and which methods are valid for the structural analysis. In this standard, no mention is ever made to numerical methods as previously issued by Juris, et al. (2019).

A literature review was conducted on studies related to freight wagon design and strength assessment. Also, applicable standards and guidelines were consulted and considered in the study.

This chapter summarises the relevant information from similar works and applicable standards that guided and supported some decisions made during the present study.

In none of the literature reviewed were found works where it was intended to evolve the design of a flat wagon with the incorporation of timber bunks and end walls like in this work.

Similar work was conducted by Stoilov V. , Slavchev, Maznichki, & Purgic (2019), where defects occurred on a flat wagon's underframe (Wagon type: Smrps; Base material S355j2 steel) after modification with stanchions were studied. In this wagon are utilized stanchions fixed directly to the underframe using bolts. Steel pipes are the goods intended to transport according to its UIC definition. In this work, the wagon and stanchions were analyzed separately using the FE method, following the load cases given at EN 12663-2 (2010). The vehicle was admitted into service by a notified body based on the observed stresses. After two years in service, high distortion was verified on the wagon's underframe in the regions where the stanchions are fastened due to the high pressures.

This occurred because, erroneously, the interaction between the two was not assessed. Then the authors created an FE model in Solidworks (CAE software) with the stanchions positioned in the flat wagon, defined virtual fastening elements and applied the loads presented in the standard for the stanchion testing. In this analysis, areas with high stresses were detected. The authors state that the deformation that occurred must be present due to impacts that occur during loading and unloading procedures, not considered by the standard. Based on these results, reinforcement measures were proposed. According to Stoilov V., Slavchev, Maznichki, & Purgic (2019), the following text should be added to the standard EN 12663-2 (2010): "The strength analysis of the side stanchions with the prescribed loads should be carried out by taking into account their impact on the wagon underframe".

In the present work's author perspective, even though this is not directly written in the standard, the complementary information given at Freight Wagons TSI (2013) implies that this verification must be made before the vehicle is put in circulation, as explained at the beginning of this chapter.

Several works reviewed compared numerical analysis results to field experimental tests and studied the suitability of Benchmarking methodologies (Stoilov, Slavchev, &

Georgieva (2011). In all these works, the applied loads are based on the load cases given at EN12663-2 (2010).

Stoilov, Slavchev, & Purgic (2016) assessed the structural integrity of an improved design of a universal flat wagon using FE method implemented in Solidworks, following the methodologies given by Stoilov, Slavchev, & Georgieva (2011). The stress and displacement results were compared between an optimized design and the existing model. According to the FE results, in some areas of the existing design, higher than allowable stresses occur. In the optimized design, some strategic changes were made to lower them to permissible levels.

Similarly, Voltr, et al. (2019), in the Innowag project, conducted a structural strength analysis following applicable standards and guidelines. This project proposes the development of a lightweight wagon with novel materials. In this work, firstly, a structural analysis was made to a conventional hopper wagon that had been in circulation for several years with no issues reported. The results were benchmarked for later comparison with the lightweight structure developed. The finite element analysis results revealed high von-Mises stresses for the existing design in some load cases, surpassing 1000 MPa in some areas. Since the wagon never had significant strength issues, the authors assumed that these atypical values may be due to modelling simplifications or small differences between the CAD model and the physical wagon.

Stoilov et al. (2019) compared the results of theoretical and experimental studies in an Sdggmrss-Twin freight wagon. Using FE methods in Solidworks software, the studies were conducted similarly to those described in the works before. Experimental testing in special rigs was performed, and the structure's deformations for different load cases were measured using strain gauges. The stress values between both FE and experimental were compared, and the authors concluded that the overall results had a good match. Similarly, Apurba & Gopal (2020) assessed the critical points of a newly designed container carrying flat wagon via the FE method and then pasted strain gauges in these locations and performed experimental tests. Here, the authors found that the measured stress is on the higher side when compared to simulation data.

Slavchev, Georgieva, Stoilov, & Purgić (2014) not only compared the experimental and theoretical results but also compared finite element models based on shell elements with models based on solid elements. Firstly, calculations were carried out, and the locations of high stresses were identified. Then, strain-gauges were duly applied in those areas. The authors found a good correlation between the results obtained experimentally with those obtained with the FEM analysis, using both shell and solid elements. Georgieva, Stoilov, & Purgić (2014) recommended the usage of 3D solid elements since those outputted results closer to experimental ones and are easier to implement. This matter is further discussed by Slavchev, Georgieva, & Stoilov (2014).

It seemed consensual between all authors of the previously presented works that the results given out by numerical analysis with finite element method were close enough to the real ones, and optimization could be done based on results given out by them.

3.1 Relevant Standards

This section presents the most relevant standards for the work developed in this thesis. Important information was summarized and presented to contextualize the decisions made later in chapters 4 and 5.

3.1.1 EN12663-2:2010 – Railway applications - Structural requirements of railway vehicle bodies - Part 2: Freight wagons

EN12663-2 (2010) specifies the structural requirements that newly designed or modified freight wagons shall fulfil before circulation. This standard provides information about the load cases that the wagon's body and associated specific equipment must sustain to be allowed in circulation. The loads prescribed are meant to be applied statically in experimental test rigs. However, in this work, this information will be adapted to the FE analysis to determine deflections and stresses, as in most of the works described in section 3.

In this standard, the wagons are split into two categories depending on the type of loads sustained in service:

- Category F-I: vehicles that can be shunted without restriction;
- Category F-II: vehicles restricted in hump and loose shunting.

The wagon in analysis falls in the F-I category because hump and loose shunting can be performed in wagon's equipped with side buffers. Even though these kinds of maneuvers are no longer allowed in Portugal due to safety concerns, the F-I category was considered in this analysis for being the most demanding one.

The static loads to apply are divided into the following groups:

- Longitudinal static loads or horizontal load cases (HLC);
- Vertical static loads or vertical load cases (VLC);
- Lifting load cases (LLC);
- Superposition of load cases (SPLC).

All longitudinal static loads shall be combined with the load due to 1 g (9,81 m/s^2) vertical acceleration of the mass m1 (table 2).

Table 2 presents the masses considered for calculation. Masses of the additional equipment (stanchions and end-walls) are not included in the m1.

Table 2 – Reference masses for load calculation.

Definition	Symbol	Mass [kg]
Mass of the vehicle body in working order	m1	13900
Mass of one bogie	m2	4500
Normal design payload	m3	57100

It is specified that the load cases must be applied in a manner that better represents the actual loading of the wagon's structure in working conditions to assess its critical features.

Longitudinal static loads:

- HLC1 - Compression force of 2000 kN applied at buffer height. Half of the value is applied at each buffer axis (figure 16).

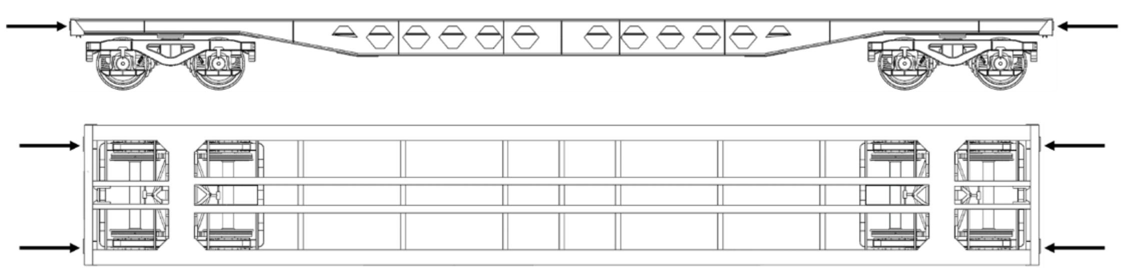

Figure 16 - Site of application of forces for HLC1.

- HLC2 – Compressive force 50mm below buffer axis 1500 kN

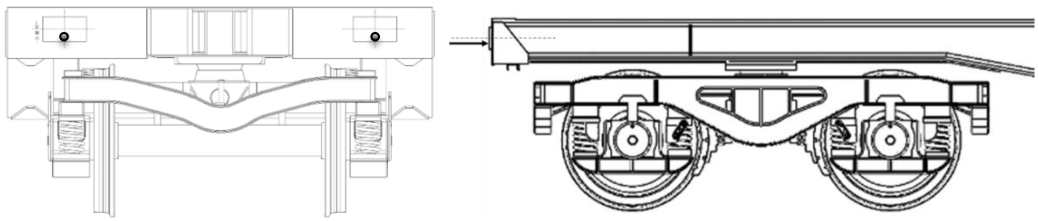

Figure 17 - Site of application of loads for HLC2.

- HLC3 – Compressive force applied diagonally at buffer level 400 kN

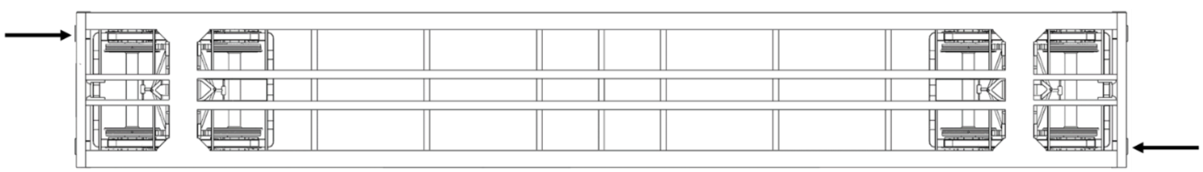

Figure 18 – Force diagonally applied at buffer level (HLC3).

- HLC4 - Tensile force in coupler, 1500 kN.

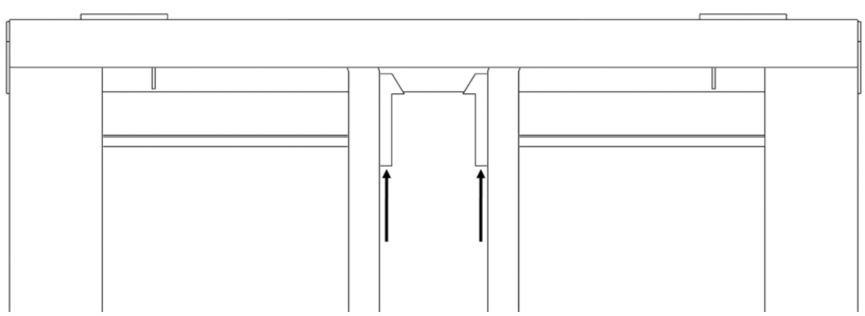

Figure 19 – Tensile force applied in the coupler face of contact with the wagon (HLC4)

Vertical static loads:

For the vertical static loads, the standard indicates the following formula, corresponding to the exceptional payload of the vehicle:

$$\text{VLC} = 1{,}3\ \times g\ \times (m_1 + m_3)\ [N] \tag{3.1}$$

m1, m3 are presented in table 2.

For the vehicle in study it corresponds to a force of 923 kN. Nowhere in the standard is indicated how this load must be applied in an experimental context. Given the information inscribed on the wagon body (figure 20) stating the maximum loads for each section, it was decided to analyze such loads in conjunction with 1 g vertical acceleration force of m1. In all the works previously reviewed the vertical loads were simulated in similar manner.

The middle column in table figure 20 corresponds to the wagon's maximum allowable payload (tons) for uniformly distributed goods, and the right column corresponds to the maximum allowable payload for bi-supported goods (UIC loading guidelines, 2021). The left column indicates the sections of the wagon where the loads are allowed. Figure 21 demonstrates the sections on the wagon.

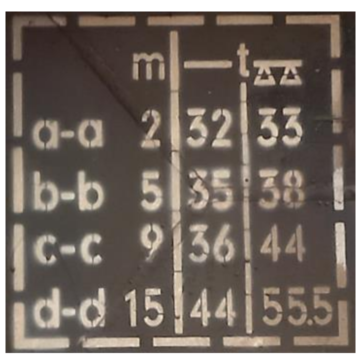

Figure 20 – Inscriptions on the wagon's underframe.

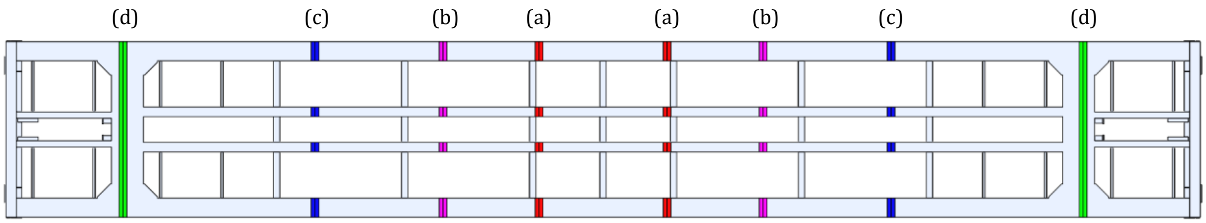

Figure 21 – Areas where vertical loads are applied.

Lifting load cases:

Lifting and jacking situations are also foreseen in this standard. One of the cases is the lifting and jacking at one end of the vehicle at the specified lifting positions. The magnitude of the load to be applied is given by the following equation:

$$\text{LLC1} = 1{,}0 \times g \times (m_1 + m_2 + m_3)\ [N] \tag{3.2}$$

m1, m2, m3 are presented in table 2.

Therefore, in this case 740 kN (LLC1) must be applied at the end of the vehicle as illustrated in figure 22.

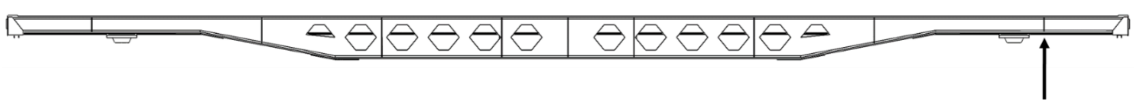

Figure 22 - Lifting load application (LLC1).

The lifting and jacking of the whole vehicle shall also be analyzed. For this case, the load is calculated according to:

$$\text{LLC2} = 1{,}0 \times g \times (m_1 + 2 \times m_2 + m_3)\ [N] \tag{3.3}$$

m1, m2, m3 are presented in table 2.

In figure 23, the application points are represented. According to the formula, 800 kN shall be applied (LLC2).

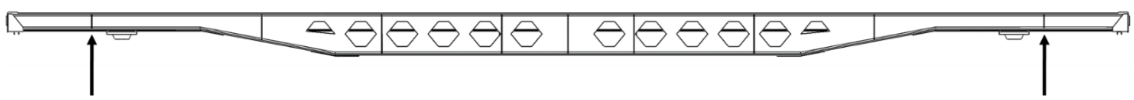

Figure 23 – Lifting of the whole vehicle (LLC2).

Lifting and jacking whit displaced support load case is also considered. For this load case, one of the lifting points must be displaced 10mm vertically relative to the plane of the other three supporting points, as illustrated in figure 24.

Figure 24 – Relative displacement of one of the lifting points (LLC3).

Superposition of static load cases for the vehicle body:

The previous load cases are analyzed individually but in working conditions, most of the time, the frame is under multiple loads simultaneously. A combination of some of the most critical load cases shall be studied to demonstrate the integrity of the structure's static strength. According to the standard, the following superposition of static loads must be analyzed:

- SPLC1 = Compression force + vertical load (HLC1+VLC1);
- SPLC2 = Tensile force + vertical load (HLC4+VLC1).

The rigidity of the frame must be assessed. It is considered well designed if the following condition is verified:

$$\partial max < 3‰ \times L \text{ [mm]}, \quad (3.4)$$

where L [mm] is the distance between bogies and ∂max [mm] the maximum resultant displacement.

Load cases for associated specific equipment

Relatively to the "Timber bunks", in chapter 7.10 of EN12663-2 (2010) are also presented methods to test the strength of the stanchions. However, as mentioned in chapter 2.3, ExTe branded stanchion system will be applied. Since those have been approved by notified body, the analysis of the stanchion itself is not within the scope of the present study. However, it is relevant to understand how the forces applied to this system are transmitted to the underframe and if that leads to excessive stresses on those locations. As stated before, Stoilov V. , Slavchev, Maznichki, & Purgic (2019) detected problems of this nature on a modified wagon where this interaction was not considered.

According to this standard, high strength stanchions shall withstand 42 kN·m in the transverse direction and 15 kN·m in the longitudinal direction, as illustrated in figure 25.

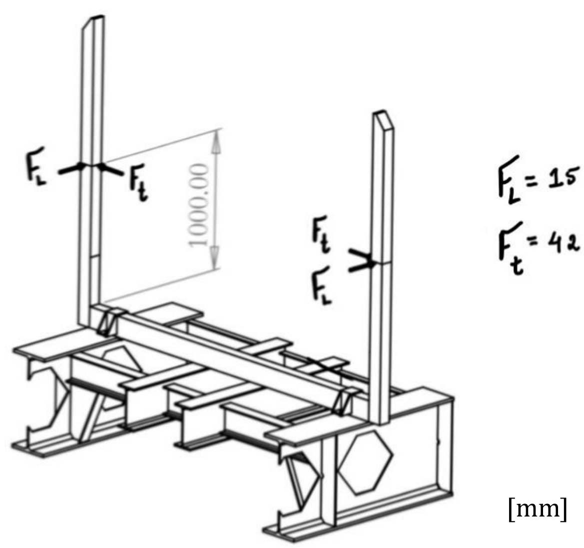

Figure 25 – Forces applied to the stanchions.

At EN 12663-2 are predicted tests of end-walls for covered wagons. Nowhere in the standard are mentioned strength tests for the type of end-walls that typically fitted in wagons for wooden logs transportation.

3.1.2 EN15273-3 Railway applications – Gauges

When adding new elements to a vehicle body, the permissible gauges must be ensured in the courses where the vehicle circulates. A gauge can be defined as an agreement between the infrastructure and the rolling stock regarding the vehicle's maximum allowable profile dimensions. It defines the maximum profile dimensions a vehicle can have to circulate safely in an infrastructure with no risk of collisions with its surroundings in all given conditions. As an example, figure 26 illustrates the importance of the loading gauge in a tunnel.

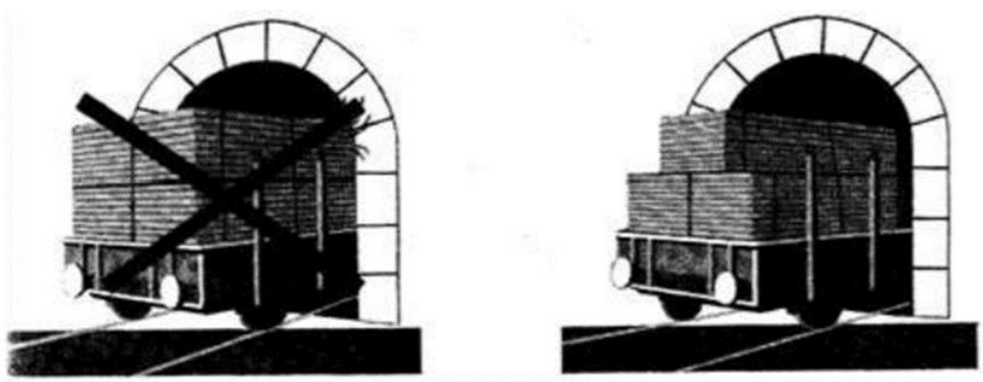

Figure 26 – Loading gauge exemplification. (source: UIC loading guidelines)

In the case in study, it had to be verified that the addition of the timber bunk system was compatible with the permissible gauges for the Iberian infrastructure.

Technical specifications for interoperability in European Union's rail system were consulted, and the requirements regarding this matter were assessed. According to these documents, the compliance of the unit with the intended reference profile must be verified using methods set out in EN15273-2 (2013). For Portugal infrastructure, PT b and PT b+ are the two most common gauges, being PT b+ predominant as seen in figure 27.

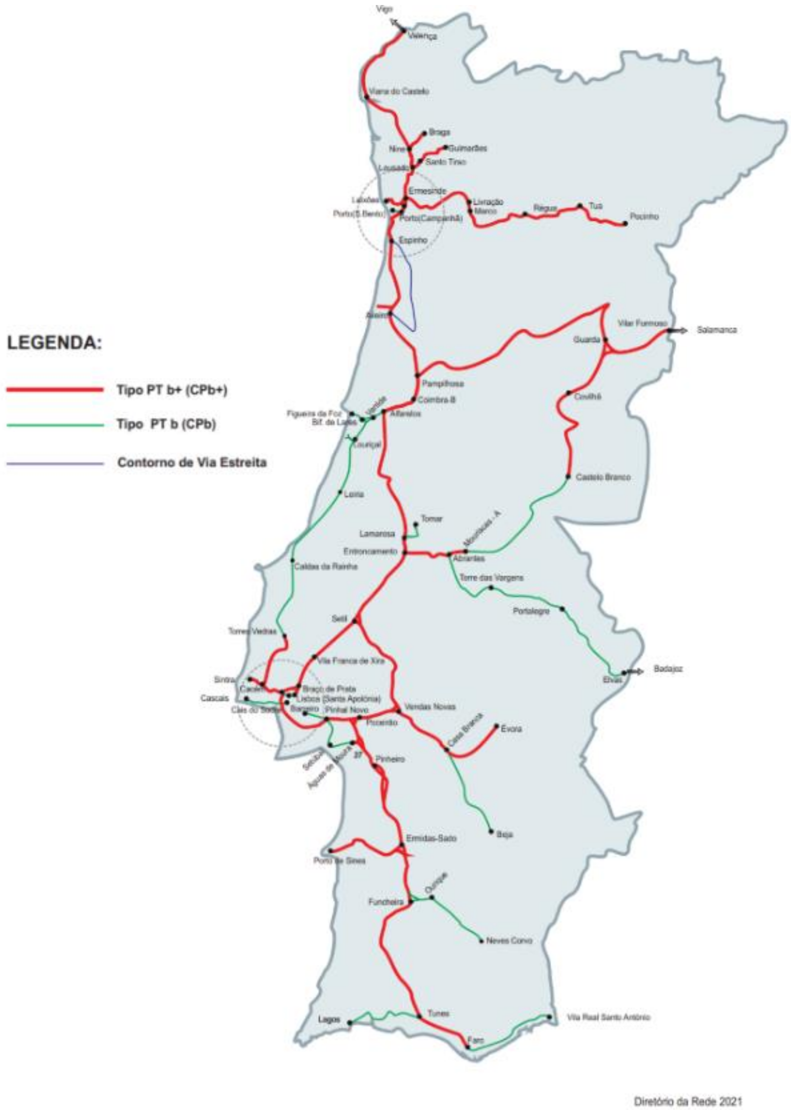

Figure 27 – Reference cinematic gauge in Portugal (source: Diretório de rede, IP)

In Spain, gauges GHE16, GEA16, GEB16, GEC16, and GEC14 are the most common. As stated before, the main goal of this wagon is the transportation of goods in Iberian territory, so the most restrictive gauge of all the stated before must be the baseline for calculation. In figure 28 is illustrated how the most restrictive gauge in Portugal (PT b) and the most restrictive gauge in Spain (GHE16) compare to each other and with the common gauge G1.

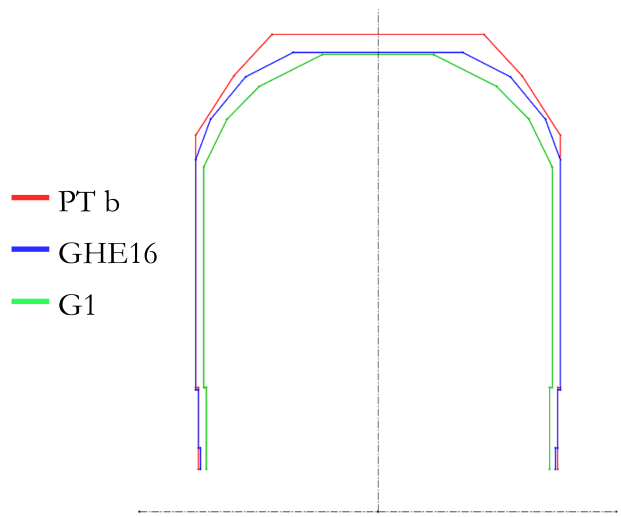

Figure 28 – Comparison of Iberian gauges.

The most restrictive gauge in Iberian soil is the GHE16. However, Medway M & R decided to have as reference gauge G1 since it allows circulation with no restrictions, allowing the vehicle body to circulate not only in Iberian infrastructure but also in European ones if ever needed, improving the interoperability of the modified wagon. As shown in figure 28, this gauge is more restrictive than Portuguese and Spanish ones in all half-widths and heights, so the reductions were made according to it.

In the methods set out in EN15273-2 (2013) for calculating the half widths and heights of the kinematic gauge for the vehicle body, several phenomena regarding its dynamics are implied. At EN15273-1 (2013) all the dynamic behaviours of the vehicle are explained in detail. Some of the critical parameters to take into consideration are:

- Nominal dimensions of the rolling stock;
- Geometric overthrow on curves (in the horizontal plane or in the vertical plane);
- Vehicle tolerances and maintenance limits;
- Excessive dissymmetry of the vehicle inclination
- Deflection under load;
- Suspension displacement and wear;
- Wheel radius differences between bogies or wheelsets;
- Adjustment devices to compensate for varying wheel diameters as well as suspension displacement and wear.

Medway M & R carried out the calculation of the maximum load gauge. In figure 29 the most critical cross section of the wagon is shown, with the timber bunk in place.

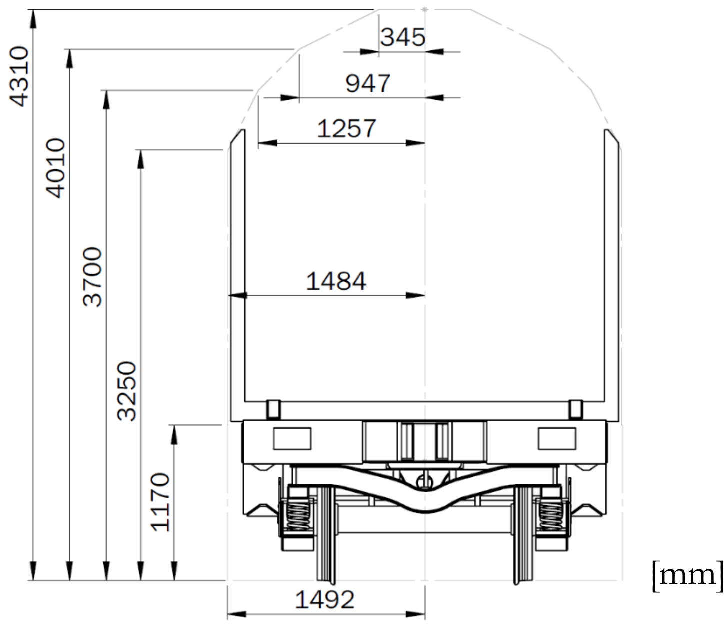

Figure 29 – Dimensions of the maximum load gauge with timber bunk in place

It can be observed that with the calculated allowed dimensions, there was no interference with the wagon with the stanchions in place. Therefore, it was verified that the addition of the timber bunks and end walls did not conflict with the maximum load gauge in all given conditions. So the circulation of the wagon is allowed with no restrictions in Iberian territory.

4 STRUCTURAL ANALYSIS OF THE WAGON'S UNDERFRAME "AS-IS"

To analyze the structure, ideally, experimental tests should be performed to assess the structural integrity of the wagon's underframe as suggested in EN12663-2 (2010). These experimental procedures must be performed in specific equipment that is not easy to access and are expensive. An alternative to these experimental tests is using advanced numerical methods to virtually assess the mechanical behaviour across the structure. Typically, the numerical method used is the Finite Element Method (FEM), using software with powerful algorithms. This chapter shows how the method was implemented considering the load cases stated in EN12663-2 (2010), previously detailed in section 3.1.1.

To have a baseline, it was decided to make a full analysis to the frame before any modification, i.e, "as-is", similarly to what was made by Voltr, et al. (2019), Stoilov, Slavchev, & Purgic (2016), and considering the methodology given by Stoilov, Slavchev, & Georgieva (2011).

4.1 Geometric Model of the Wagon

4.1.1 Reverse Engineering Procedure

Since no CAD model of the wagon's chassis was available, the physical model had to be reverse engineered. An accurate real scale geometric model of the wagon's underframe was made using software Solidworks, based on some 2D drawings provided by Medway M & R and measurements of the actual wagon. Insignificant features for the structural analysis were not considered in the 3D model in order to avoid later issues in the FE model, as suggested by Kurowski (2020) and Akin (2010). Figure 30 shows some views of the chassi's 3D model developed.

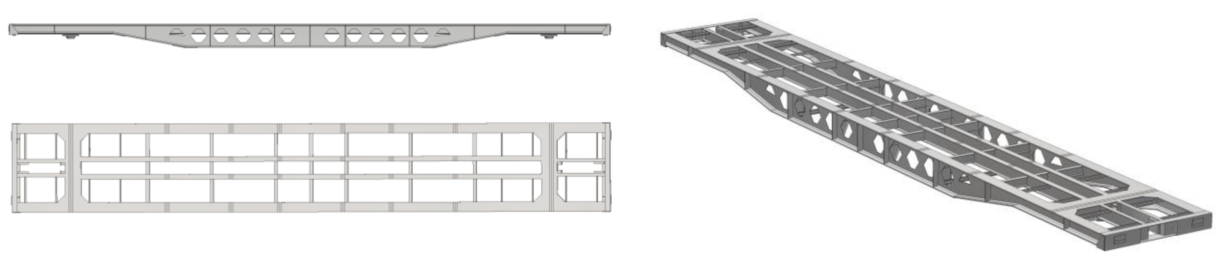

Figure 30 – 3D model views.

4.1.2 Mechanical Properties of the Material

Before any analysis, the mechanical properties of the wagon material must be assessed. The critical mechanical properties to implement a linear static analysis using FEM are longitudinal elastic modulus (E), and Poisson's coefficient (ν). Tensile strength data is also important for results interpretation. A tensile strength test is typically used to obtain these properties, consisting of straining a test specimen in tension until rupture.

For the context of the present work, six material test pieces (three round and three flat – figure 31 (a)) were machined from a plate removed from the wagon's structure. The material test pieces, and the tests were carried out according to EN10002-1 (2001). Tensile tests were performed in ISEC facilities in an INSTRON 5584 universal testing machine (figure 31 (b)). Only the cylindrical specimen's data are considered due to equipment malfunction during the flat specimens tests.

(a) (b)

Figure 31 – (a) Wagon's steel test pieces; (b) Tensile test

Graphic 1 presents the results obtained from the tensile tests of the three cylindrical test pieces.

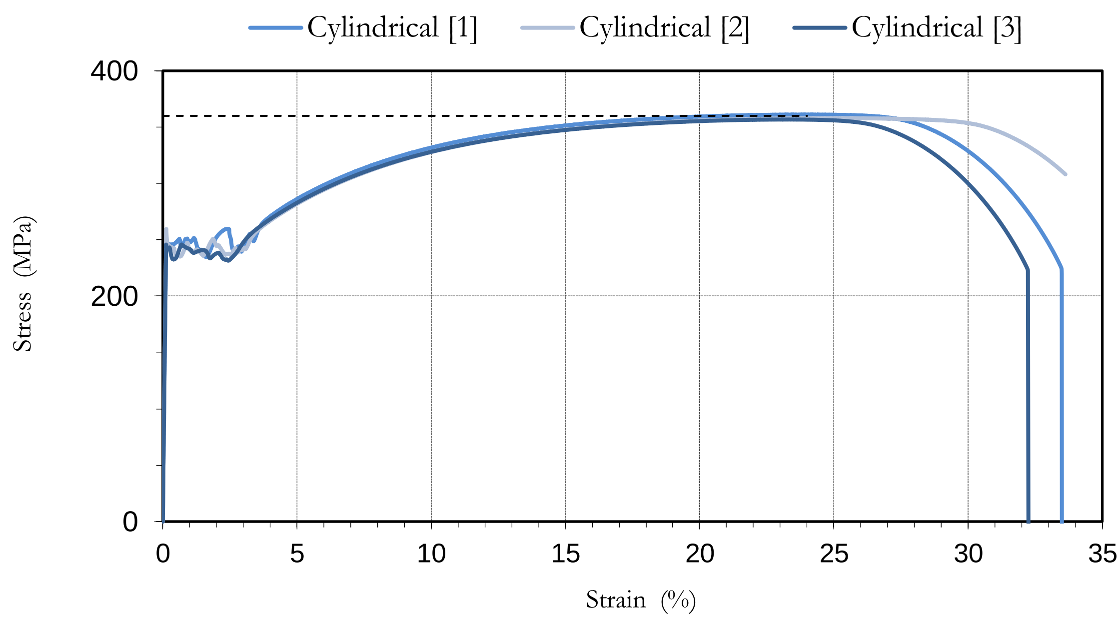

Graphic 1 – Stress-strain curves of wagon's steel test pieces.

Graphic 1 indicates similar behaviors between test specimens. Elastic, transition, and plastic phases are identifiable. During the tests, high deformation until fracture was observed (figure 32), as graphic 1 indicates.

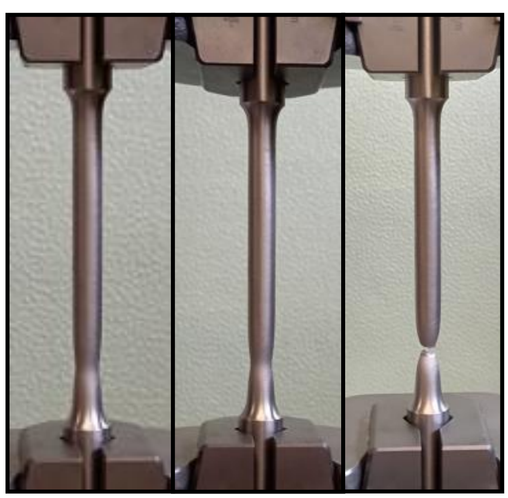

Figure 32 – Straining progress of the specimen's during tensile test.

Theoretically, the yield-strength (σ_y) is the point where the transition from elastic domain to plastic domain occurs. This is sometimes hard to identify for some materials, and, in these cases, the so-called "offset method" is applied to determine the yield-strength. This method consists in offsetting by 0.2% the initial elastic line in a stress-strain graphic. The yield stress corresponds to where this line crosses the test curve. In graphic 2 is shown the application of this method for this case.

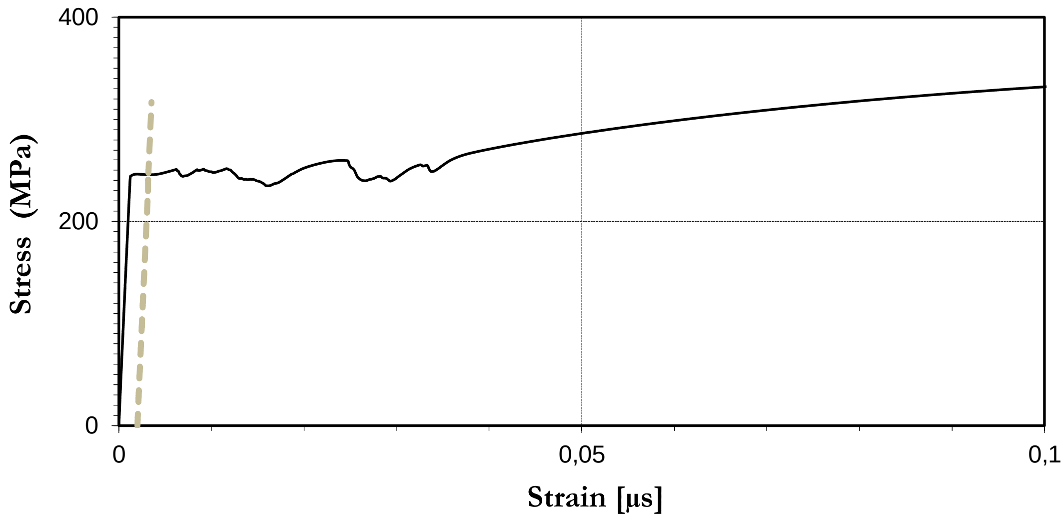

Graphic 2 – 0.2% offset method for yield strength determination

The mean values of the mechanical properties determined and considered for the study are present at table 3.

Table 3 – Material mechanical properties.

Young modulus	206 ± 2 GPa
Poisson's coefficient	0.3*
Yield strength	245 ± 5 MPa
Ultimate strength	359 ± 1 MPa

*Not calculated

The results suggest that ductile construction steel was utilized in the wagon's chassis. Even though its yield strength is relatively low compared to an high strength steel, its ability to receive permanent deformation without fracturing is a significant advantage for this application. It allows plastic deformations to occur locally without compromising the overall structural integrity. This property is handful in the event of a collision (high impact) or overload where sudden rupture can be catastrophic. Ductility allows some of the energy to be absorbed in the form of deformation.

In EN 12663-2 (2010), some materials typically used in underframes are presented. Based on the results obtained experimentally, it seems that the steel used for this wagon was S235 or similar. In the works reviewed in chapter 3, the most commonly used steel was S355, with a yield strength of 355 MPa.

4.2 Finite Element Model of the Wagon "as-is"

For solving a structural mechanic problem, several analytical methods can be used. However, applying these methods is intricate when analyzing structures with complex geometries, loads, and materials. In some cases, a significant degree of simplification is needed, resulting in accuracy loss. The finite element method is a technique for numerically solving differential equations and approximate calculating solutions using computational power. It was initially used to solve complex structural problems in civil and aeronautical engineering but nowadays is utilized in many engineering fields. It is not easy to accurately indicate the date of the invention of this method, but its early development can be attributed to A.Hrennikoff and R. Courant in the early 1940s (Crahmaliuc, 2020). Using this method, time and resources that would otherwise be necessary to evaluate a physical system may not be needed, allowing virtual optimization.

To fully define complex engineering problems, along with differential equations, the system's boundary and load conditions must be defined. For structural analysis, these conditions correspond to the forces and moments applied to the structure, the fixation points, and material properties. The goal of the FEM is to transform the complex differential equations and boundary conditions into simple linear systems of equations.

After defining the problem physically, the geometry in the analysis is split into a finite number of small elements connected at nodes. In simple terms, the elements behave like springs with a given stiffness. If a load is applied at one of his nodes, these will suffer a displacement, determined by the magnitude of the load and the stiffness of the "spring". This step is often called "Discretization" of the model, and the set of elements is called a "mesh".

Element stiffness matrices are then defined for all the elements of the domain. These define how much each node of the element will displace. Then, a global stiffness matrix is defined, where all the individual element stiffness matrices are assembled based on the element connectivity. This global stiffness matrix defines how the structure will respond to external loads.

The present study will consider a static linear elastic model, similar to the experimental test conditions in which wagons are analyzed. In this type of analysis, the FE method's primary goal is to determine the displacement of each node of the model when loads are applied. The calculation of the displacements across the structure is based on equilibrium equations.

The last step of this cycle is the validation of the model. It is often overlooked even though it is crucial to ensure that the results obtained in the FE analysis are accurate. This validation can be, for example, the development of an instrumented scale model to compare results in critical areas.

For the study of the wagon's underframe "as-is", the FE method was implemented in two Softwares: Solidworks 2020 and MSC Apex 2021.1. The goal was to compare the results outputted by each and validate the FE model using different Softwares and models as Akin (2010) suggests for studies where no experimental tests are made.

In the following chapters, the essential steps of the development of the FE models for this study are detailed.

4.2.1 Boundary conditions

Nowadays, software's are advanced to the point where anyone with engineer and computer skills can easily perform a FE analysis and obtain results. The difficulty comes with making a correct physical definition of the problem and the awareness of the specifics for applying this method. A user input error can lead to results opposite to the real ones. According to Akin (2010) and Kurowski (2020) most errors when performing FE analysis occur in the definition of the restrains of the model, followed by the definition of the contacts between components.

For the wagon's underframe, several cases were studied and required different boundary conditions to be assigned. The degrees of freedom that the actual physical interactions restrain must be defined accordingly in the FE model. This must be a well-thought-out assignment since over-constraining the model may create over-stiffened models, leading to the underestimation of displacements and stresses.

When defining a constraint, the user essentially assigns a no-displacement condition to a node or group of nodes in a specified direction. In static analysis, equilibrium must be achieved, and so the FE model must have absolute zero displacements in at least one node; otherwise, the FE solver will abort the analysis (Batchu, 2015). Sometimes, to achieve a no rigid body mode condition, additional constraints must be added in a way that the physics of the system is not influenced.

Constraints used in this study must be applied as close as possible to the conditions of the experimental tests recommended at EN12663-2 (2010). The following constraints were considered:

Constraints:

- Pivot – no displacement condition in the vertical and transversal direction on the wear faces of the pivot (as in free body diagram presented in figure 7).
- Side bearers – no displacement constraint in the vertical direction on the wear faces of the side bearers (as in free body diagram presented in figure 7);
- Buffer reactions* – restrained displacement condition in longitudinal direction applied in buffer mounting surfaces, both aligned with the axis or below it, depending on the load case;
- Draw gear reaction* – restrains longitudinal movement at the draw gear stops.
- Underframe's base* – restrains vertical displacements of the bed of the underframe.
- Lifting areas* – restrains vertical displacements in the points assigned for instances where the wagon needs to be lifted;

*Constrains used for FE model stabilization purposes in different load cases.

For HLC's, the forces are placed on the opposite end where the buffer and draw gear constraints are applied. Symmetry boundary conditions could have been implemented to improve simulation efficiency since the wagon's underframe is symmetrical in two planes. However, for unknown reasons, in MSC Apex, this condition was not working, even when defined manually. So, to have a fair comparison between Softwares, it was decided to create a model with the whole geometry in both with the same boundary conditions and study the horizontal load cases (HLC), vertical load cases (VLC) and lifting load cases (LLC), previously described in chapter 3. The remaining studies were carried out in the software that best performed in these studies. In figure 33 the areas of application of the constraints are illustrated. Some of the constrains defined were also considered in other works developed by Voltr, et al. (2019) and Slavchev, Maznichki, Stoilov, & Purgic (2018).

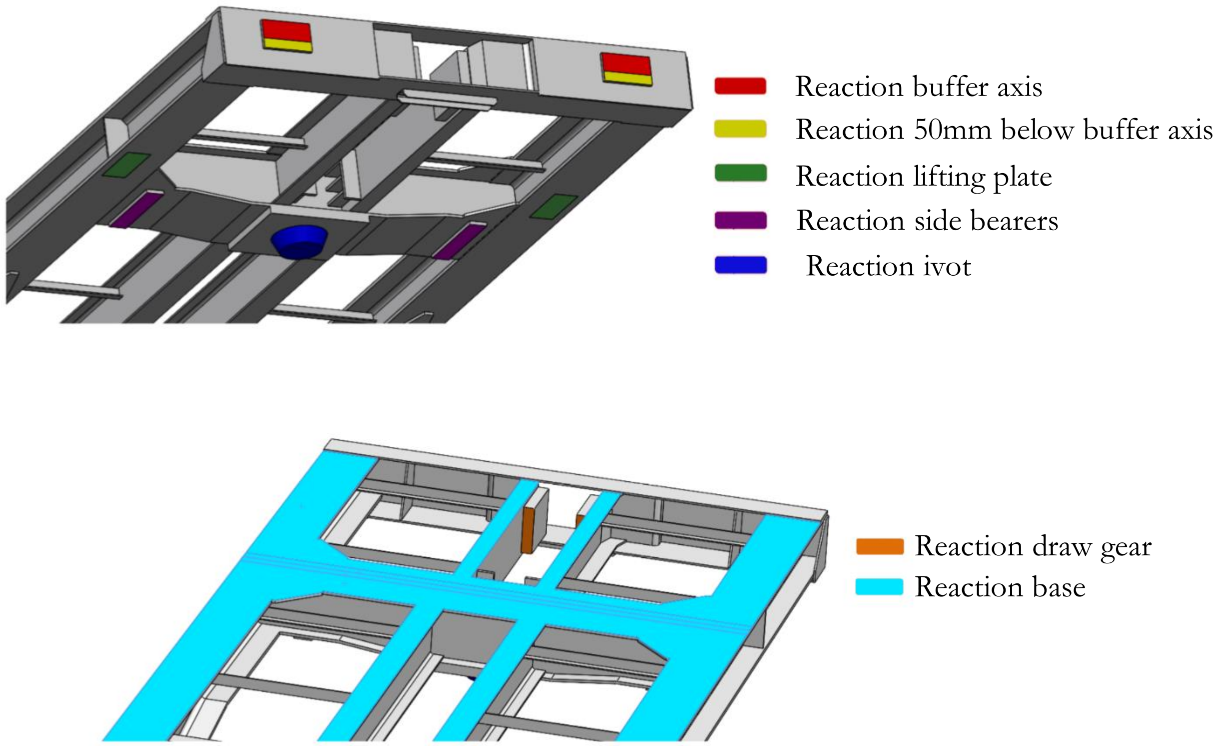

Figure 33 – Constraints location in the geometric model.

Tables 4 to 6 show the boundary conditions for all the load cases.

Table 4 – Horizontal load cases (HLC)

Load cases	Bogie pivot 1 (x,z)	Side bearers 1 (z)	Buffer axis 1 (y)	Buffer axis 2 (y)	Buffer Axis 3 (y)	Buffer 1 & 2 (50mm below) (y)	Draw Gear 1 (y)	Bogie pivot 2 (x,z)	Side bearers 2 (z)	Gravity force 1G	Buffer axis 3 & 4 (2000 kN)	Buffer 3 & 4 (50mm below) (1500 kN)	Buffer axis 1 & 4 (400 kN)	Draw Gear 2 (1500 kN)
HLC1	Y	Y	Y	Y				Y	Y	Y	Y			
HLC2	Y	Y				Y		Y	Y	Y		Y		
HLC3	Y	Y		Y	Y			Y	Y	Y			Y	
HLC4	Y	Y					Y	Y	Y	Y				Y

Table 5 – Vertical load cases (VLC)

Load case	Bogie pivot 1 (x,z)	Side bearers 1 (z)	Buffer axis 1 (y)	Buffer axis 2 (y)	Buffer Axis 3 (y)	Buffer Axis 4 (y)	A-A Bi Supported (330 kN)	B-B Bi Supported (380 kN)	C-C Bi Supported (440 kN)	D-D Bi Supported (555 kN)	A-A Uniform Distribution (320 kN)	B-B Uniform Distribution (350 kN)	C-C Uniform Distribution (360 kN)	D-D Uniform Distribution (440 kN)
VLC1	Y	Y	Y	Y	Y	Y	Y							
VLC2	Y	Y	Y	Y	Y	Y		Y						
VLC3	Y	Y	Y	Y	Y	Y			Y					
VLC4	Y	Y	Y	Y	Y	Y				Y				
VLC5	Y	Y	Y	Y	Y	Y					Y			
VLC6	Y	Y	Y	Y	Y	Y						Y		
VLC7	Y	Y	Y	Y	Y	Y							Y	
VLC8	Y	Y	Y	Y	Y	Y								Y

Table 6 – Lifting load cases (LLC)

Load case	Bogie pivot 1 (x,z)	Side bearers 1 (z)	Buffer axis 1 (y)	Buffer axis 2 (y)	Base (z)	Lifting plate 1,2,3 (z)	Lifting plate 1 & 2 (740 kN)	Lifting plate 1,2,3,4 (800 kN)	Lifting plate 4 (10mm relative displacement)
LLC1	Y	Y	Y	Y	Y		Y		
LLC2					Y			Y	
LLC3						Y			Y

4.2.2 Mesh Generation

The discretization of the model is one of the most critical steps in a FE analysis, and its quality plays a vital role in the study's success. It is one of the components of the FEM that is user-defined and requires empirical knowledge for complex analysis.

For the discretization of a model, different types of elements can be used: Line elements, shell elements or solid elements. The choice of the elements depends on the geometry and the degree of complexity required. Line elements are used to analyze simplified structures composed of low-complexity geometries like, for example, beams, where stress distribution is not relevant. Shell elements are applied to geometries where one dimension, typically thickness, is much smaller than the others, such as stamped sheet metal components. Solid elements are used in complex geometry components when, for example, the previous elements are not applicable.

Solid and shell elements can be first-order elements (draft-quality) or second-order elements (high-quality). For demanding applications where stress is one of the field variables to evaluate, second-order or parabolic elements must always be applied (Solidworks online help, 2020). These consist of elements with mid nodes that more accurately represent the deformation within the element (figure 34). Furthermore, because of their geometry, these form meshes that more accurately describe the domain in study, therefore increasing accuracy. They also increase the number of degrees of freedom and, consequently, computational time.

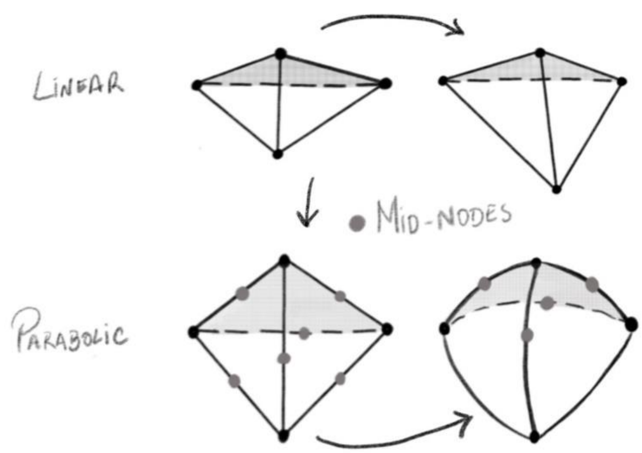

Figure 34 – Linear vs parabolic elements.

As assessed before in chapter 3, several authors have studied geometries similar to those in analysis using solid and shell elements. Some recommend the use of solid elements. In the present work, it was decided to create FE models using both types of elements to investigate this matter further and allow the author to develop skills regarding the creation of 2D elements FE models.

For meshing, general guidelines/empirical notes provided by Ho (2021), (Solidworks online help, 2020) and Thieme (2016) were followed. Some of them were:

- When using solid elements, have at least 3 elements across the thickness to accurately calculate bending stresses;
- Evaluation of mesh quality rating utilizing software tools and plots for mesh distortion, such as "Aspect ratio";
- Mesh convergence analysis.

The more elements a structure is divided into, the more DOF's it has and the better it will capture its mechanical behaviour. However, excessive DOF's lead to more complexity, increasing computation time. One way to develop an efficient model is by performing a mesh convergence or mesh independence study. This study consists of the analysis of the behaviour of the results when the number of elements changes. A mesh convergence is achieved when the variation of the number of degrees of freedom in the model does not significantly impact the results. Mesh independence studies were made for all the models studied to ensure that the results were not dependent on mesh size.

4.2.3 Solid Model

FE models using solid elements were created both in MSC Apex and Solidworks. A new material with the properties assessed in chapter 4.1.2 was created and assigned to the geometry in both Softwares. Then, the fixtures and external loads were assigned to the models, according to the load case in analysis. No point loads/constraints were applied to prevent the occurrence of singularities in the vicinity of boundary conditions and, instead, distributed loads with equivalent effects.

While in Solidworks, distributed loads and boundary conditions can be directly assigned to faces (i.e., to all nodes present in that feature), in MSC Apex, only remote loads/constraints or pressures can be applied to faces. Because of this, to apply the loads similarly in both softwares, the area of the face that the load was to be assigned had to be calculated beforehand to then divide by the load and finally calculate the equivalent pressure. For the constrainment of the model in MSC Apex, remote constraints were utilized. In figure 35, as an example, are presented the boundary conditions and loads assigned to the models for HLC1 in both softwares.

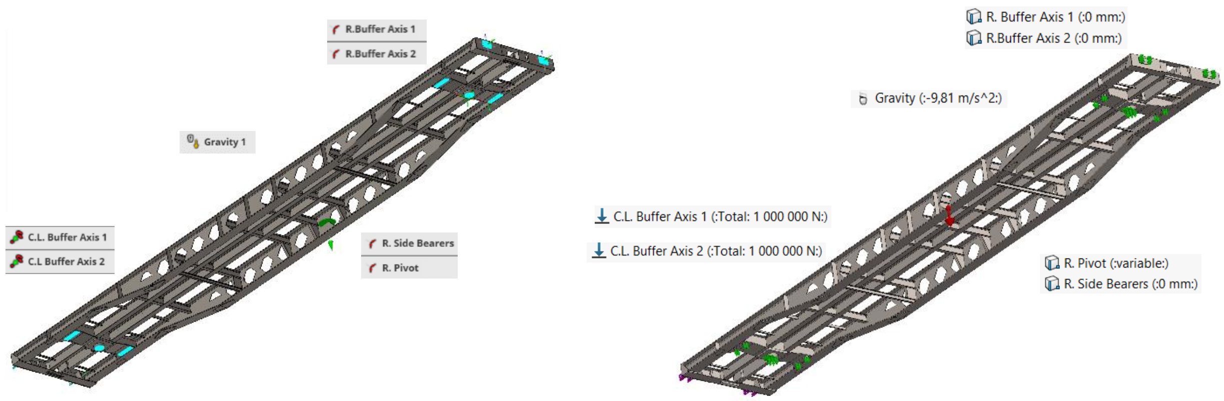

Figure 35 – Boundary conditions assigned to FE models for HLC1. (Left – MSC Apex; right – Solidworks).

In both Softwares, second-order tetrahedral elements were considered to define the models. Each element has ten nodes, and each node has three degrees of freedom (translations).

Softwares have integrated tools to evaluate the quality of the mesh. MSC Apex is more advanced in this regard, considering more factors, as illustrated in figure 36. In Solidworks, the quality can be assessed by plotting aspect ratio or Jacobian and evaluating the mesh details.

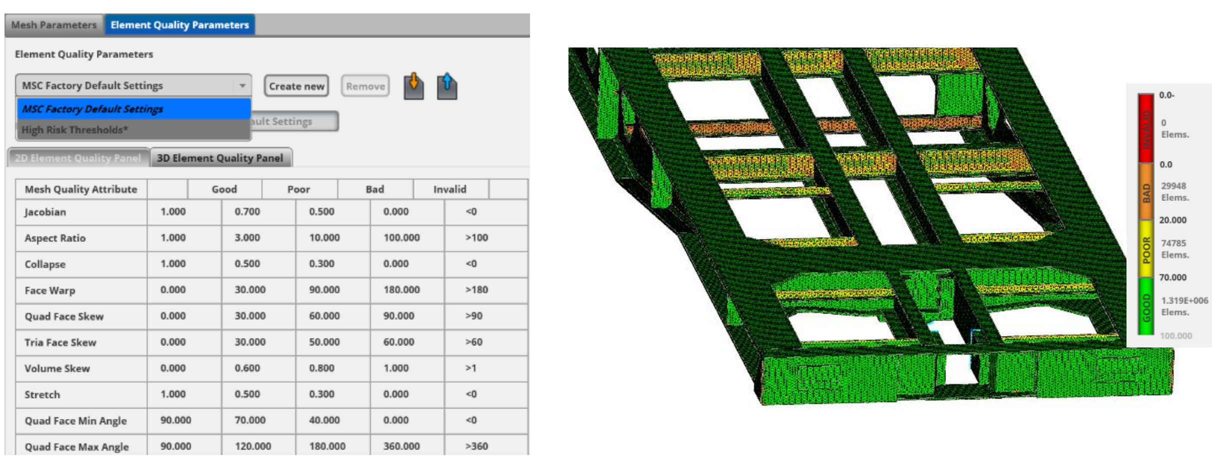

Mesh Quality Attribute		Good	Poor	Bad	Invalid	
Jacobian	1.000	0.700	0.500	0.000	<0	
Aspect Ratio	1.000	3.000	10.000	100.000	>100	
Collapse	1.000	0.500	0.300	0.000	<0	
Face Warp	0.000	30.000	90.000	180.000	>180	
Quad Face Skew	0.000	30.000	60.000	90.000	>90	
Tria Face Skew	0.000	30.000	50.000	60.000	>60	
Volume Skew	0.000	0.600	0.800	1.000	>1	
Stretch	1.000	0.500	0.300	0.000	<0	
Quad Face Min Angle	90.000	70.000	40.000	0.000	<0	
Quad Face Max Angle	90.000	120.000	180.000	360.000	>360	

Figure 36 – Element quality parameters in MSC Apex.

In both, the mesh was evaluated with the tools provided and, according to them, the mesh had good quality. To further confirm that the results are not dependent on the mesh, a convergence analysis was made. Relative errors in between analysis are calculated as follows:

$$[\%]\ Relative\ error = \frac{|Ares - Pres|}{Pres} * 100 \tag{4.1}$$

where Pres is the Previously obtained result and Ares is the actual result.

The convergence of the FE model was studied using HLC1 loads and boundary conditions. The convergence of model was achieved based solely on the displacements in both Softwares. The maximum von-Mises stresses did not converge to a value. Even tough in graphics 3 and 4 it might appear that the errors tend to decrease, a slight variation in the element size resulted in extreme stresses in the vicinities of boundary conditions or in geometric discontinuities. This phenomenon is called a singularity and was expected to happen even with the geometry treatment since it also occurred in several of the reviewed works, such as PĂTRAȘCU (2020) and Voltr, et al. (2019). Figure 37 shows an example of an extreme stress with a typical abrupt distribution of singularities.

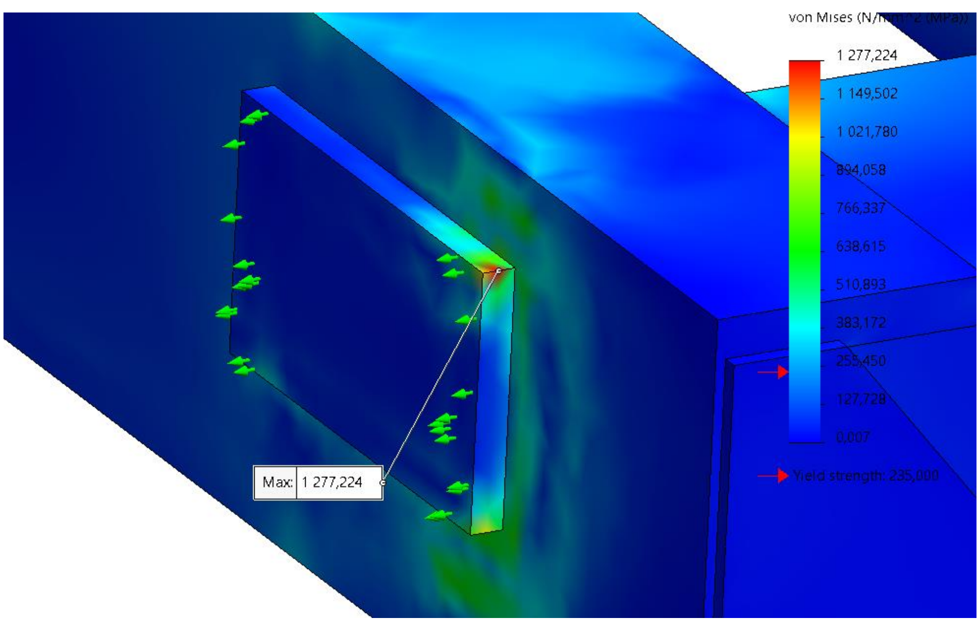

Figure 37 – Singularity in the vicinity of boundary condition.

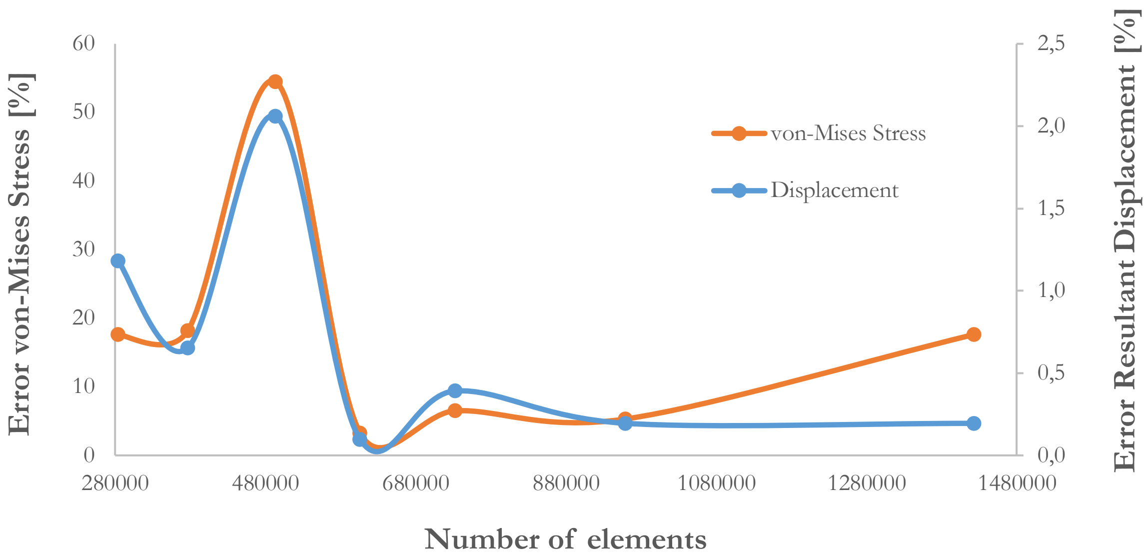

Graphic 3 - Mesh independence study MSC Apex - Solid elements

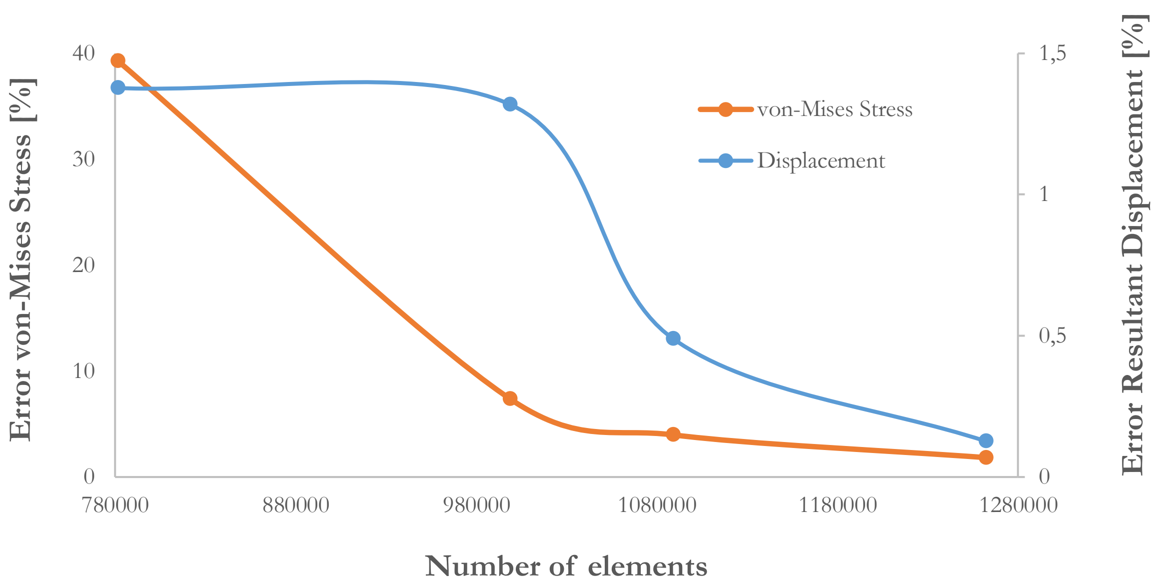

Graphic 4 - Mesh independence study Solidworks - Solid elements

Apurba & Gopal (2020) proved the convergence of the results by measuring the stress in different sections of the wagon, where no geometric discontinuities or boundary conditions exist. Similarly, for the present study the stress was evaluated at the regions identified in figure 38.

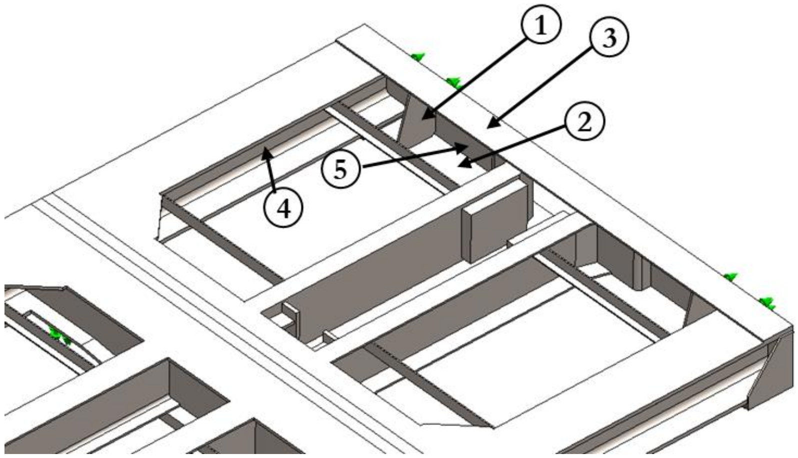

Figure 38 – Points utilized for Stress convergence assessment.

A sensor was assigned to a defined node at each region and the von-Mises stresses were calculated for different mesh sizes. Since none of these points is on a geometric discontinuity, the von-Mises stresses converge to a value seen in graphic 5. Hence, with proper precautions, the FE model is also valid for stress assessment.

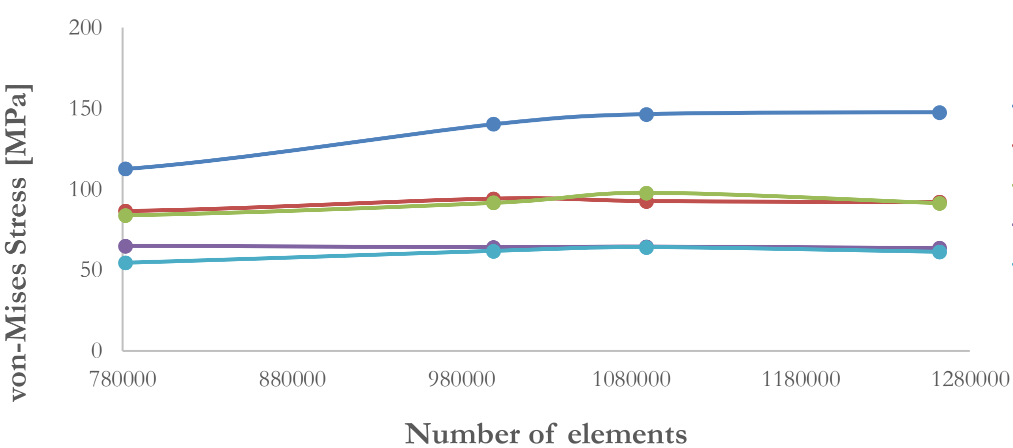

Graphic 5 – Convergence verification in specific locations.

Final mesh element size for the MSC Apex model was 20mm, resulting in a model with 1423450 elements. In Solidworks, the maximum element size 30mm and the minimum 6mm, resulting in a model with 1262253 elements. In figure 39 the meshes of both models are shown.

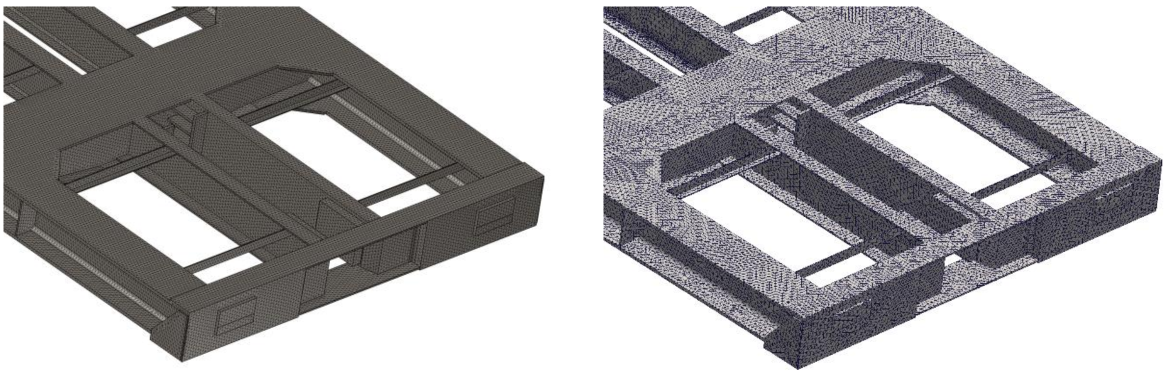

(a) (b)

Figure 39 – Final mesh. (a) MSC Apex; (b) Solidworks.

Results

Predicting when the failure occurs in a complex geometry subjected to multi-axial solicitations can be difficult. In ductile materials, such as the one in analysis, failure is typically determined by the occurrence of plastic deformation. In a uniaxial solicitation, like the one presented in chapter 4.1.2, this transition is identifiable and well defined as the yield point stress. However, when dealing with multi-axial stress, predicting failure is not easy. Several empirical methods have been used for a long time for different materials to analyse the structure's stress state and aid this prediction. Failure criteria considered in all the studies was maximum distortion energy theory (von Mises yield criterion) since it is one of the most popular and reliable failure theories for ductile materials (Aadnøy & Looyeh, 2019).

It was found that the results given by both softwares were similar, both for stresses and displacements. In figure 40 are illustrated, side by side, the von-Mises stress and displacement distributions for HLC1, as an example. In Appendix are shown the results for all the load cases.

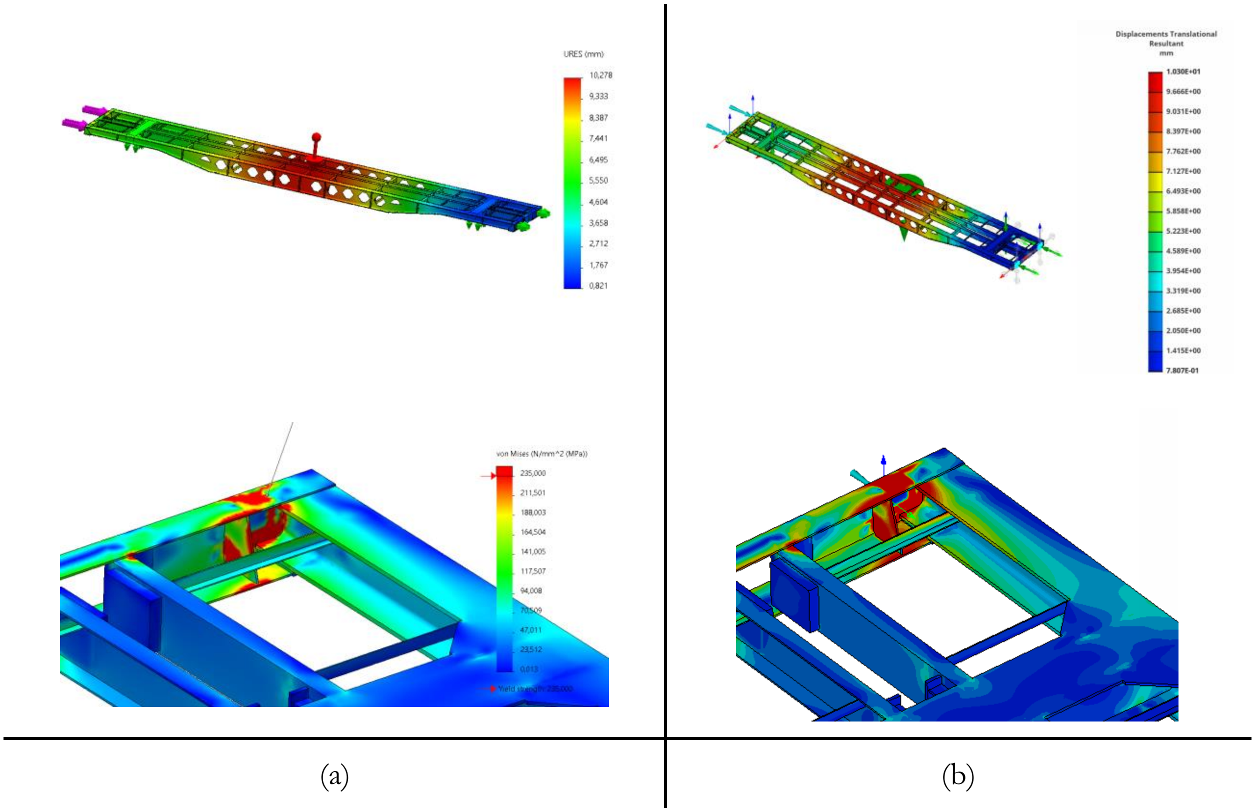

(a) (b)

Figure 40 – Comparison of HLC1 results. (a) Solidworks; (b) MSC Apex.

In table 7 and 8 are presented respectively the deviation between the outcomes of the maximum resultant displacements and the maximum von-Mises Stress for both Softwares. The absolute deviation is calculated, according to:

$$Absolute\ deviation = |Result(Solidworks) - Result(Apex)| \tag{4.2}$$

Table 7 – Comparison of maximum resultant displacements.

	Solidworks [mm]	MSC Apex [mm]	Abs. Deviation [mm]
HLC1	10.28	10.30	0.02
HLC2	7.64	7.65	0.02
HLC3	4.66	4.65	0.01
HLC4	6.62	6.63	0.13
VLC1	21.88	22.01	0.06
VLC2	20.13	20.19	0.05
VLC3	13.21	13.26	0.00
VLC4	0.57	0.57	0.08
VLC5	21.97	22.05	0.14
VLC6	22.15	22.29	0.05
VLC7	19.35	19.40	0.07
VLC8	15.11	15.18	0.00
LLC1	0.54	0.54	0.00
LLC2	0.29	0.29	0.20
LLC3	11.04	11.24	0.06

The maximum resultant displacements occurred in expected areas, and there was a high correlation between the models in both location and magnitude.

On the other hand, relatively high deviations were found when comparing the maximum von-Mises stresses between the FE models. This was expected and reinforces the existence of stress singularities.

Table 8 - Comparison of the maximum von-Mises stresses.

	Solidworks [MPa]	MSC Apex [MPa]	Abs. Deviation [MPa]
HLC1	1300.65	1682.0	382.00
HLC2	1387.35	1804.0	417.00
HLC3	852.80	674.4	178.40
HLC4	436.43	569.5	133.10
VLC1	748.40	828.1	79.70
VLC2	800.92	880.4	79.50
VLC3	735.81	805.4	69.60
VLC4	165.93	128.4	37.53
VLC5	731.87	808.5	76.53
VLC6	780.65	861.8	81.15
VLC7	752.30	826.6	74.30
VLC8	663.49	725.5	62.01
LLC1	186.87	188.4	1.53
LLC2	101.03	102.4	1.37
LLC3	358.30	346.7	11.60

For these studies particularly, MSC Apex software was not as efficient as Solidworks. The simulation time was higher, and the size of the result files was more extensive (approximately 15 times). Also, the visualization of the stresses was clearer in Solidworks since it allowed to perform section views for hidden parts of the model. For the VLCs, for example, this was needed to visualize the region where the maximum von-Mises stresses were located and in MSC Apex this was not possible (Appendix-tables of VLCs).

Because of this, the remaining simulations, i.e., the superposition load cases, and the analysis of the wagon equipped with timber bunks (chapter 5), were only performed using the software Solidworks.

At EN12663-2 (2010), a rigidity criterion is given. "The maximum deflection of the under-frame under the normal design payload shall not exceed 3 ‰ of the wheelbase or of the bogie pivot pitch from the initial position (including the effects of any counter-deflection)". In the wagon in analysis, 3 ‰ of 14860 mm corresponds to an allowable deflection of 44.58 mm. This value wasn't surpassed in any of the load cases studied. The maximum resultant displacement obtained was 29.58mm in SPLC1 and occurred in the middle of the wagon as expected for this load case (figure 41).

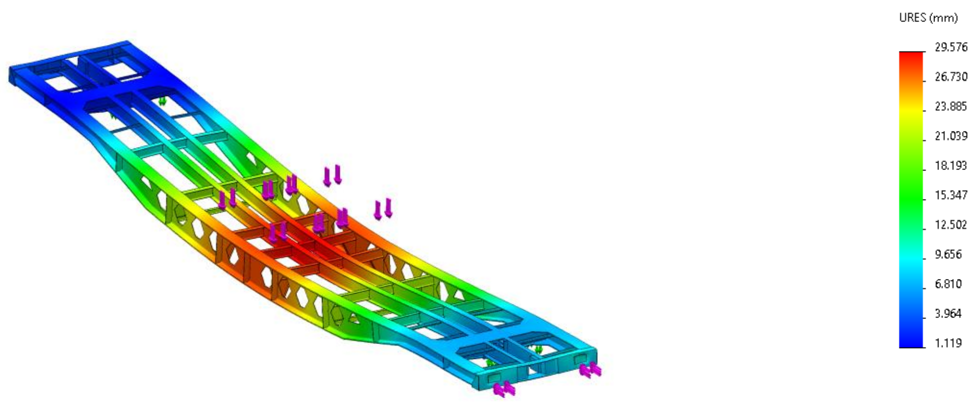

Figure 41 – Resultant displacement distribution for SPLC1.

According to the numerical results obtained, von-Mises stresses surpassed the yield strength in most load cases. However, the stress gradient, the location of the peak stresses, and the fact that the stresses in these areas were inversely proportional to mesh size, suggest that in most cases, these are singularities. Voltr, et al. (2019) had similar occurrences in Innowag project. Because most cases showed signs of this kind of phenomenon, to be more objective, it was decided to evaluate the stress distribution relative to the yield strength rather than to the maximum stress. This allows a clear visualization of the regions where the yield strength is surpassed. In the tables of Appendix are illustrated the stress and displacement gradients for all the cases studied on the wagon “as-is”.

In figure 42 is shown the von-Mises stress distribution for the most critical load case, SPLC1. Areas (A) and (B) of figure 42 (c) highlight the regions where the yield strength is surpassed. Area (B) shows small areas of high stresses, mostly on geometric discontinuities. Area (A), however, presents a vast stain where the yield strength is exceeded, indicating that it is really a problematic region.

After close inspection of several physical wagon's underframes, no visible damage was detected in area (B). In area (A), significant permanent deformation was detected, as illustrated in figure 42 (d).

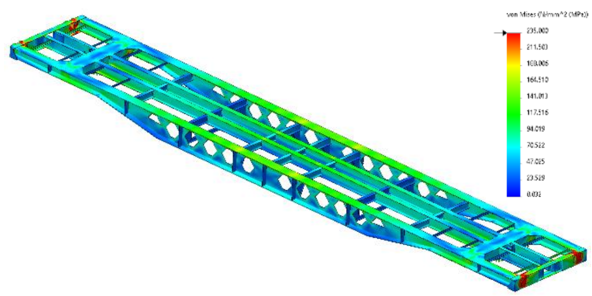

(a)

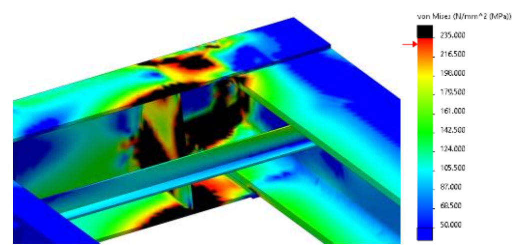

(b)

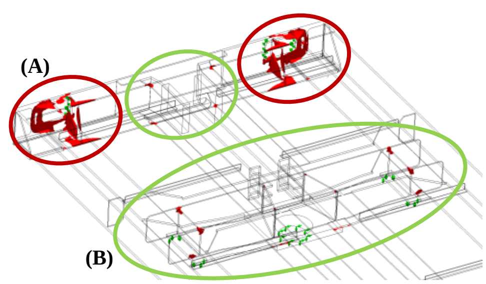

(c)

(d)

Figure 42 – Detailed view of von-Mises stresses for the most critical load case (SPLC1). (a) General stress distribution; (b) Critical area; (c) Critical areas and singularities; (d) Deformation on critical area in real wagon.

Other areas presented high deformation, as illustrated in figure 43. However, this seems to be either due to non-predicted impacts or not considered loading cases in the standard since none of the numerical studies identified these areas as problematic.

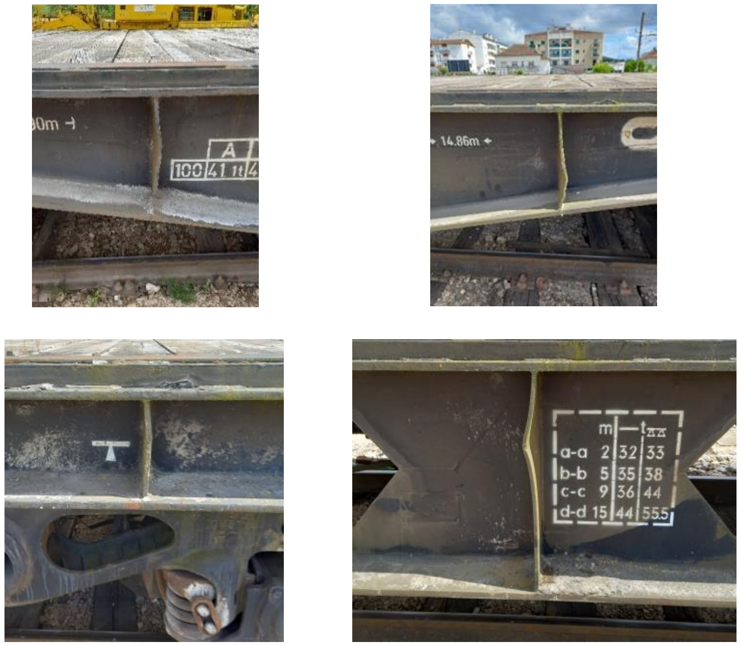

Figure 43 – Deformation regions identified in the chassis.

4.2.4 Shell model

The first step to creating a FE model with shell elements is converting the existing tridimensional geometry into a set of 2D surfaces. This process is usually called "mid-surfacing" preparation. MSC Apex is known for its geometry editing tools, especially the mid-surfacing extracting and editing tools for existing 3D models. In figure 44 is illustrated the Shell geometric model extracted using these tools.

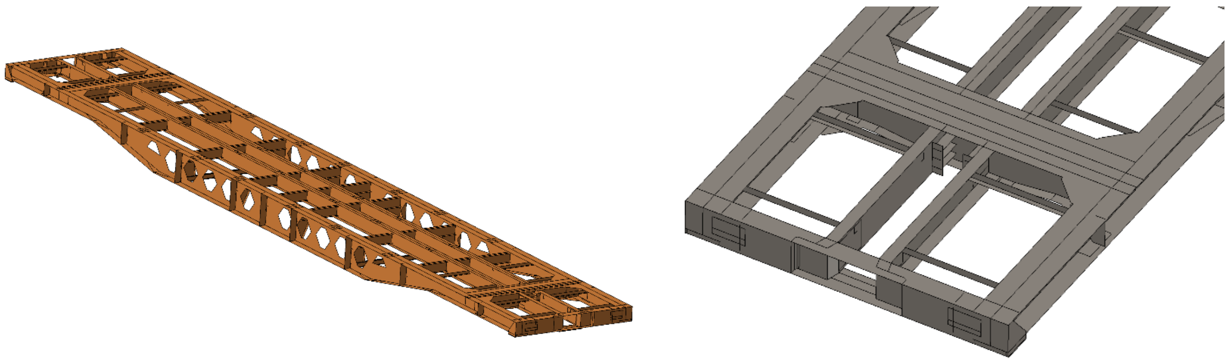

Figure 44 – Shell geometric model.

Then, to fully define the geometry, "virtual" thicknesses have to be assigned to each model section with the appropriate offsets. Although MSC Apex has tools that allow these operations to be carried out semi-automatically, most thicknesses and offsets had to be defined manually in the present model. They required multiple iterations due to user inexperience, making the process of creating the 2D model was quite time-consuming, similarly to what Slavchev, Georgieva, & Stoilov (2014) described. It was verified that this step was performed correctly by visualizing the model with the thicknesses assigned "virtually" (figure 45).

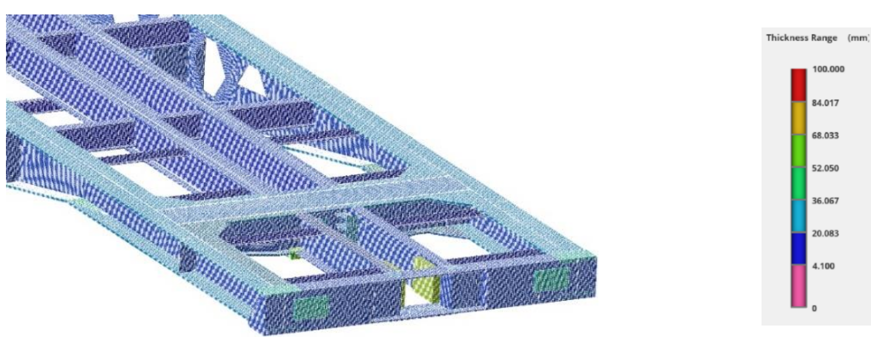

Figure 45 – Thickness assignment to shell model.

The mesh quality can also be assessed for 2D elements similar to what was shown for the solid mesh FE model. A significant difference and advantage of working with MSC apex on a shell model is the possibility of easily manipulating the mesh with the integrated tools, automatically updating the quality of the elements, allowing a fine treatment of the mesh. Even though this is a time-consuming task, in critical areas is fundamental to ensure a good quality mesh. In figure 46 are presented some of the steps involved in the improvement of the mesh.

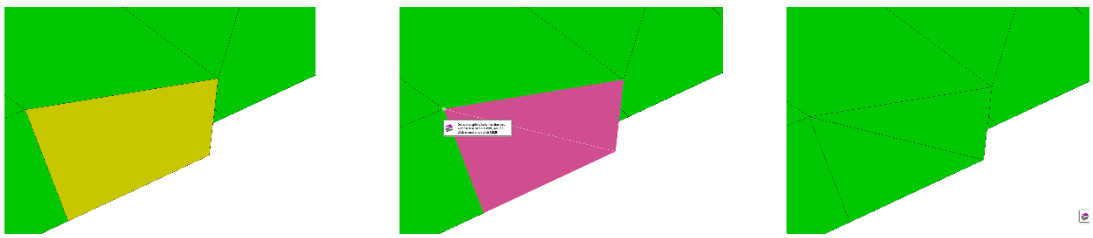

(a) (b) (c)

Figure 46 – Splitting of an element to increase mesh quality. (a) Poor quality element; (b) Element split functionality; (c) Good element quality.

For this model were used linear elements, with 4 nodes, 6 DOF each (3 translations and 3 rotations), with a mapped meshing strategy. Element size was defined as 10 mm. The FE model had in total 838862 elements with high quality.

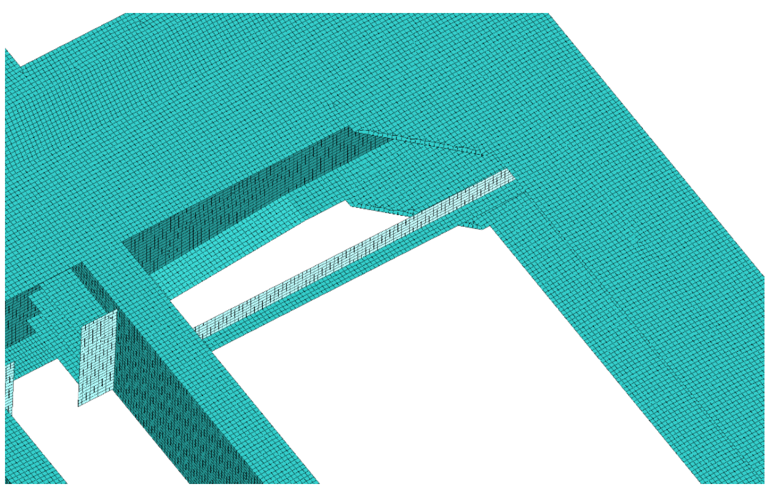

Figure 47 – Shell model mesh.

The boundary conditions assigned to this model are the previously detailed at 4.2.1, with slight modification regards the constraints. In shell elements the rotational degrees of freedom are modeled and therefore the constraints must be adjusted accordingly.

Results

One of the goals of creating this shell model was to assess how it performed compared to FE models using solid elements. Since the deviation between Softwares using solid models was low, and to have a "direct" comparison exclusively between types of meshes, it was decided to compare both models created in MSC Apex.

Generally, the results obtained using the shell element model were similar to those obtained with the solid elements models previously shown. The singularities issues encountered before are also found in this model. In figure 48 and 49 are shown side by side the resultant displacement and von-Mises stress distributions of the shell model and the solid model in MSC Apex, for HLC1 as an example.

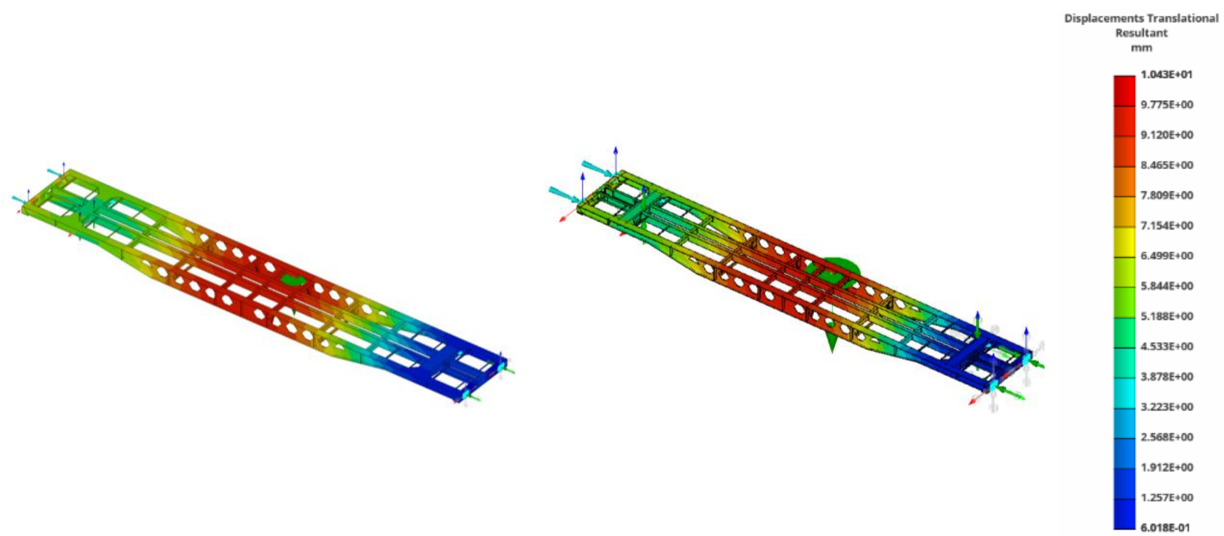

(a) (b)

Figure 48 – Resultant displacements comparison for HLC1. (a) Shell model (Max=10.43 mm); (b) Solid model (Max=10.30 mm)

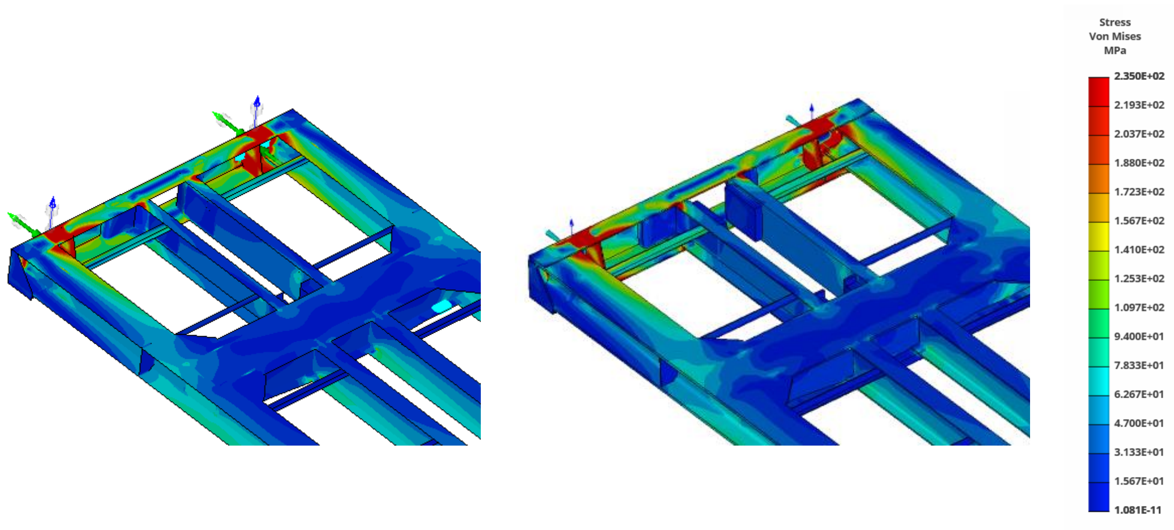

(a) (b)

Figure 49 – von-Mises stress distribution comparison for HLC1. (a) Shell model (Max=2035 MPa); (b) Solid model (Max=1682 MPa)

In tables of Appendix are presented images of the distribution of the von-Mises stresses and maximum resultant displacements for the load cases studied with the shell model.

Table 9 and 10 present the deviation between the 3D and shell models, according to:

$$Absolute\ deviation = |Result(Apex\ Solid) - Result(Apex\ Shell)| \qquad (4.2)$$

Table 9 – Maximum resultant displacement comparison for different type of mesh.

	Solid [mm]	Shell [mm]	Abs. Deviation [mm]
HLC1	10.30	10.43	0.13
HLC2	7.65	7.72	0.07
HLC3	4.65	4.29	0.36
HLC4	6.63	6.24	0.39
VLC1	22.01	21.47	0.54
VLC2	20.19	19.66	0.53
VLC3	13.26	12.85	0.41
VLC4	0.57	0.56	0.01
VLC5	22.05	21.61	0.44
VLC6	22.29	21.81	0.48
VLC7	19.40	18.29	1.11
VLC8	15.18	14.78	0.40
LLC1	0.54	0.66	0.12
LLC2	0.29	0.36	0.07
LLC3	11.24	11.13	0.11

Table 10 - Maximum von-Mises stress comparison for different type of mesh.

	Solid [MPa]	Shell [MPa]	Abs. Deviation [MPa]
HLC1	1682	2035	353.0
HLC2	1804	2117	313.0
HLC3	674.4	815.8	141.4
HLC4	569.5	411.5	158.0
VLC1	828.1	618.9	209.2
VLC2	880.4	663.7	216.7
VLC3	805.4	613.8	191.6
VLC4	128.4	111.9	16.5
VLC5	808.5	606.1	202.4
VLC6	861.8	647.3	214.5
VLC7	826.6	623.1	203.5
VLC8	725.5	550.7	174.8
LLC1	188.4	229.6	41.2
LLC2	102.4	125.4	23.0
LLC3	346.7	441.3	94.6

The errors obtained between the displacement values of the solid element model and the shell model were higher than between solid models, but still relatively low. However, their location was similar.

The von-Mises stress values also varied between the 3D elements and shell models, with higher errors, similar to that of the comparison between solid models. Other observation is that the maximum von-Mises stresses of the shell model are lower in all the vertical load cases and mostly higher on the others.

4.3 Discussion

In most of the load cases, apart from the extreme von-Mises stresses observed in certain locations due to the occurrence of singularities, the stresses across the structure were acceptable and suggest that the underframe can sustain the loads considered in simulation.

The cases of horizontal compression load (HLC1, HLC2, HLC3) are the only ones that raise some concern as they present vast regions with von-Mises stresses higher than the yield stress in the headstock region. After close inspection of several of the real wagons significant deformation was found on that location in most of them, corroborating the results of the simulation.

In HLC4 were also detected higher than desired stresses in the center longitudinal beams. However, it is important to note that the coupling system gives a lot of rigidity to these beams, and, erroneously, it was not considered in the simulation of this load case.

Vertical loads generally showed extreme maximum stresses, arising in geometric discontinuities. When analyzing plots in which the yield stress is the reference, it is visible that the stresses across the structure are mostly reasonable. The peak stress occurred consistently in a region of the main cross beam where exists an interior plate. An abrupt transition of the stress (characteristic of singularities) is identifiable in all the images for the VLC's. Several wagon's were inspected in these regions and no damage was verified. Hence, based on this, it is also safe to say that the wagon sustains the simulated VLC's.

Regards the Softwares utilized for the analysis, based on the results, for this specific study Solidworks was superior with the solid elements model. It allowed for a better visualization of the results, needing less time and space to perform the simulations. Because of this, the following analysis made in the context of this thesis are based on the FE model created in Solidworks.

5 WAGON WITH TIMBER BUNKS IN PLACE

An important part of the work is presented in this chapter, where an assessment of the viability of application of stanchions to this wagon's underframe is made. This study evolved as follows:

- Study of the implementation of the timber bunk system in the chassis with no structural reinforcements and assessment of the displacements and stresses;
- Optimization of the structural strength for this case study based on the results obtained.

As previously mentioned in chapter 2.3 the goal is to fit seven sets of these timber bunks. For this study, a simplified version of the timber bunk system and respective fastening system were created and positioned on top of the wagon's underframe. An assembly compatibility assessment was made, and it was found that the lateral frame stopper had to be removed for one of the timber bunks to fit.

The over-yoke fastening system attaches the timber bunk system to the wagon's underframe using two M20 bolts per side. Holes were incorporated in the geometric model where these bolts pass through the chassis. It was the only geometric modification made to the chassis in the first analysis. Figure 50 shows the geometric model with timber bunks in place.

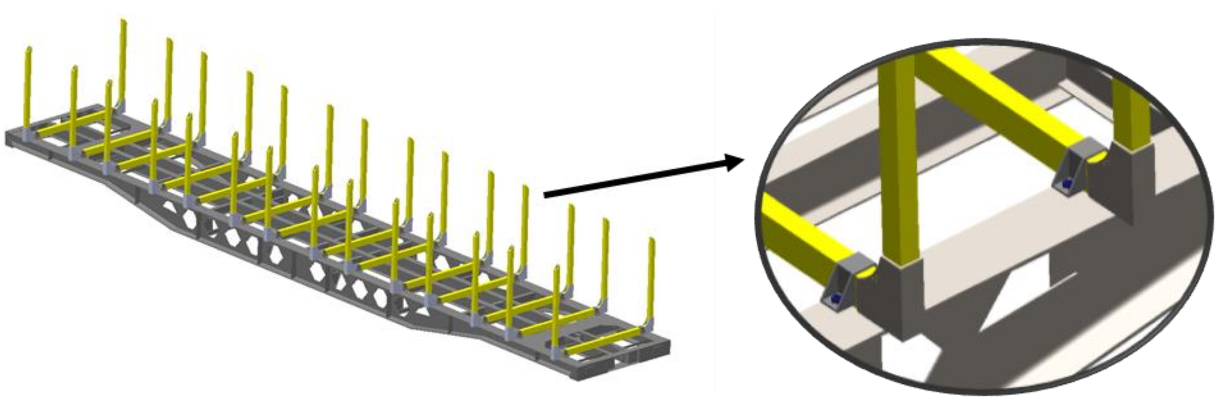

Figure 50 – Wagon with timber bunk system in place

An FE model was created for the case study with the timber bunks in place based on the Solidworks FE model described in chapter 4.

5.1 Boundary and Load conditions

For the stanchions that will be utilized, according to manufacturer, the allowable payload is 8 tons In the FE model, the distribution of the forces caused by the payload must be defined in the stakes and yoke.

Since no experimental tests were conducted, it is difficult to predict the lateral forces, as a lot of uncertainties and variabilities arise such as wood density, log length and girth, method used for volume measurement, among others.

Faced with similar difficulty, Lisowski & Lisowski (2020) conducted experimental tests on stanchions of a timber truck and determined the magnitude of the transversal loads based on the displacements of the free end of the stanchion. In this experiment the logs were positioned on top of two sets of timber bunks rated for 5 tons each. The static payload of the vehicle was 140 kN, meaning that there was a 40% overload. Looking at the results obtained by the Lisowski & Lisowski (2020), and calculating an equivalent torque on the pivot point of the stanchion based on the forces obtained, as given in EN12663-2 (2010), for this payload, the logs exerted and equivalent torque of approximately 16.34 kN·m to the stanchion transversally. These values are much lower than the loads that railway stanchions must be subjected for approval according to EN12663-2 (2010) as shown in chapter 3.1.1. This may be because in this standard the impact loads occurred during loading and unloading procedures are considered, and because most of the times the limit payloads are exceeded, as also addressed Lisowski & Lisowski (2020). The loads considered for this analysis were those described at EN12663-2 (2010), detailed previously in chapter 3.1.1 to be more conservative in the study.

The ExTe timber-bunks with an over-yoke fastening system utilizes M20 bolts and nuts to fix the timber bunk to the structure. It also utilizes, in series with the nut, a rubber puck to mitigate vibrations during transportation (figure 51). For simplification purposes, in the FE model, the rubber puck was not considered, rather a rigid connection.

Figure 51 – Timber bunk fastened with rubber pucks.

Bolts and nuts were located, and the 180 N.m torque specified by the manufacturer was assigned to each. “No-penetration” contact sets were applied to all the faces in contact between components. Friction between components was not considered. Loads stated in section 3.1.1 regards the stanchions were considered in conjunction with a vertical load correspondent to the maximum payload that each timber bunk system is rated for (8 ton. According to manufacturer) and gravity force.

5.2 Model simplification and mesh

This analysis is more complex than previous ones since it requires modelling the contact interaction between the components and incorporating virtual bolts.

Some attempts to simplify the model were made. Firstly, a portion of the wagon was split, and simplification tests were made, comparing with the same splitted portion without simplifications.

As previously mentioned, the stanchion system intended to be applied is certified, so it is not an object of analysis. Ideally, this system would be removed from the analysis to decrease model complexity. One of the first simplification approaches was to assess the bolt reaction forces and only analyze the chassis with those forces applied.

Using only the reaction forces of the bolts resulted in wrong displacement results. The yoke of the timber bunk adds significant rigidity and bending resistance to the outer profile flanges due to the increased moment of inertia, minimizing its displacement and stresses. Because of this effect, the yoke geometric model is mandatory to keep.

Then, the next attempt to simplify the FE model was to maintain only the yoke, replacing the stanchions with remote loads. In figure 52 is illustrated how the different simplified models compare to each other.

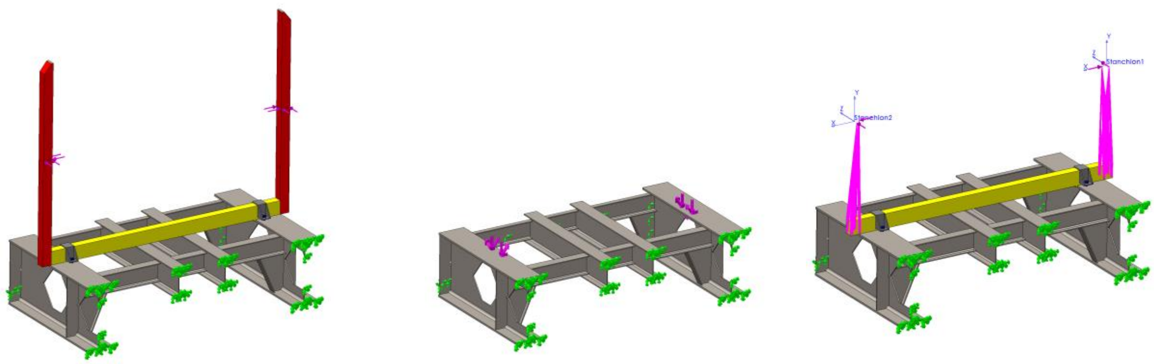

(a) (b) (c)

Figure 52 – (a) Non-simplified model; (b) Reactions only; (c) Yoke only with remote loads.

Table 11 – Comparison of results between simplified models.

	Full model	Bolt reactions only	Yoke only
Displacement [mm]	2.09	4.36	2.09
von-Mises Stress [MPa]	875.08	870.20	877.38

This way, the results are very similar to the model without simplification, so a full model was created with these simplifications. The simulations were carried out using a simplified model of the timber bunk presented in figure 52 (c) , maintaining only the yoke and the over-yoke fastening system.

In this sectioned model, the influence of the number of elements across the thickness of the flanges was also studied. The results using the same mesh as the one used in chapter 4 were compared with a refined mesh that had three elements across the thickness. In figure 53 are illustrated the differences.

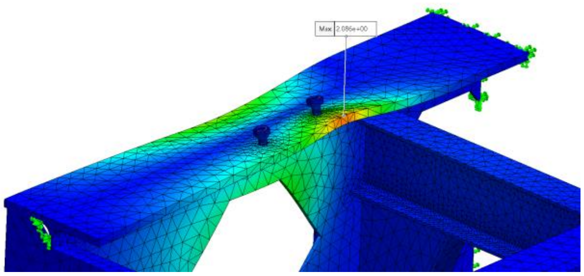

Max displacement = 2.086 mm

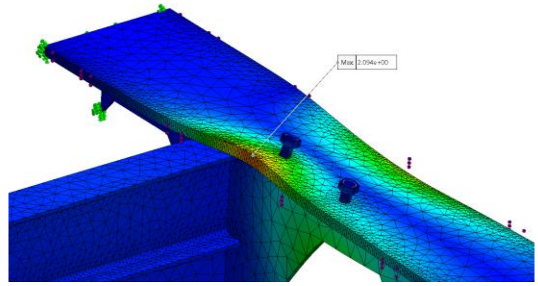

Max. Displacement = 2.094 mm

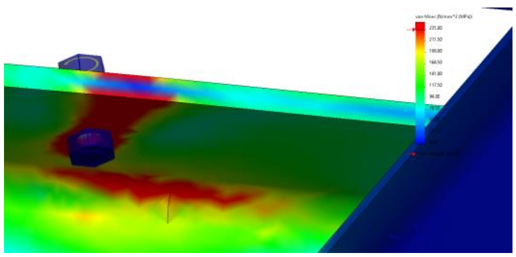

Poor perception of stress distribution at flange level

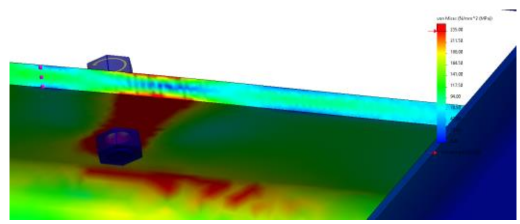

Smooth stress gradient

(a) (b)

Figure 53 – Comparison of results between original and refined mesh. (a) Mesh with 1 element across thickness; (b)Mesh refined at flange level with 3 elements across the thickness.

With 3 elements across the thickness the gradients are smoother allowing the assessment of the stress distribution across the flange's thickness. However, the differences in the absolute results for the displacement is negligible. It was decided to utilize the original mesh to not increase FE model complexity and interpret the obtained results considering the results of this analysis.

For the full FE model, symmetry constraints for the longitudinal and transversal axis of the vehicle were defined, and the restrictions were applied as before in chapter 4 for the pivot and side bearers.

For the chassis, since the geometric modifications were minimal (bolt holes), the same mesh size as in chapter 4 was utilized. For the remaining components, mesh refinements were applied until there were at least three elements across its thickness. This model had in total 543253 elements, a smaller number than the model utilized to analyse the wagon "as-is", even though it has more components. This is largely because for this case symmetry conditions were used.

In figure 54 is represented the simplified model with the boundary conditions in place. For this analysis "Large-problem direct sparse" solver had to be used due to the contact modelling. Otherwise, the simulation would not run due to solver errors.

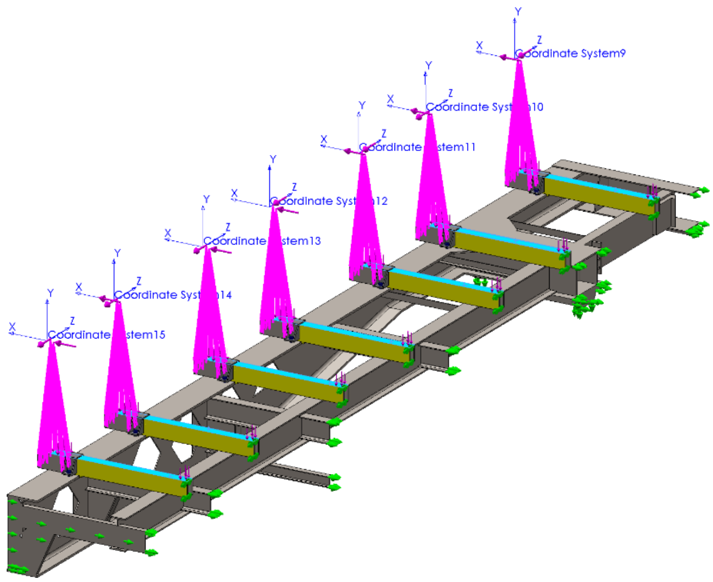

Figure 54 – FE model for wagon “as-is” with stanchions.

5.3 Results

The timber bunk system, as previously referred, is certified, and so it is not the object of study. Therefore, only the wagon's underframe is plotted and analysed.

The maximum resultant displacement for this case study was 23.96 mm and occurred in the middle of the wagon as expected (figure 55). The transversal and longitudinal components have a low contribution to the resulting displacement, which is dominant in the vertical component. It is lower than that observed for SPLC1, so the rigidity criteria given in EN12663-2 (2010), enunciated in chapter 4 is also verified for this case study (allowable deflection of 44.58mm).

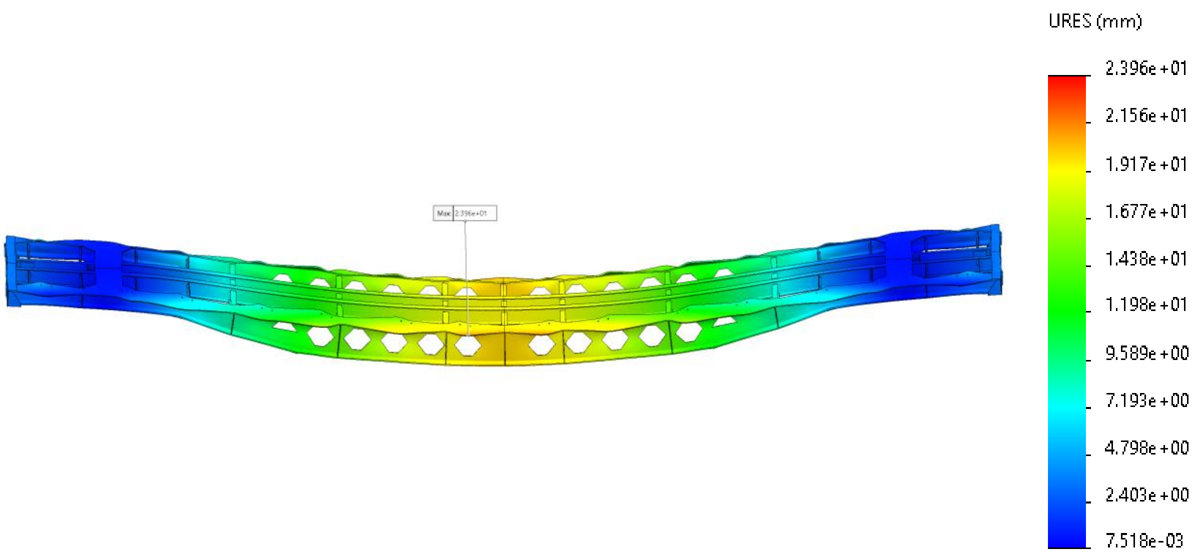

Figure 55 - Maximum Resultant Displacement.

Because virtual connectors were used, extremely high stresses in their vicinity were found. These are fictional and should be ignored, according to Soliworks technical paper (2021). Therefore, because the maximum von-Mises stress was located in that area, it is not a valid indicator. It was decided to analyse the stress distribution relative to the yield strength, as done in chapter 4, to be more objective. This analysis found that in the most exterior beam, directly in line with each stanchion, areas with high stresses were visible at flange level. This phenomenon is highlighted when the results are plotted with an elevated deformation scale (20 x), as illustrated in figure 56. Stress singularities exist once again in the vicinity of some boundary conditions and geometric discontinuities, but, as previously, these were not considered critical spots.

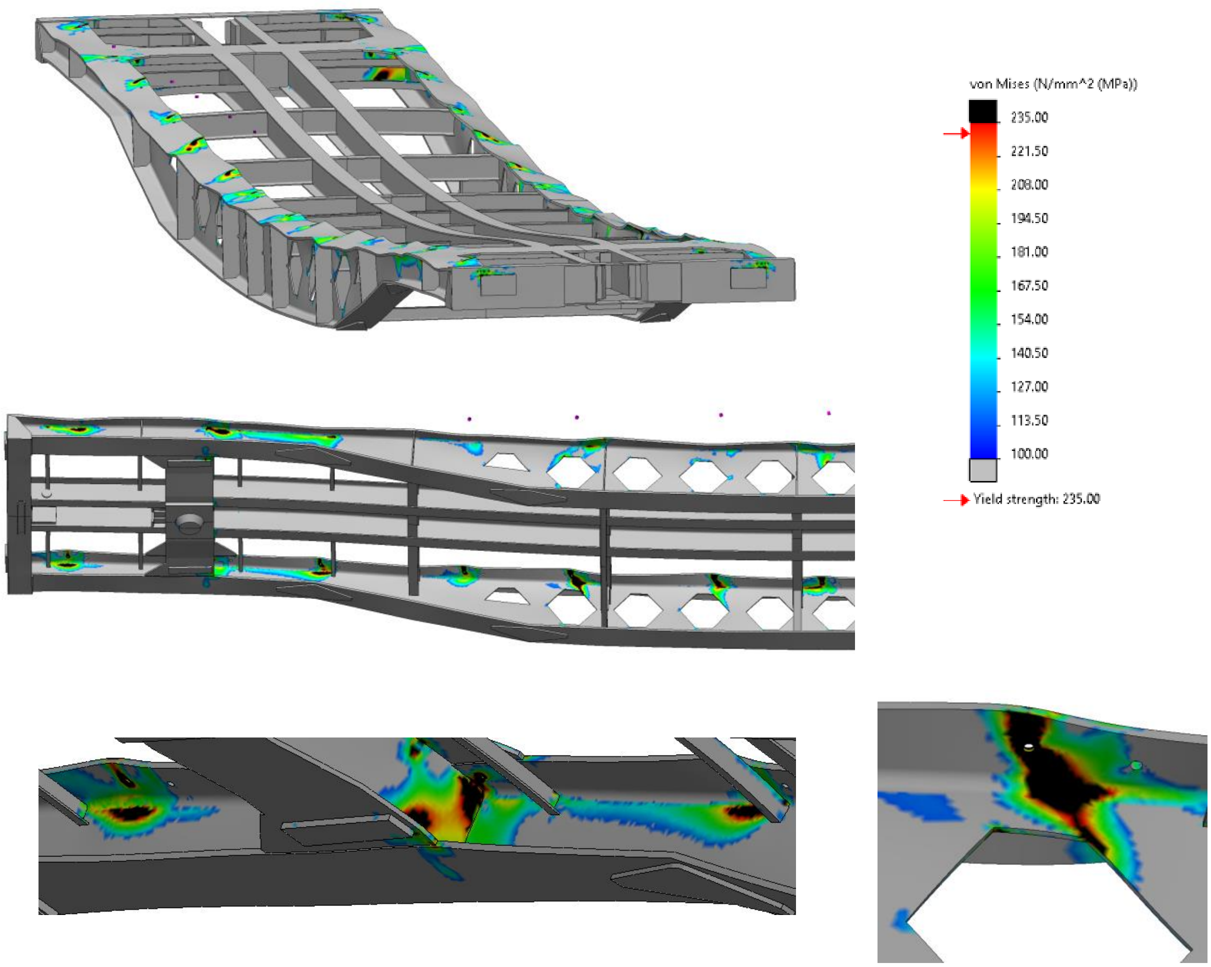

Figure 56 – Von-Mises stress distribution for wagon "as-is" with timber bunk system in place (timber bunks hidden).

5.3.1 Discussion

For the considered loads, the results show that the direct implementation of a timber bunk system in the wagon "as-is", would result in permanent deformations in the exterior beam flanges. In figure 56 the vast black stains observed in these areas correspond to stresses higher than the yield strength and are therefore problematic regions that must be reinforced to sustain the considered loads.

5.4 Optimized version with structural improvements

Based on the results obtained, the addition of structural reinforcements was studied to enable a safe implementation of the timber bunk system. The goal is to strategically reinforce the wagon's underframe with an easy fabrication geometry, maintaining the added mass as low as possible. Materials with better mechanical properties could have been chosen for better mass design optimization, but it was decided to consider the same base material for convenience purposes.

These geometric modifications were made directly on the FE model utilized in the previous analysis, shown in figure 54 (section 5.2). The same mesh parameters were considered.

The observation of the exaggerated deformation was essential as a starting point. The first iteration consisted in the addition of 10 mm steel plate reinforcements transversally, in both sides of the beam, where the relative deformation was high to mitigate the bending effect observed on the beam's flange.

As shown in figure 57, the addition of these steel plates results in lower displacements and reduces substantially the overall stain of von-Mises stresses higher than the yield strength observed before. However, between these plates, there is still a region where the yield strength is surpassed and, therefore, the reinforcements can be optimized.

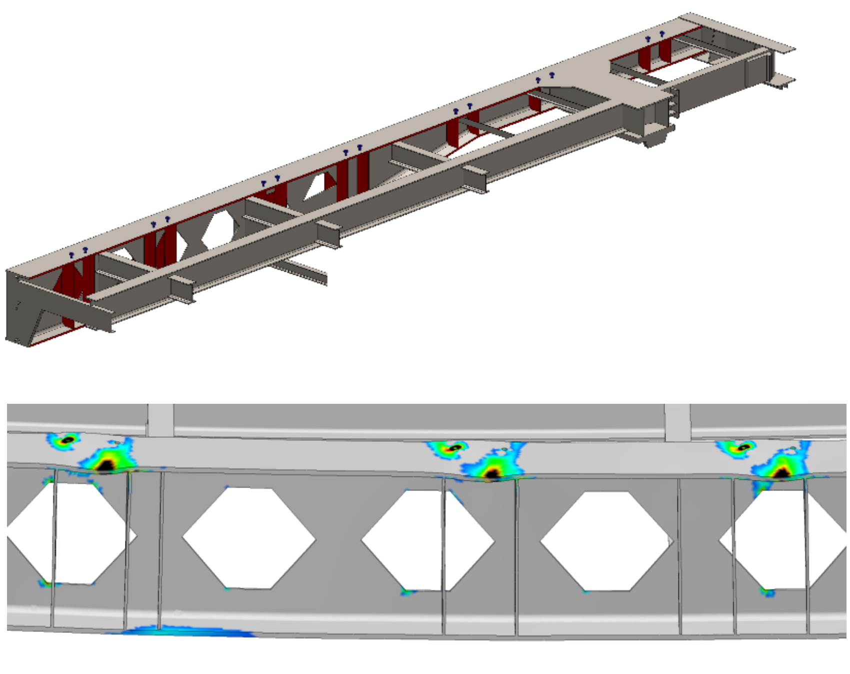

Figure 57 – First structural reinforcements iteration.

The optimization phase took several iterations, where several structural reinforcement designs were simulated, and its performance assessed. In figure 58 are presented some of the design iterations studied.

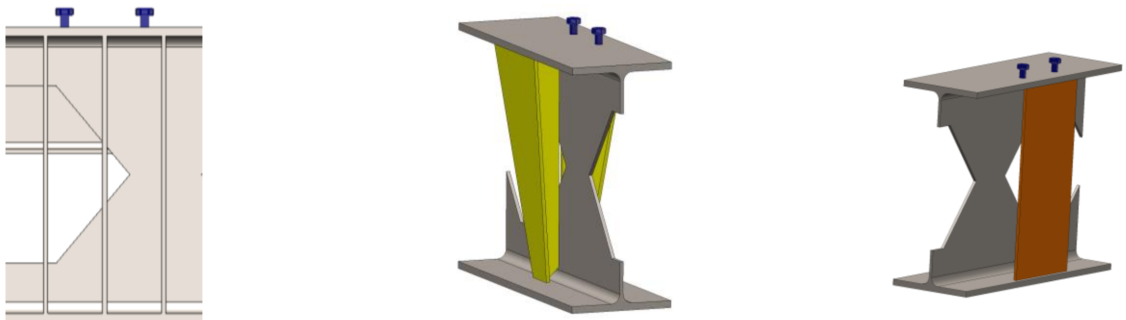

Figure 58 – Design iterations of the structural reinforcements.

It was found that the steel plates worked better if placed longitudinally rather than transversally, and that there's no need to place them in both sides of the exterior beam. The design presented in figure 59 was the best performing one, eliminating the high stresses observed below the stanchions. It consists in 10mm steel plates made from the material as the chassis, placed only on the interior of the beam for the most part, that are tensioned when the timber bunk is loaded. In total these add approximately 360 kg to the own weight of the underframe (1.4 % of the wagon's total mass).

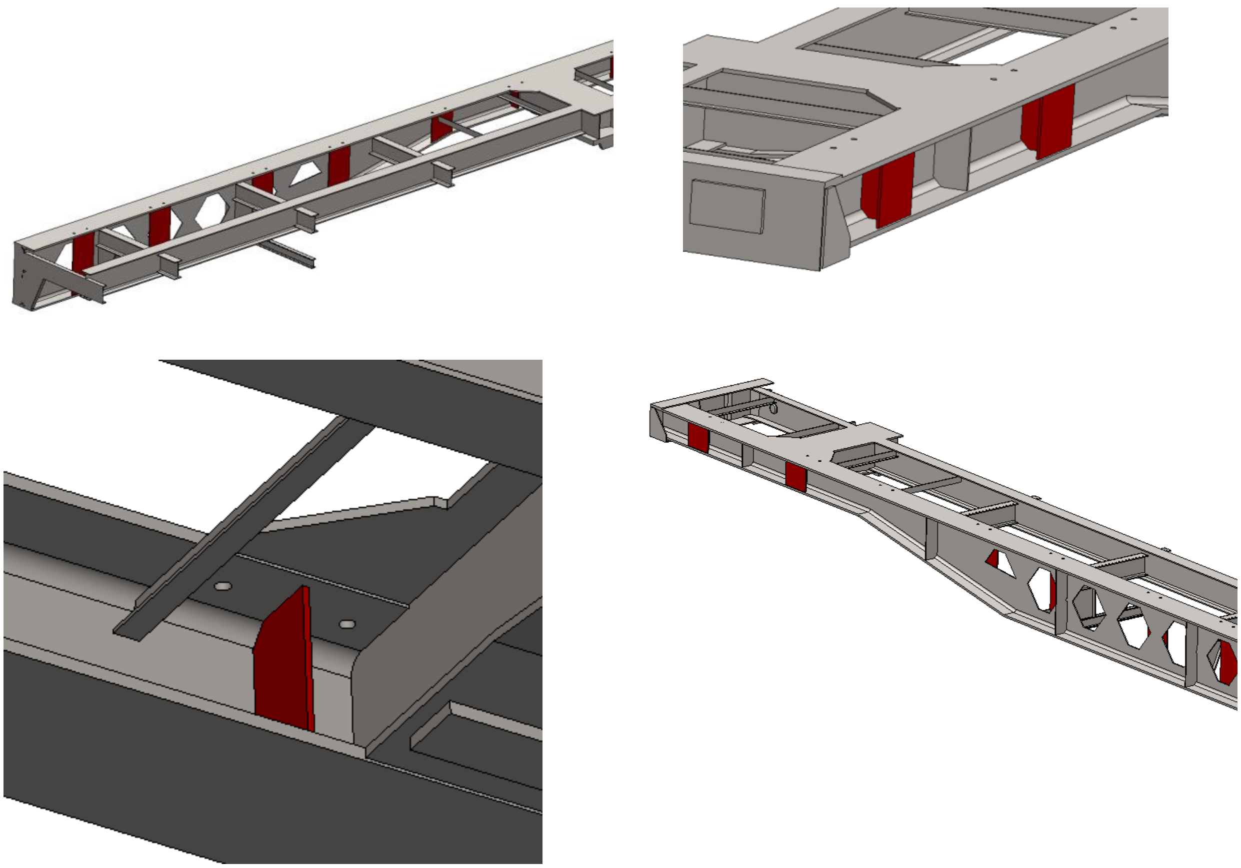

Figure 59 –Reinforcement plates location.

In figure 60 is presented the von-Mises stress distribution for the wagon with the reinforcements implemented.

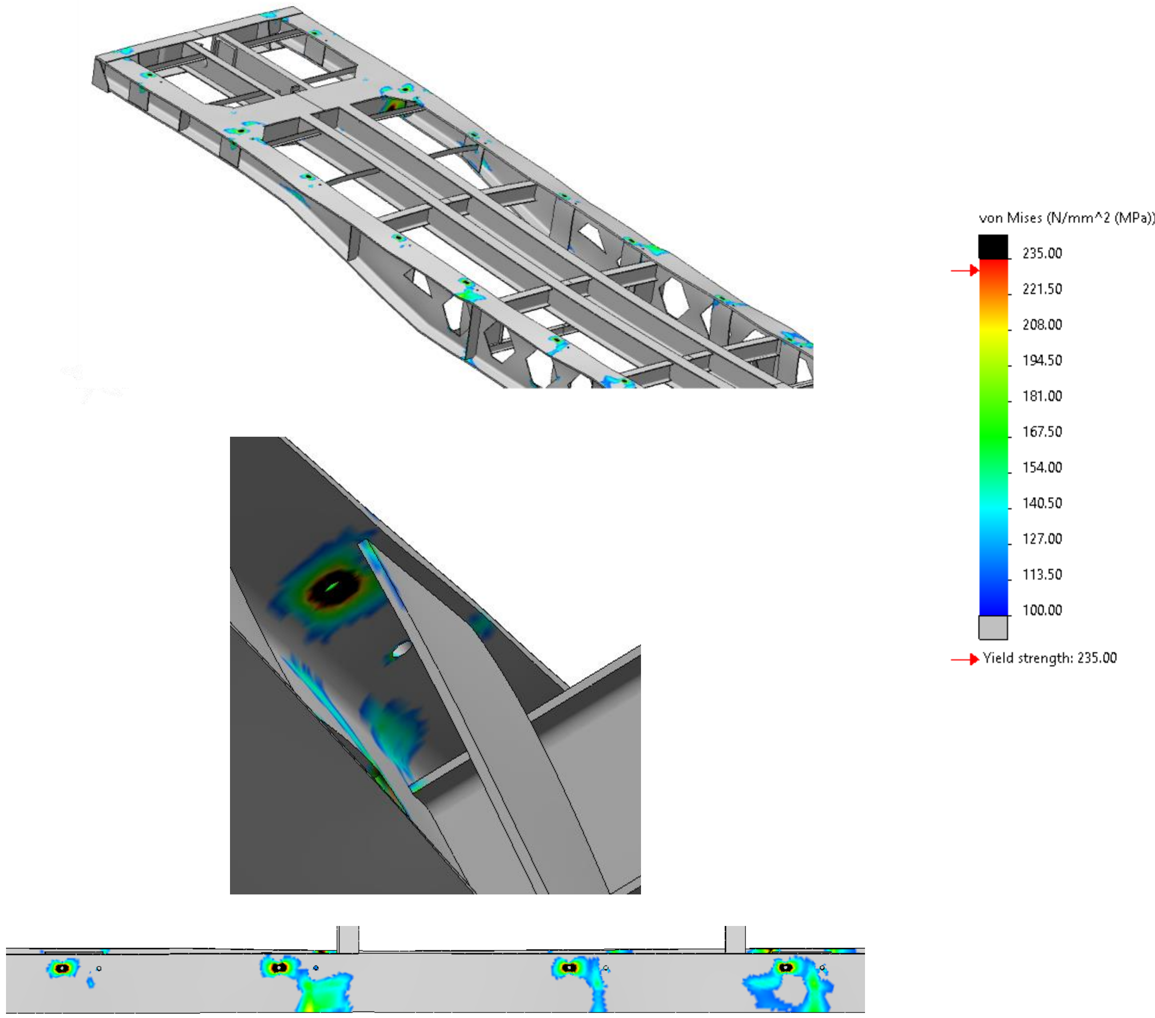

Figure 60 – Von-Mises Stress distribution after reinforcements.

According to the results, the von-Mises stresses are mostly below the material's yield strength. Similarly to the results obtained previously, in the vicinity of the bolts and some geometric discontinuities are observed high stresses that can safely be deemed as fictitious and ignored.

5.4.1 Fatigue verification

Cyclic loads can lead to failure even if their range is below the material's yield strength. In the case in study, loading and unloading procedures may provoke premature failure. After verification of static strength, fatigue was also object of a simplified analysis.

According to table 28 presented at EN 12663-2 (2010), evolved designs don't necessarily have to pass fatigue and/or service tests if other methods show sufficient fatigue strength. In chapter 6.2.3 of the standard are provided guidelines to experimentally prove the fatigue strength. These are complex and difficult to adapt for numerical methods solving. Still, taking this into consideration, it was decided to make a simplified fatigue analysis in Solidworks.

Fatigue failure occurs due to the formation and propagation of cracks in the material. It is a three-stage process: crack formation, crack growth and fracture. Materials have different fatigue strengths, defined by its characteristic S-N curve. These curves are obtained experimentally, using specialized equipment that mimic cyclic loadings in test specimens.

Numerical model

For the fatigue simulation the finite element is also a valid method. A study considering constant amplitude was created in Solidworks, based on the static study previously described in chapter 5.2.

Because the S-N curve for the wagon's underframe steel was not determined experimentally, one was approximated based on the material's Young Modulus with ASME method, embed in Solidworks software.

For this case, the loading condition that best represents the loading and unloading procedures that may cause fatigue is a zero-based load (R=0), where the applied load is varied between zero and the value of the load.

Considering that the mean distance traveled in each trip by a freight train is 280 km (INE 2020), 35000 cycles correspond to roughly ten million kilometers of life. In the analysis 35000 cycles were simulated.

According to Solidworks Manual (2019), the Gerber method is the most suitable for ductile materials and so it was considered in this study.

Results

Fatigue simulations are based on the static results shown previously. As expected, in regions where the stresses were fictitiously exceeded, fatigue life is also not correct. Because of this the "Damage percentage" plot ranges were modified for better visualization and evaluation of the results.

In figure 61 it can be observed that most of these high damage regions correspond to areas where the stress values were high and not real. Besides those, high damage percentage is also visible in some areas that might require geometric changes or reinforcements.

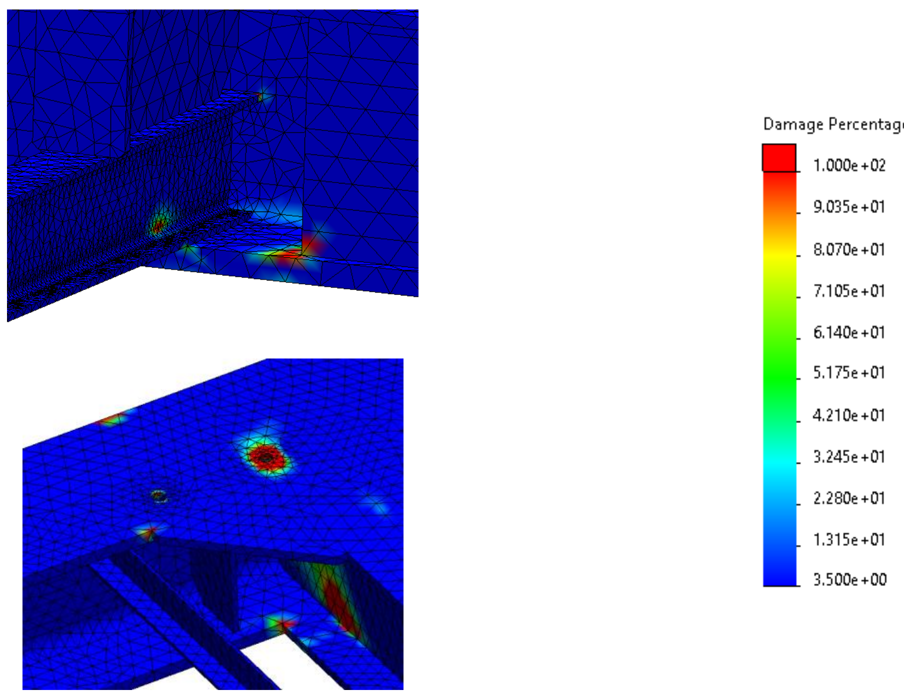

Figure 61 – Damage percentage plot.

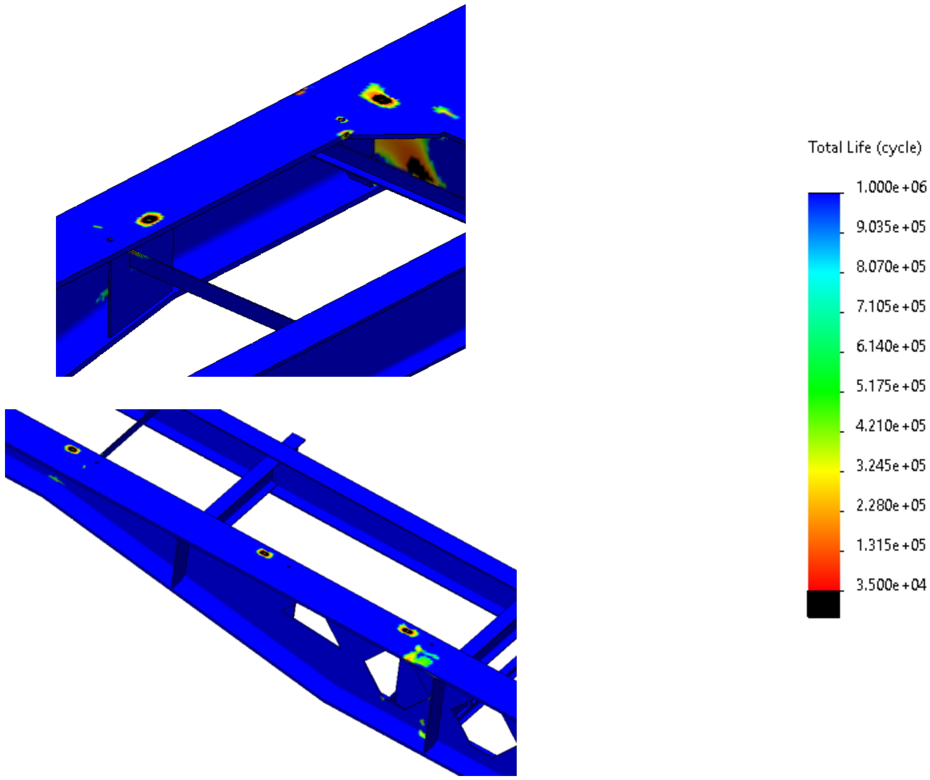

Figure 62 - Total Life (cycles)

Discussion

The life for most of the underframe is above one million cycles. Regions below 35000 cycles are identified in figure 51 as a black stain. These are mostly coincident with the areas where the stresses were high, like what was verified before for the damage.

This simulation is very superficial and has a lot of uncertainties factored. A proper characterization of the material's fatigue strength is required for correct fatigue life assessment.

6 CONCLUSIONS

This thesis incorporates an ongoing project started by Medway M&R where the viability of implementing a timber bunk system to the flat wagon Rlps 81 94 383 2 001/065, intended to transport wooden logs, is assessed.

A review of applicable standards and guidelines was made, as well as a review of the EC requirements for certification of modified railway vehicles. The wagon's underframe geometry was reverse engineered, and a CAD model was created in Solidworks. The properties of the chassis's steel were assessed by straining until failure test pieces in a universal testing machine.

The structural analysis went through three distinct main phases: Structural analysis of the conventional flat wagon for benchmarking purposes; Study of the implementation of the timber bunk system in the wagon "as-is"; Creation and analysis of an optimized wagon with structural reinforcements. For this analysis, different types of FE models were created and tested, achieving a model that can be used to quickly test the addition of structural elements to the wagon in study in a virtual fascia.

For the optimized version a fatigue verification was made, and regions of concern determined. Due to the diverse uncertainties during the definition of this analysis, the results must be viewed as a simplified, with debatable veracity.

For the case study can be concluded that installing seven sets of the timber-bunk systems ExTe SR8+ with the structural reinforcements suggested in this thesis is viable. With this configuration, the maximum gross weight for this wagon is approximately 81 tons, still relatively far from the ideal 90 tons to take full advantage of the infrastructure's bearing load. However, with gauge G1 and fixed wagon length would be difficult to achieve this kind of payloads given the relatively low specific mass of wood and high volumetric necessities.

6.1 Future developments

Regards future works, the following are suggested to further gather information and optimize the wagon for wood logs transportation.

- Instrumentation of the wagon's underframe based on the points of interest established in the numerical analysis to further validate the FE model created;
- Experimental measurement, in real working conditions, of the transversal load exerted by the wood logs on the stanchions. With this information optimize the mass design of the proposed reinforcements.
- Characterization of the wagon's underframe S-N curves for accurate fatigue life assessment;
- Realization of CFD simulations to assess the aerodynamic performance of the wagon's end-walls and eventual optimization to minimize drag;

BIBLIOGRAPHY

Aadnøy, B. S., & Looyeh, R. (2019). *Petroleum Rock Mechanics (Second Edition).* Gulf Professional Publishing.

Ahmad, N., Cole, C., Spiryagin, M., Spiryagin, Q., & Sun, Q. (2015). Integrated Methodology for Investigation of Wagon Design Concepts by Simulations. *Proceedings of the ASME 2014 International Design Engineering Technical Conferences and Computers and Information in Engineering Conference. Volume 6: 10th International Conference on Multibody Systems, Nonlinear Dynamics, and Control.* Buffalo, New York, USA.

Akin, J. E. (2010). *Finite Element Analysis Concepts.* USA: World Scientific Publishing Co. Pte. Ltd.

Apurba, D., & Gopal, A. (2020). Compression, tension & lifting stability on a meter gauge flat Wagon: an experimental approach. *Australian Journal of Mechanical Engineering*.

Batchu, S. (2015, 03 19). *Stress book*. Retrieved from Stress Ebook LLC.: https://www.stressebook.com/rigid-body-mode/

Batista, E., Hedberg, J., Christmann, R., Beutel, R., Alza, M., & Schraud, J. (2017). *D5.1 State of the art of numerical and system validations and gap analysis description.*

Castagnetti, F., Toubol, A., & Rizzi, G. (2016). C4R project increases rail capacity without laying down new tracks. *Transportation Research Procedia 14*, 672-678.

Crahmaliuc, R. (2020, 11 10). 75 Years of the Finite Element Method (FEM).

EN10002-1. (2001). Metallic materials - Tensile testing - Part 1: Method of test at ambient temperature. *European Standard*.

EN12663-2. (2010). Railway applications - Structural requirements of railway vehicle bodies - Part 2 Freight wagons. *European Standard*.

EN15273-1. (2013). Railway applications - Gauges - Part 1 General - Common rules for infrastructure and rolling stock. *European standard*.

EN15273-2. (2013). Railway applications - Gauges - Part 2 Rolling stock gauge. *European Standard*.

Freight Wagons TSI. (2013). *Technical specification for interoperability relating to the subsystem 'rolling stock'.* Official Journal of the European Union.

Ho, B. (2021, 04 15). *5 Tips on How to Create a High-Quality Mesh*. Retrieved from Simscale: https://www.simscale.com/blog/2018/03/tips-high-quality-mesh/

Juris, M., Nguyen-Tajan, M.-L., Garner, P., Jakobi, D., Terron, E., & Solabarrieta, I. (2019). *Virtual Certification: State of the art, gap analysis and barriers identification, beneficts for the railway industry.* PLASA 2.

Kurowski, P. M. (2020). *Engineering Analysis with SOLIDWORKS Simulation 2020.* USA: SDC Publications.

Lisowski, F., & Lisowski, E. (2020). Testing and Fatigue Life Assessment of Timber Truck Stanchions. *Applied Sciences*.

PĂTRAȘCU, A. I. (2020). *Study of increasing the load capacity of an open high-walls wagon.* Bucharest: PhD Thesis Summary.

Slavchev, S., Georgieva, K., & Stoilov, V. (2014). Issues of wagon modeling with shell elements. *XVI International Scientific-expert Conference on Railways*, (pp. 33-36). Serbia.

Slavchev, S., Georgieva, K., Stoilov, V., & Purgić, S. (2014). Analysis of the results of theoretical and experimental studies of freight wagon FALS. *XVI International Scientific-expert Conference on Railways*.

Slavchev, S., Maznichki, V., Stoilov, V., & Purgic, S. (2018). Strength analysis of hopper freight wagon with regard to lightweight design. *BulTrans-2018 Conference Proceedings* , (pp. 106-109).

Solidworks Manual. (2019). *Mean Stress Correction.* Retrieved from http://help.solidworks.com/2019/english/SolidWorks/cworks/c_Mean_Stress_Correction.htm

Solidworks online help. (2020). *Meshing tips*. Retrieved from Help Solidworks: https://help.solidworks.com/2020/english/SolidWorks/cworks/c_Meshing_Tips.htm#klj1450460201166

Solidworks Technical Paper. (2021). *Understanding Connectors - Technical Paper.* Retrieved from https://blog.tekyaz.com/wp-content/uploads/2020/06/Understanding-Connectors.pdf

Stoilov, V., Simić, G., Purgić, S., Milković, D., Slavchev, S., & Radulović, S. (2019). Comparative analysis of the results of theoretical and experimental studies of freight wagon Sdggmrss-twin. *IOP Conference Series: Materials Science and Engineering.*

Stoilov, V., Slavchev, S., & Georgieva, K. (2011). Methodology for applying of comparative approach to proof the strength of wagons body.

Stoilov, V., Slavchev, S., & Purgic, S. (2016). Static strength study of body of universal flat wagon. *XVII International Scientific-expert Conference on Railways.* Serbia.

Stoilov, V., Slavchev, S., Maznichki, V., & Purgic, S. (2019). Analysis of some problems in the theoretical wagon strength studies due to the imperfection of the European legislation. *IOP Conference Series: Materials Science and Engineering.*

Thieme, C. (2016). *Whiteparer - How to Create a Good Quality FE Model.* Retrieved from MSC software: https://documents.mscsoftware.com/sites/default/files/whitepaper_how_to_create_a_good_fe_model.pdf

Timber Transport Forum. (2020). *The Road Haulage of Round Timber Code of Practice.* Retrieved from timbertransportforum.org.uk: https://timbertransportforum.org.uk/attachments/article/24/Timber%20Transport%20Forum%20Road%20Haulage%20of%20Round%20Timber%205%20Ed%20Digital.pdf

Ulianov, C., Önder, A., & Peng, Q. (2018). Analysis and selection of materials for the design of lightweight railway vehicles. *IOP Conference Series: Materials Science and Engineering*.

Ulianov, C., Shaltout, R., & Balan, A. C. (2015). Lightweight Vehicle Structural Design with Advanced Steel Grades and Profiles. *Applied Mechanics and Materials*, pp. 1199-1204.

Voltr, P., Ulianov, C., Hsaine, N., Hyde, P., Shi, D., & Fartan, M. (2019). *Modelling and analyses of novel lightweight design solutions.* INNOWAG.

APPENDIX

In this appendix are presented images for the results obtained for the analysis of the wagon "as-is" in the three FE models developed in this work. The plots considered more relevant are shown: Resultant displacements, von-Mises stress, and von-Mises stress with adjusted scale.

Load case: Horizontal Load Case 1 (HLC1)

Description: Compression force at buffer height – 2000 kN

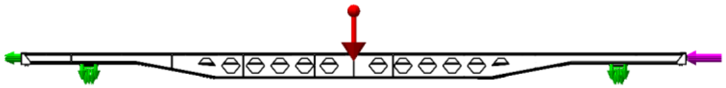

	Solidworks (Solid elements)	*MSC Apex* (Solid elements)	*MSC Apex* (Shell elements)
Displacement	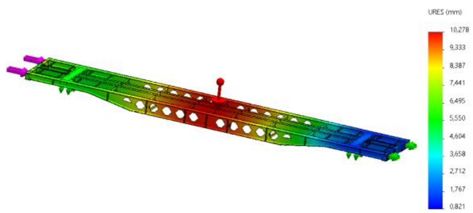	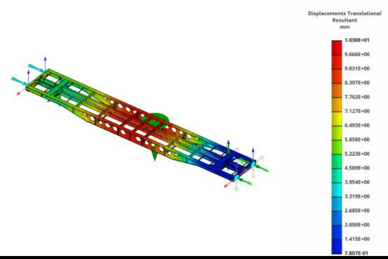	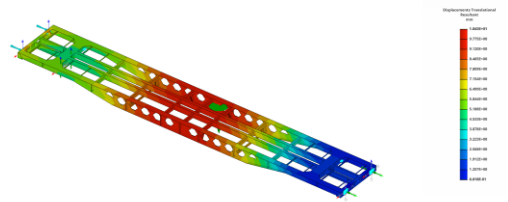
	δ =10.28 mm	δ = 10.30 mm	δ = 10.43 mm
Max. von-Mises Stress	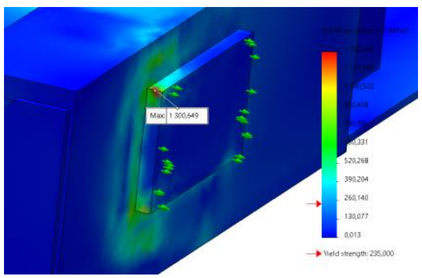	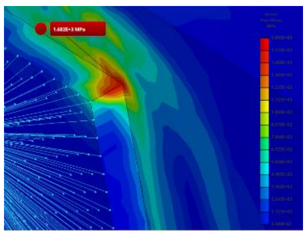	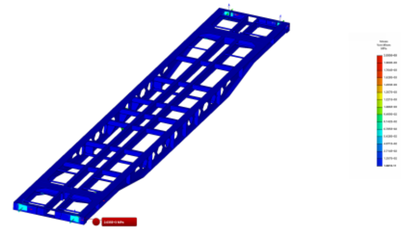
	$\sigma_{von\text{-}Mises}$=1300 MPa	$\sigma_{von\text{-}Mises}$=1682 MPa	$\sigma_{von\text{-}Mises}$= 2035 MPa
Stress > Yield Strength	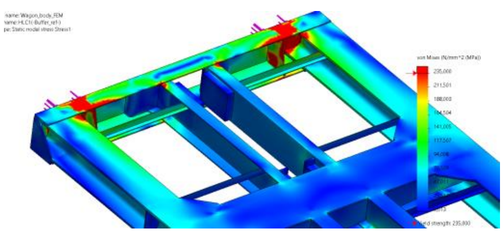	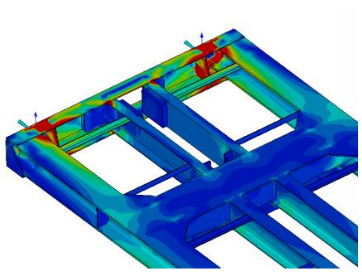	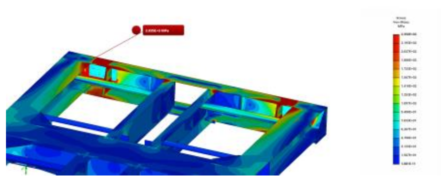

Load case: Horizontal Load Case 2 (HLC2)

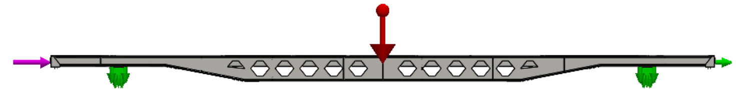

Description: Compression load applied 50mm below buffer axis - 1500 kN

	Solidworks (Solid elements)	*MSC Apex* (Solid elements)	*MSC Apex* (Shell elements)
Displacement	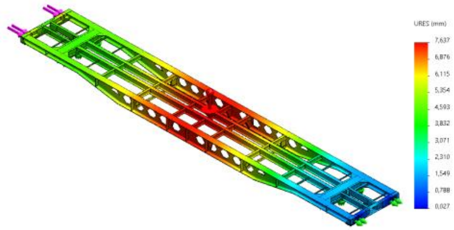	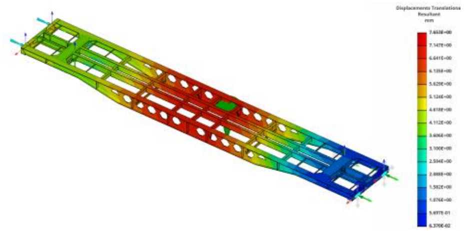	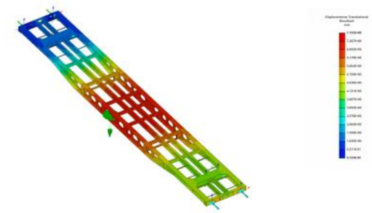
	δ = 7.637 mm	δ = 7.653 mm	δ = 7.722 mm
Max. von-Mises Stress	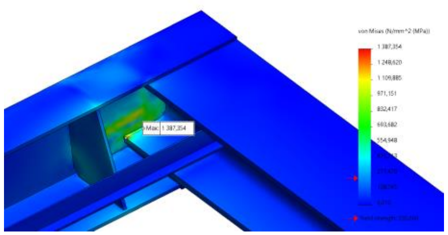	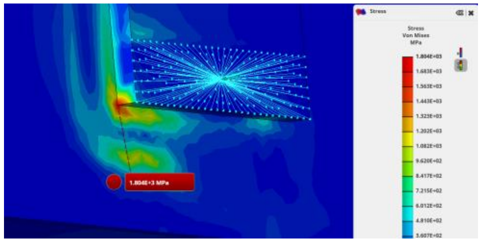	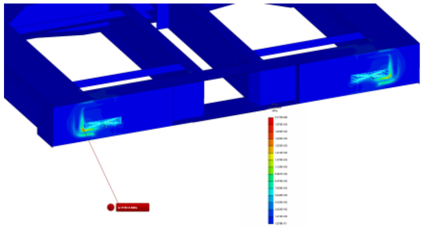
	$\sigma_{von\text{-}Mises}$= 1387 MPa	$\sigma_{von\text{-}Mises}$= 1804 MPa	$\sigma_{von\text{-}Mises}$= 2117 MPa
Stress > Yield Strength	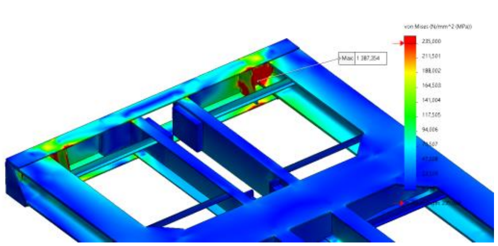	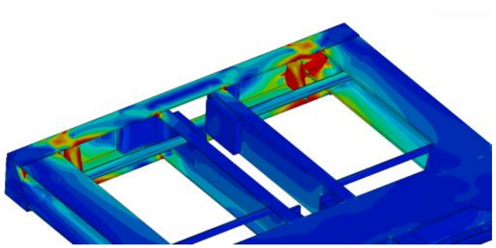	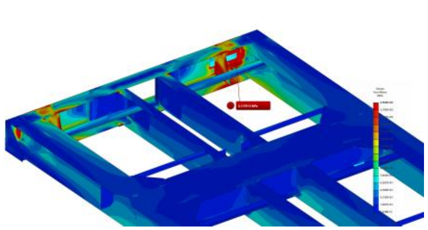

Load case: Horizontal Load Case 3 (HLC3)

Description: Compressive force applied diagonally at buffer level - 400 kN

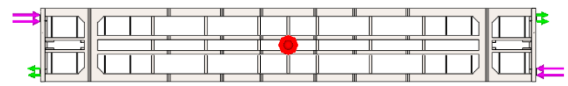

	Solidworks (Solid elements)	*MSC Apex* (Solid elements)	*MSC Apex* (Shell elements)
Displacement	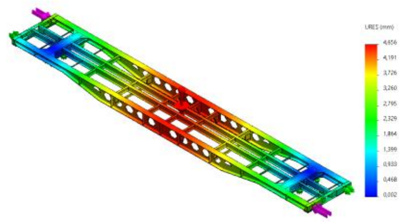	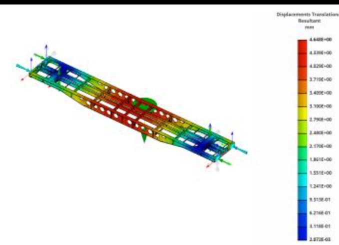	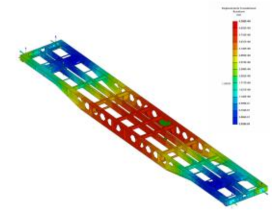
	δ = 4.656 mm	δ = 4.648 mm	δ = 4.288 mm
Max. von-Mises Stress	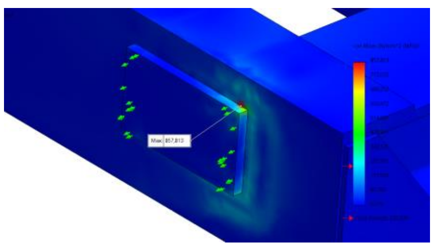	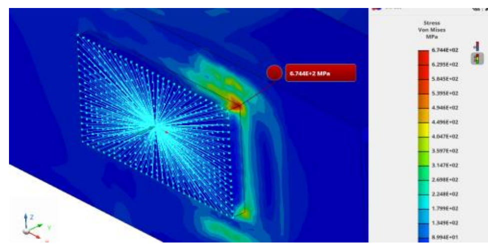	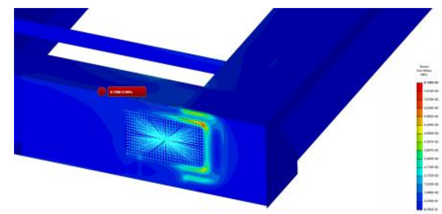
	$\sigma_{von\text{-}Mises}$= 852.8 MPa	$\sigma_{von\text{-}Mises}$= 674.4 MPa	$\sigma_{von\text{-}Mises}$= 815.8 MPa
Stress > Yield Strength	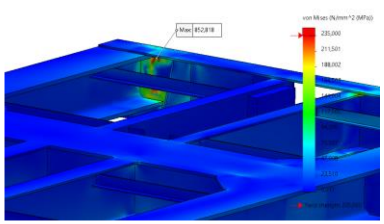	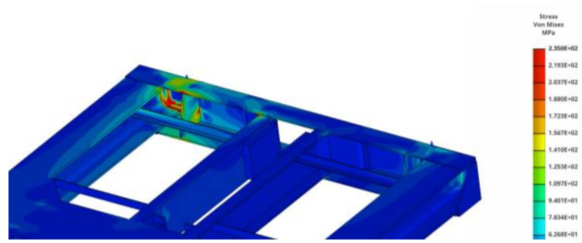	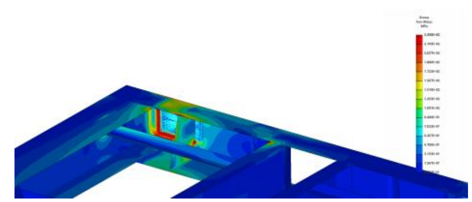

Load case: Horizontal Load Case 4 (HLC4)

Description: Tensile force in coupler - 1500 kN

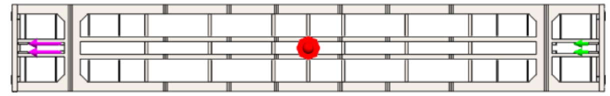

	Solidworks (Solid elements)	*MSC Apex* (Solid elements)	*MSC Apex* (Shell elements)
Displacement	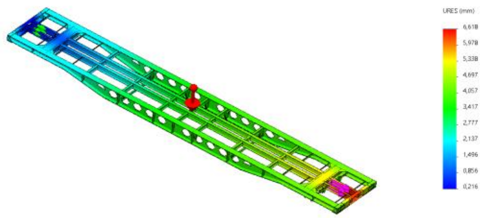	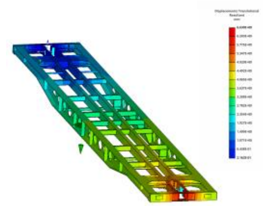	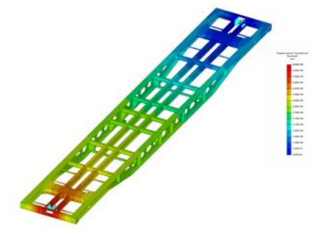
	δ = 6.618 mm	δ = 6.63 mm	δ = 6.243 mm
Max. von-Mises Stress	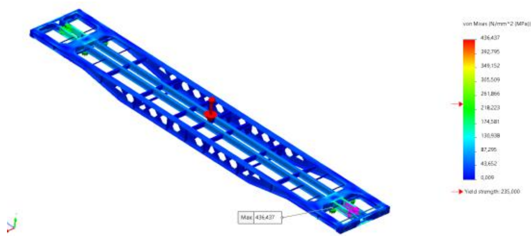	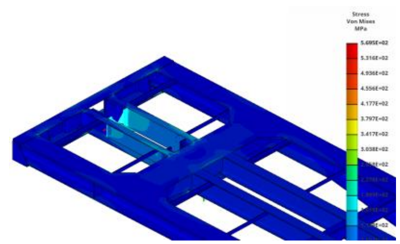	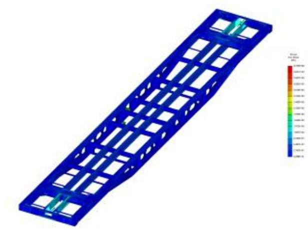
	$\sigma_{von-Mises}$= 436.437 MPa	$\sigma_{von-Mises}$= 569.5 MPa	$\sigma_{von-Mises}$= 411.5 MPa
Stress > Yield Strength	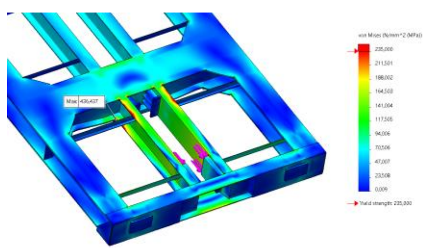	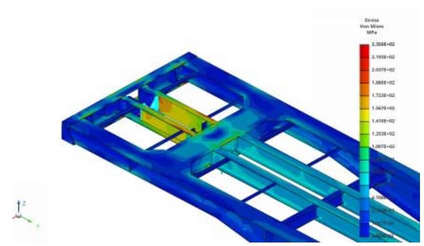	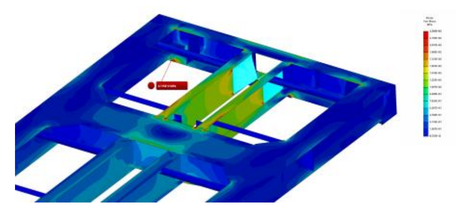

Load case: Vertical Load Case 1 (VLC1)

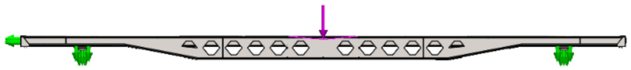

Description: 330 kN bi-supported A-A

	Solidworks (Solid elements)	*MSC Apex* (Solid elements)	*MSC Apex* (Shell elements)
Displacement	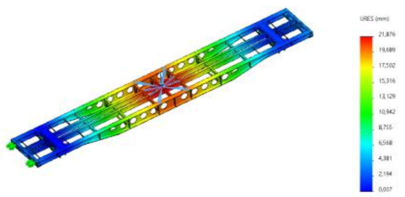	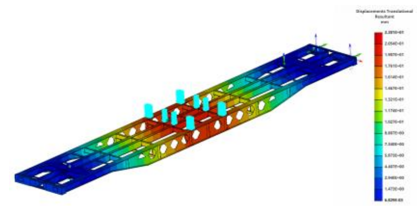	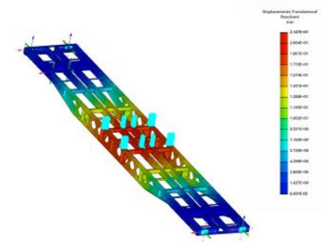
	δ = 21.88 mm	δ = 22.01 mm	δ = 21.47 mm
Max. von-Mises Stress	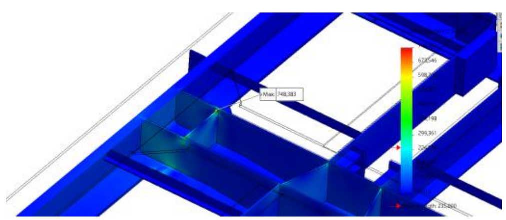	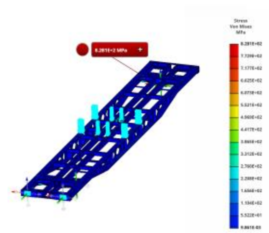	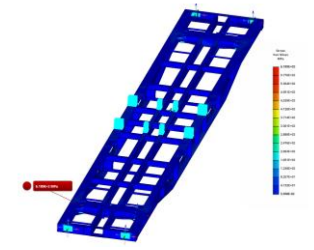
	$\sigma_{von\text{-}Mises}$= 748.4 MPa	$\sigma_{von\text{-}Mises}$= 828.10 MPa	$\sigma_{von\text{-}Mises}$= 618.90 MPa
Stress > Yield Strength	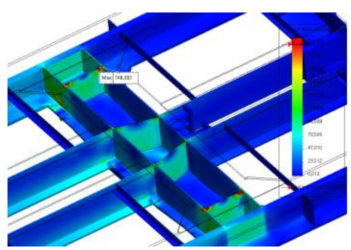	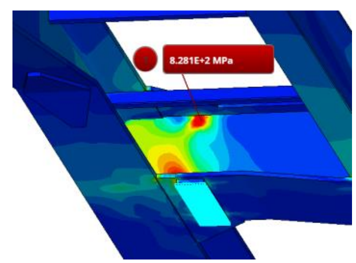	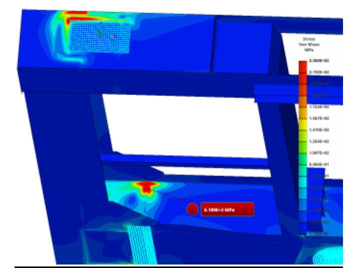

Load case: Vertical Load Case 2 (VLC2)

Description: 380 kN bi-supported B-B

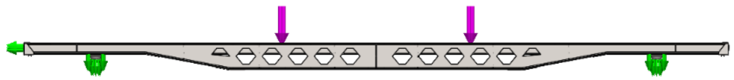

	Solidworks (Solid elements)	*MSC Apex* (Solid elements)	*MSC Apex* (Shell elements)
Displacement	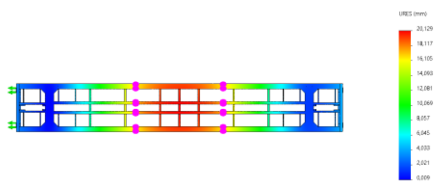	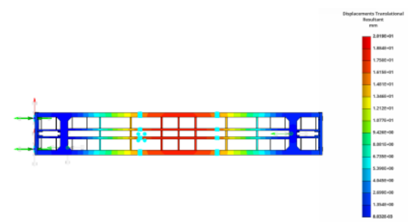	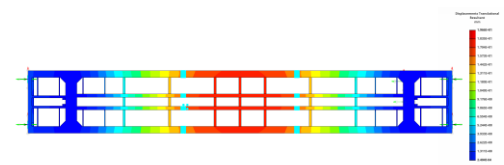
	δ = 20.13 mm	δ = 20.19 mm	δ = 19.66 mm
Max. von-Mises Stress	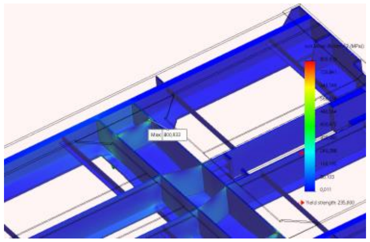	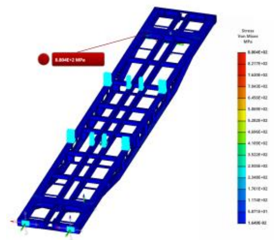	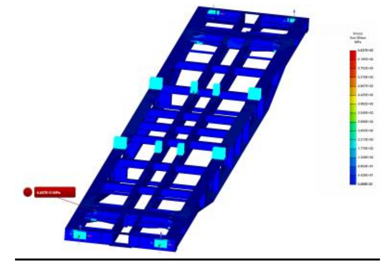
	$\sigma_{von\text{-}Mises}$= 800.90 MPa	$\sigma_{von\text{-}Mises}$= 880.40 MPa	$\sigma_{von\text{-}Mises}$= 663.70 MPa
Stress > Yield Strength	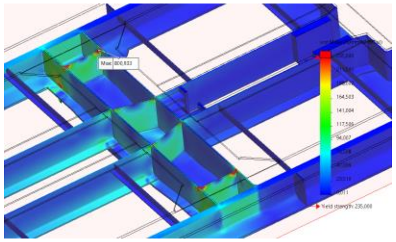	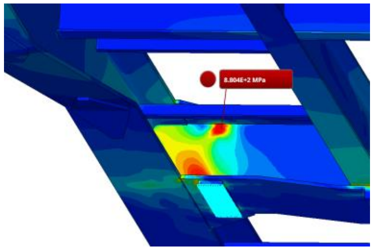	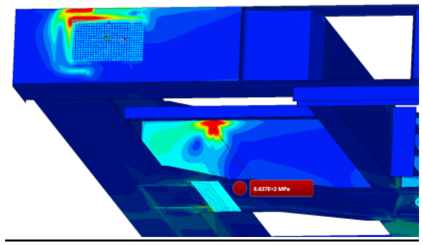

Load case: Vertical Load Case 3 (VLC3)

Description: 440 kN bi-supported C-C

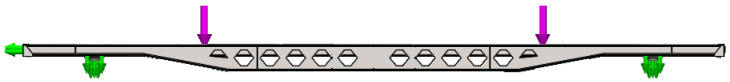

	Solidworks (Solid elements)	*MSC Apex* (Solid elements)	*MSC Apex* (Shell elements)
Displacement	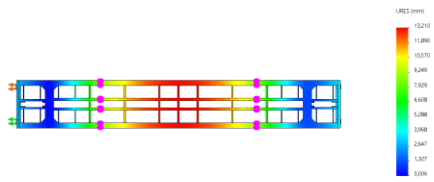	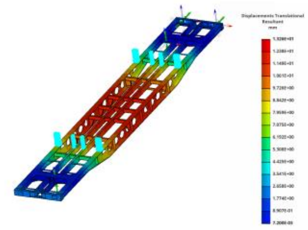	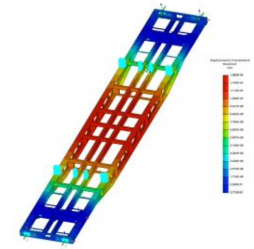
	δ = 13.21 mm	δ = 13.26 mm	δ = 12.85 mm
Max. von-Mises Stress	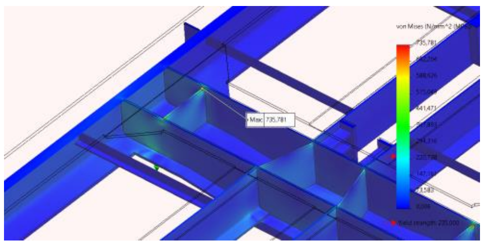	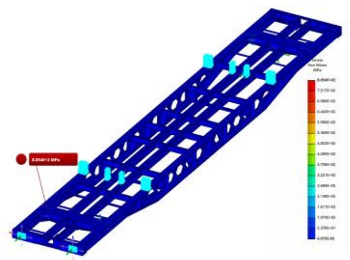	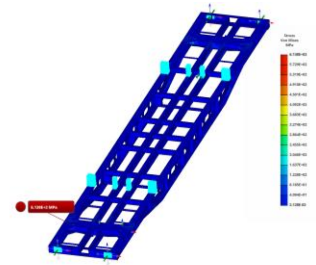
	$\sigma_{von\text{-}Mises}$= 735.8 MPa	$\sigma_{von\text{-}Mises}$= 805.40 MPa	$\sigma_{von\text{-}Mises}$= 613.80 MPa
Stress > Yield Strength	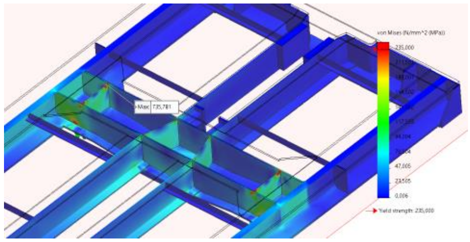	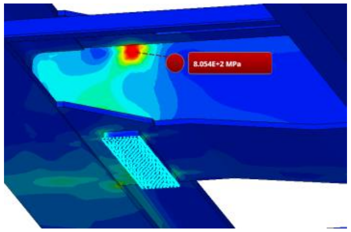	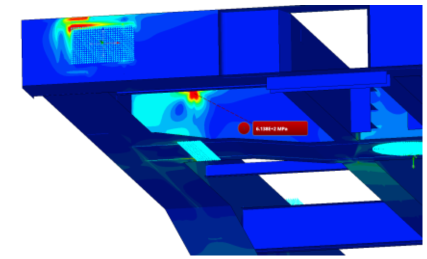

Load case: Vertical Load Case 4 (VLC4)

Description: 555 kN bi-supported D-D

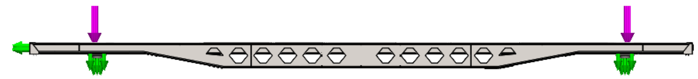

	Solidworks (Solid elements)	*MSC Apex* (Solid elements)	*MSC Apex* (Shell elements)
Displacement	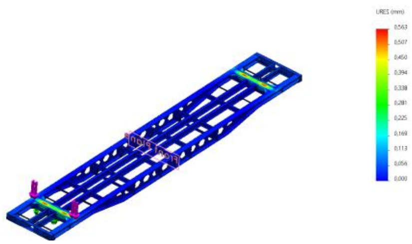	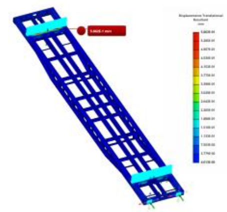	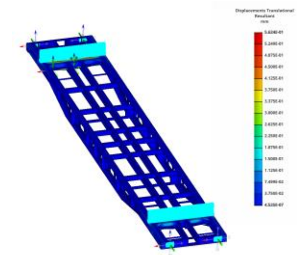
	δ = 0.56 mm	δ = 0.57 mm	δ = 0.56 mm
Max. von-Mises Stress	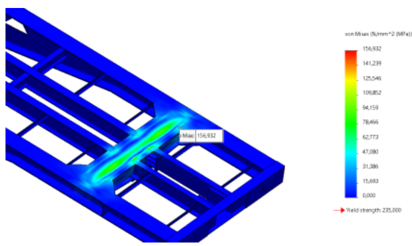	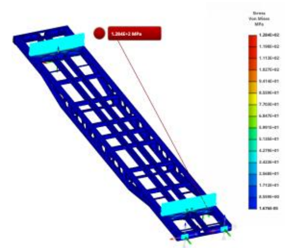	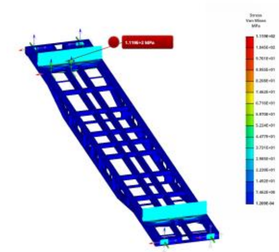
	$\sigma_{von\text{-}Mises}$= 165.93 MPa	$\sigma_{von\text{-}Mises}$= 128.40 MPa	$\sigma_{von\text{-}Mises}$= 111.90 MPa
Stress > Yield Strength	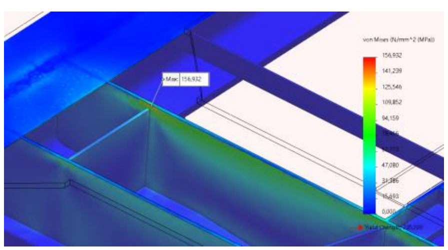	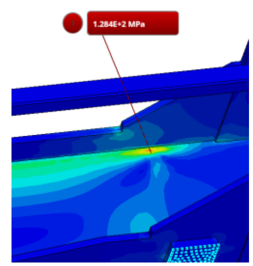	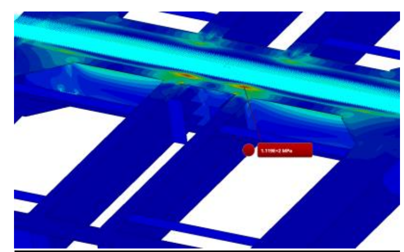

Load case: Vertical Load Case 5 (VLC5)

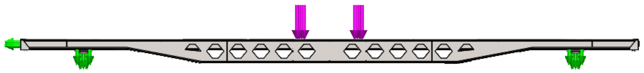

Description: : 320 kN Uniform Distribution A-A

	Solidworks (Solid elements)	*MSC Apex* (Solid elements)	*MSC Apex* (Shell elements)
Displacement	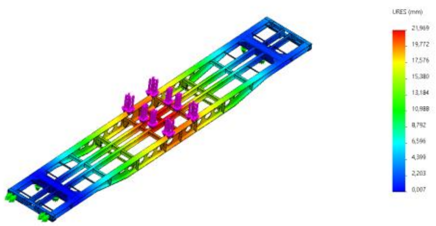	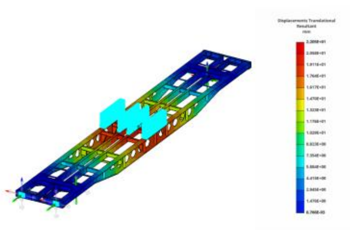	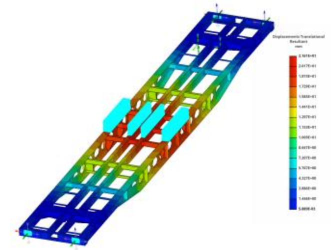
	δ = 21.97 mm	δ = 22.05 mm	δ = 21.61 mm
Max. von-Mises Stress	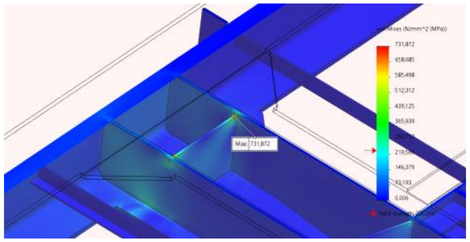	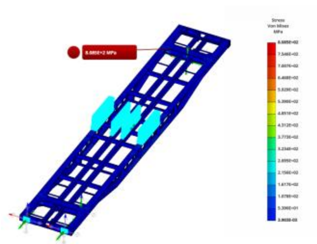	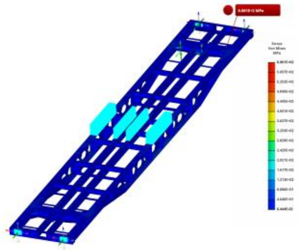
	$\sigma_{\text{von-Mises}}$= 731.872 MPa	$\sigma_{\text{von-Mises}}$= 808.50 MPa	$\sigma_{\text{von-Mises}}$= 606.10 MPa
Stress > Yield Strength	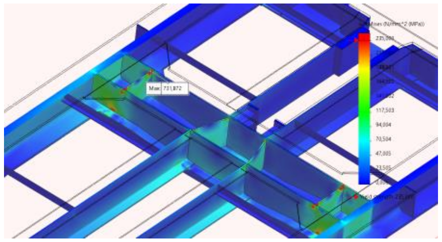	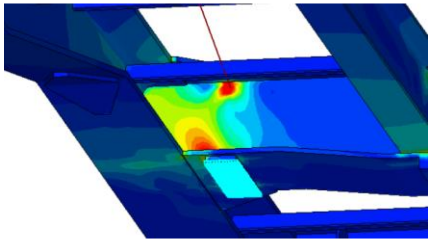	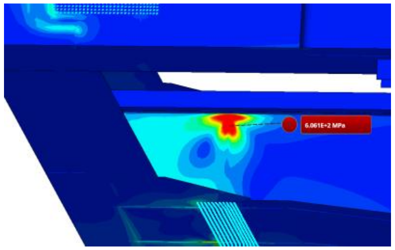

Load case: Vertical Load Case 6 (VLC6)

Description: 350 kN Uniform Distribution B-B

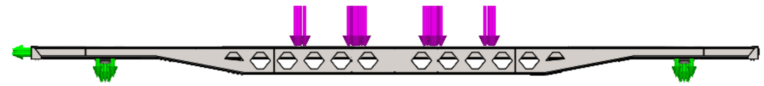

	Solidworks (Solid elements)	*MSC Apex* (Solid elements)	*MSC Apex* (Shell elements)
Displacement	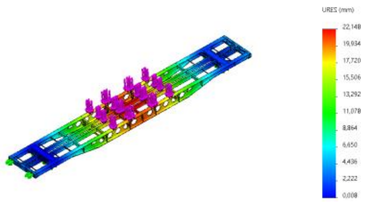	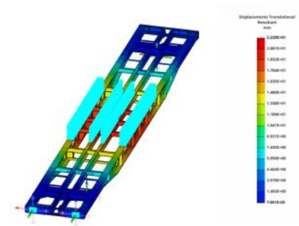	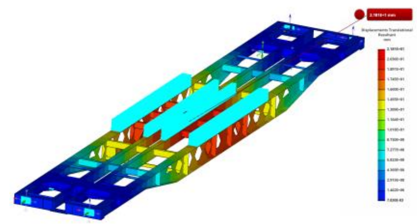
	δ = 22.15 mm	δ = 22.29 mm	δ = 21.81 mm
Max. von-Mises Stress	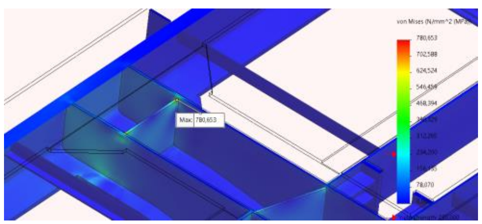	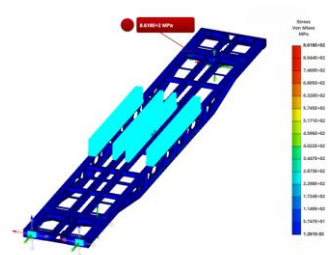	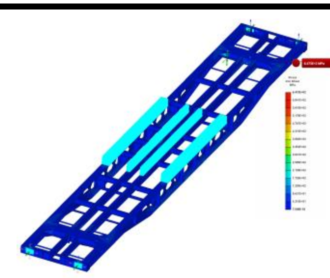
	$\sigma_{von\text{-}Mises}$= 780.65 MPa	$\sigma_{von\text{-}Mises}$= 861.80 MPa	$\sigma_{von\text{-}Mises}$= 647.30 MPa
Stress > Yield Strength	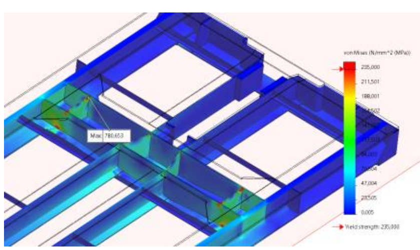	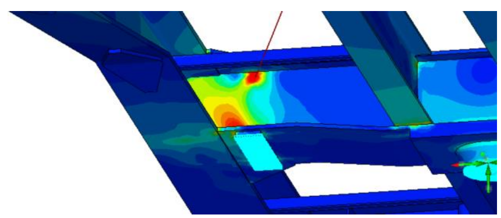	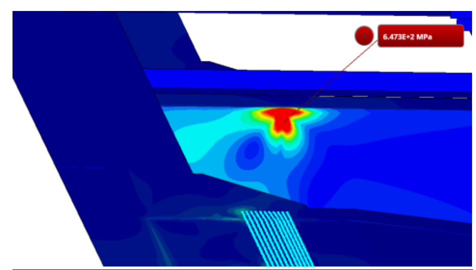

Load case: Vertical Load Case 7 (VLC7)

Description: 360 kN Uniform Distribution C-C

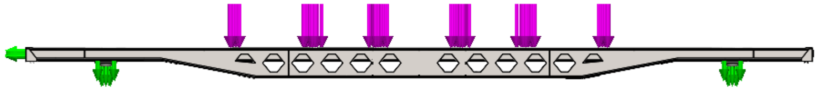

	Solidworks (Solid elements)	*MSC Apex* (Solid elements)	*MSC Apex* (Shell elements)
Displacement	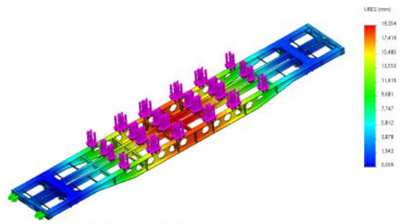	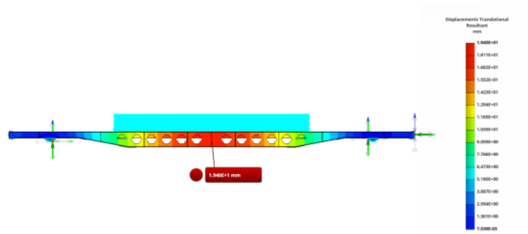	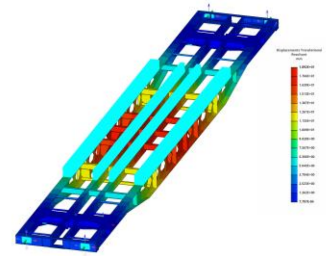
	δ = 19.35 mm	δ = 19.40 mm	δ = 18.29 mm
Max. von-Mises Stress	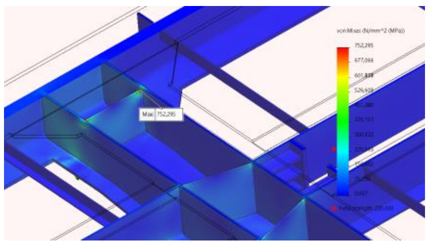	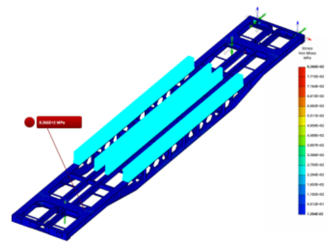	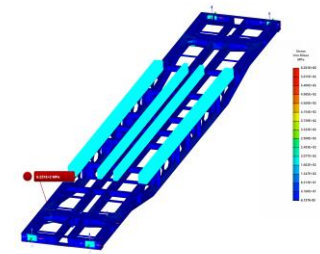
	$\sigma_{\text{von-Mises}}$= 752.30MPa	$\sigma_{\text{von-Mises}}$= 826.60 MPa	$\sigma_{\text{von-Mises}}$= 623.10 MPa
Stress > Yield Strength	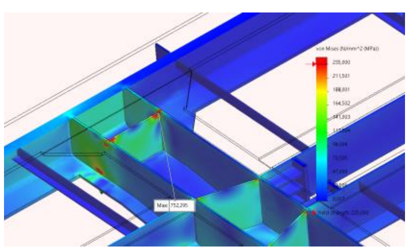	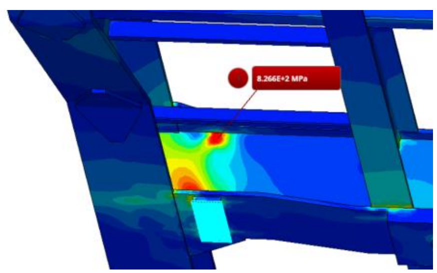	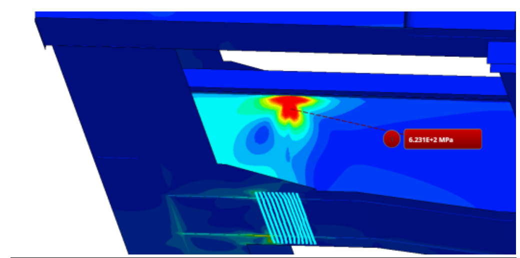

Load case: Vertical Load Case 8 (VLC8)

Description: 440 kN Uniform Distribution D-D

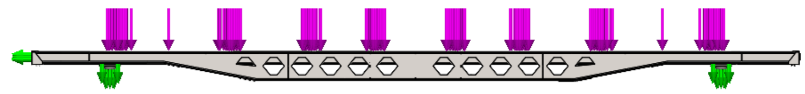

	Solidworks (Solid elements)	*MSC Apex* (Solid elements)	*MSC Apex* (Shell elements)
Displacement	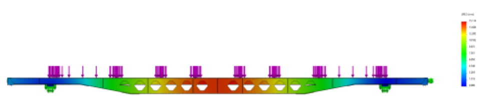	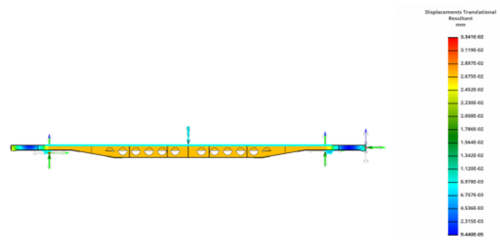	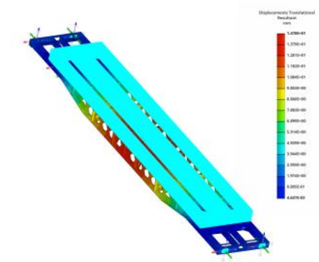
	δ = 15.11 mm	δ = 15.18 mm	δ = 14.78 mm
Max. von-Mises Stress	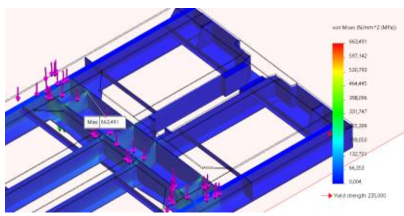	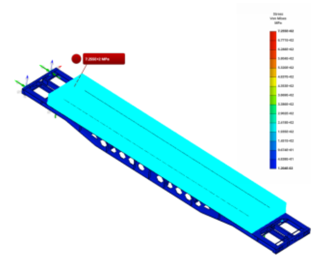	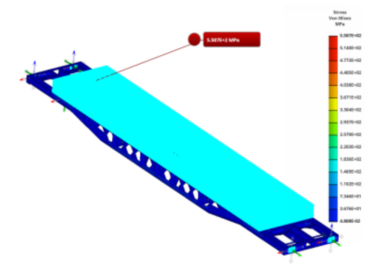
	$\sigma_{von\text{-}Mises}$= 663.49 MPa	$\sigma_{von\text{-}Mises}$= 725.50 MPa	$\sigma_{von\text{-}Mises}$= 550.70 MPa
Stress > Yield Strength	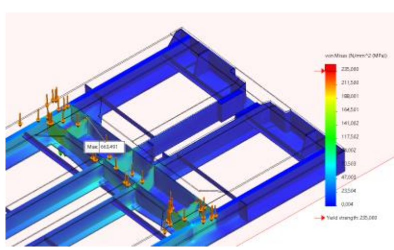	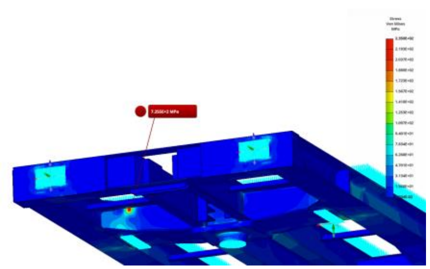	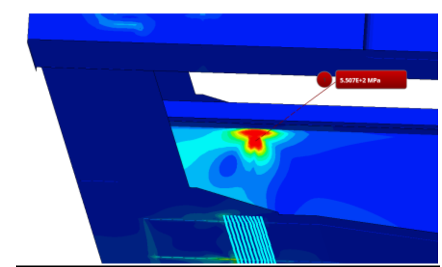

Load case: Lifting Load Case (LLC1)

Description: Lifting of one of the ends – 740 kN

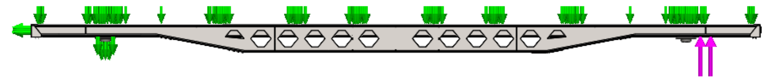

	Solidworks (Solid elements)	*MSC Apex* (Solid elements)	*MSC Apex* (Shell elements)
Displacement	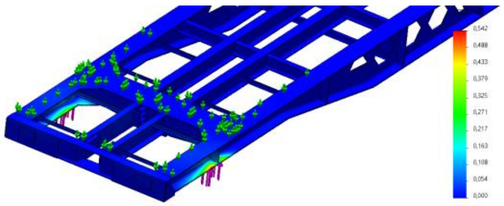	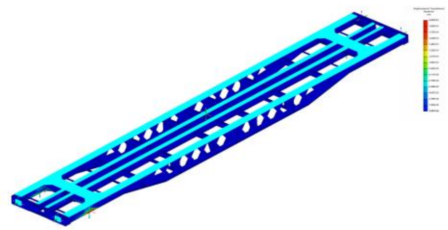	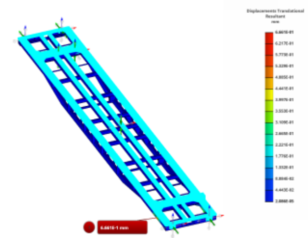
	$\delta = 0.542$ mm	$\delta = 0.543$ mm	$\delta = 0.661$ mm
Max. von-Mises Stress	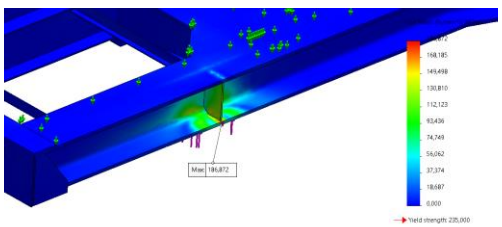	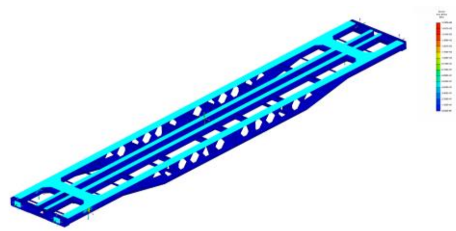	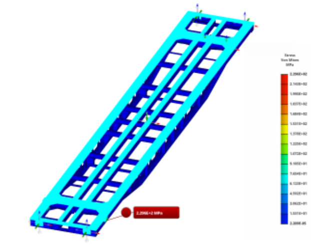
	$\sigma_{von\text{-}Mises}$= 186.87 MPa	$\sigma_{von\text{-}Mises}$= 188.40 MPa	$\sigma_{von\text{-}Mises}$= 229.6 MPa
Stress > Yield Strength	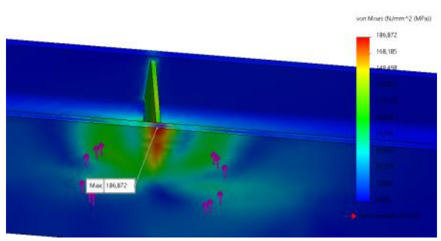	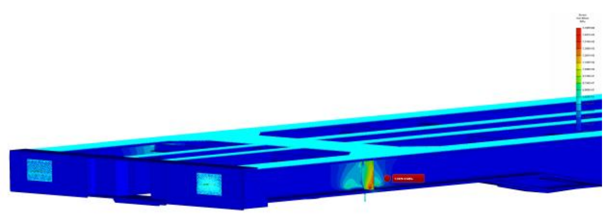	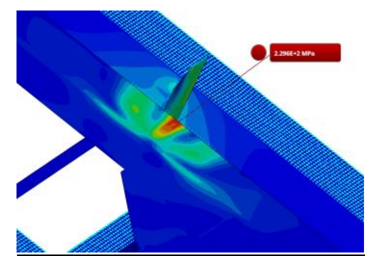

Load case: Lifting Load Case (LLC2)

Description: Lifting of the full vehicle – 800 kN

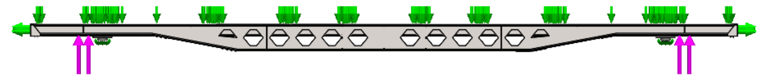

	Solidworks (Solid elements)	*MSC Apex* (Solid elements)	*MSC Apex* (Shell elements)
Displacement	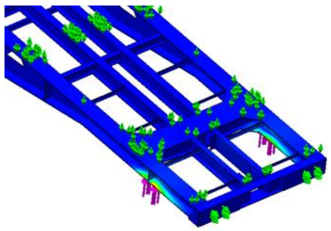	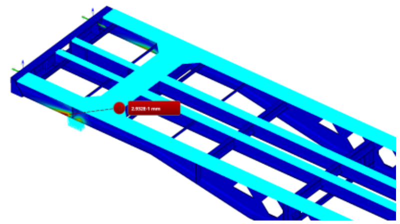	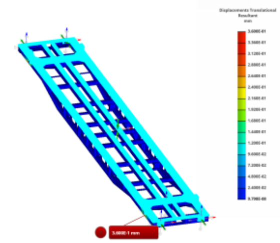
	$\delta = 0.293$ mm	$\delta = 0.293$ mm	$\delta = 0.360$ mm
Max. von-Mises Stress	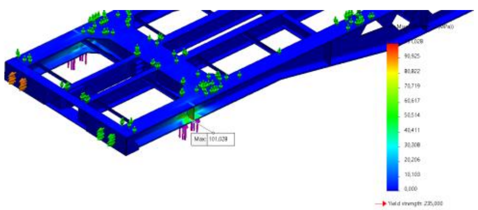	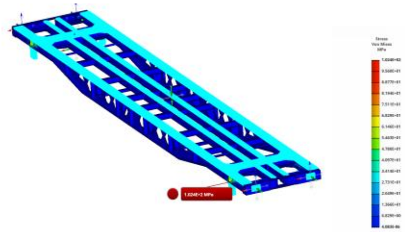	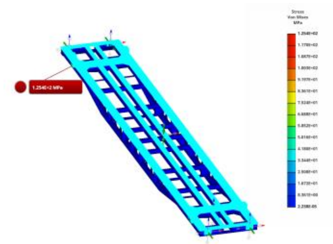
	$\sigma_{\text{von-Mises}}$= 101.03 MPa	$\sigma_{\text{von-Mises}}$= 102.4 MPa	$\sigma_{\text{von-Mises}}$= 125.4 MPa
Stress > Yield Strength	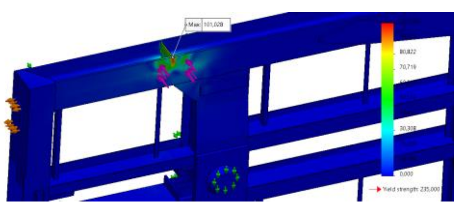	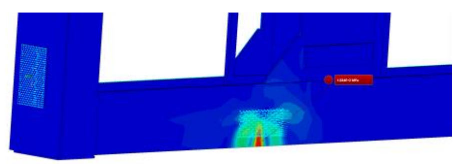	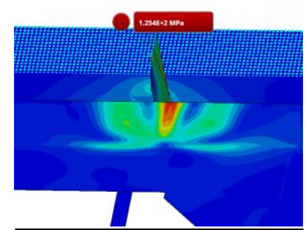

Load case: Lifting Load Case (LLC3)

Description: 10mm relative displacement

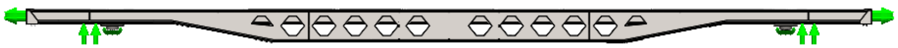

	Solidworks (Solid elements)	*MSC Apex* (Solid elements)	*MSC Apex* (Shell elements)
Displacement	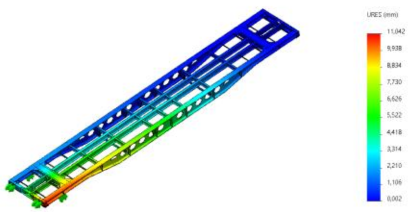	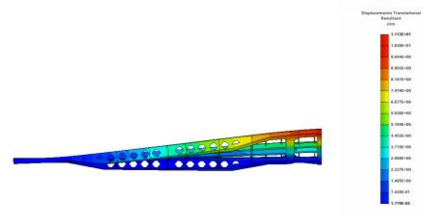	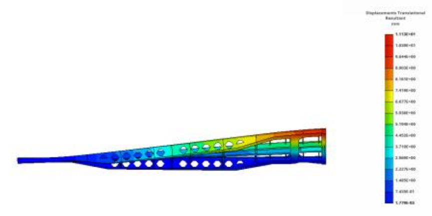
	δ =11.042 mm	δ = 11.24 mm	δ = 11.13 mm
Max. von-Mises Stress	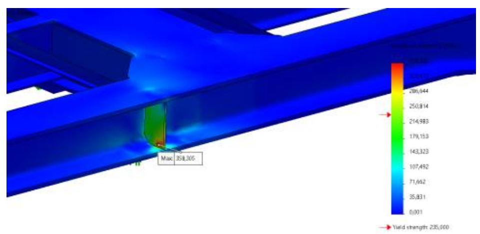	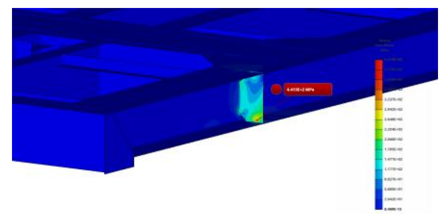	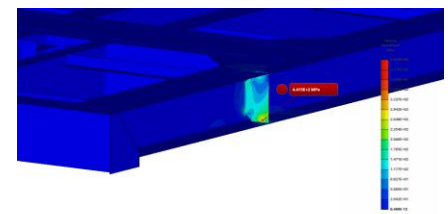
	$\sigma_{von\text{-}Mises}$= 358.3 MPa	$\sigma_{von\text{-}Mises}$= 346.7 MPa	$\sigma_{von\text{-}Mises}$= 441.3 MPa
Stress > Yield Strength